UNCLASSIFIED

GE DOCUMENT No. 78SDR2195

ADVANCED OPTICAL CERAMICS

PHASE "O"

May 15, 1978

Final Technical Report
Contract No. N00014-77-C-0649
(DARPA ORDER NO. 3387)

Technical Work Performed
August 15, 1977 through February 15, 1978

for

Office of Naval Research
800 N. Quincy Street
Arlington, Virginia 22217

GENERAL ELECTRIC
Re-entry & Environmental Systems Division
3198 Chestnut St., Philadelphia, Pa. 19101

UNCLASSIFIED

UNCLASSIFIED

SECURITY CLASSIFICATION OF THIS PAGE (When Data Entered)

REPORT DOCUMENTATION PAGE

READ INSTRUCTIONS BEFORE COMPLETING FORM

1 REPORT NUMBER | 2. GOVT ACCESSION NO. | 3. RECIPIENT'S CATALOG NUMBER

4 TITLE (and Subtitle)
Advanced Optical Ceramics Phase 'O'
Final Report

5. TYPE OF REPORT & PERIOD COVERED
Technical Aug. 15, 1977 thru Feb. 15, 1978

6. PERFORMING ORG. REPORT NUMBER
78SDR2195

7 AUTHOR(s)
S. Musikant, R.A. Tanzilli, R. J. Charles, G.A. Slack, W. White, R.M. Cannon

8. CONTRACT OR GRANT NUMBER(s)
N00014-77-C-0649
DARPA Order No. 3387

9 PERFORMING ORGANIZATION NAME AND ADDRESS
GENERAL ELECTRIC COMPANY, RESD
3198 Chestnut Street
Philadelphia, Pa. 19101

10. PROGRAM ELEMENT, PROJECT, TASK AREA & WORK UNIT NUMBERS
NR 032-577/6/21-77 (471)

11 CONTROLLING OFFICE NAME AND ADDRESS
Office of Naval Research
800 N. Quincy Street
Arlington, Virginia 22217

12. REPORT DATE
May 15, 1978

13. NUMBER OF PAGES
164p.

14 MONITORING AGENCY NAME & ADDRESS (if different from Controlling Office)

15. SECURITY CLASS. (of this report)
UNCLASSIFIED

15a. DECLASSIFICATION/DOWNGRADING SCHEDULE
N/A

16 DISTRIBUTION STATEMENT (of this Report)

This document has been approved for public release and sale; its distribution is unlimited.

DDC
DISSEMINATED
JUN 12 1978
F

17 DISTRIBUTION STATEMENT (of the abstract entered in Block 20, if different from Report)
Final technical rept. 15 Aug 77-15 Feb 78,

18 SUPPLEMENTARY NOTES The views and conclusions contained in this document are those of the authors and should not be interpreted as necessarily representing the official policies, either expressed or implied of the Defense Advanced Research Projects Agency or the U.S. Government.

19 KEY WORDS (Continue on reverse side if necessary and identify by block number)
IR domes, radome, missile, ceramics, antenna window, window, absorption coefficients.

20 ABSTRACT (Continue on reverse side if necessary and identify by block number)
The Advanced Optical Ceramics Phase 'O' study was designed to firstly identify advanced DoD missions which will impose performance requirements on electro-optical/electro-magnetic (EO/EM) windows beyond the current state of the art as it is now progressing.

over

DD FORM 1 JAN 73 1473 EDITION OF 1 NOV 65 IS OBSOLETE

UNCLASSIFIED

SECURITY CLASSIFICATION OF THIS PAGE (When Data Entered)

404 884

LB

The second aspect of the study was to identify advanced EO/EM window materials which should be investigated for their potential application to the advanced missile window problem.

A survey of missions was performed and reported in a separate classified report. A review was conducted of ceramic materials which are refractory, hard and have the potential for meeting the EO/EM requirements. This review identified a wide variety of materials which can potentially meet the performance requirements. The selected candidates included simple compounds in the oxide, nitride and ternary sulfide families, oxynitrides, and a wide variety of mixed oxides. A program plan was devised to synthesize, and characterize these materials so that a selection of the few most promising ones can be made for further development and application to transparent enclosures for advanced missiles.

FOREWORD

This Final Report covers the unclassified results of the Advanced Optical Ceramics Phase "O" study performed by the General Electric Company, Re-entry and Environmental Systems Division (GE-RESD) under Office of Naval Research Contract No. N00014-77-C-0649. The ONR contract monitor was Dr. A. M. Diness, while the program manager was Dr. Solomon Musikant (GE-RESD). The work was sponsored under the Defense Advanced Research Projects Agency (DARPA) Materials Sciences (Dr. A. Bement, Jr., Director), DARPA Order No. 3387. The period of performance for the technical effort was August 15, 1977, through February 15, 1978.

Task 1 of this study identified the advanced DoD missions which will impose performance requirements on electro-optical/electro magnetic (EO/EM) windows beyond the state-of-the-art as it is currently progressing. A classified (confidential) report covering this aspect of the study has been issued.

Advanced Optical Ceramics
Task 1 Report - Advanced Mission Survey and Ceramic Window Performance Requirements
GE No. 78SDR2196
by J. Greshock (GE-RESD) November 30, 1977

The classified volume is a comprehensive review of ongoing and planned (to the year 2000) developments of advanced guided missiles as well as ballistic re-entry vehicles which will require advanced optical/electromagnetic windows for successful mission performance. The volume reviews the bandpasses of interest, the aerothermal loading, and the projected laser threats which will be imposed on these windows. The rain erosion problem is evaluated specifically for the SCRAM hypersonic vehicle.

Acknowledgments

The primary contributors to this study have been:

Dr. R. M. Cannon, Jr., Assistant Professor, Ceramics,
Department of Materials Science and Engineering, MIT

Dr. R. J. Charles, Manager, Ceramics Branch,
GE-Corporate Research and Development

J. P. Greshock, Systems Engineer
GE-Re-entry and Environmental Systems Division

H. W. Rauch, Ceramist, GE-Space Division

Dr. G. A. Slack, Physicist
GE-Corporate Research and Development

Dr. R. A. Tanzilli, Consulting Materials Scientist
GE-Re-entry and Environmental Systems Division

Dr. W. B. White, Professor Geochemistry
Materials Research Laboratory, Pennsylvania State University

Mr. R. A. Middleton, Curator of Minerals, Philadelphia Academy of Natural Sciences, provided natural crystals for optical measurements of various of the candidate materials.

Significant technical contributions were made to this study by many GE scientists and engineers in various General Electric divisions. The following acknowledges some (but not all) of these important contributors:

J. Brazel	GE-Reentry and Environmental Systems Div.
Dr. J. J. Gebhardt	
J. O. Hanson	
R. M. Ross	
V. N. Saffire	
Dr. E. Feingold	GE-Space Division
A. Gatti	
L. R. McCreight	
H. W. Rauch	
Dr. R.H. Arendt	GE-Corporate Research and Development
Dr. C. D. Greskovich	
Dr. I. C. Huseby	
Dr. S. Prochazka	

H. P. Bovenkirk — GE-Specialty Material Business Dept.
Dr. F. Corrigan
Dr. P. Gigl
Dr. P. D. St. Pierre

We are indebted to the numerous personnel in the various DoD Laboratories and agencies who have contributed to the contents of these volumes, and to Dr. A. M. Diness, Office of Naval Research, Program Monitor, for his guidance during the performance of this study.

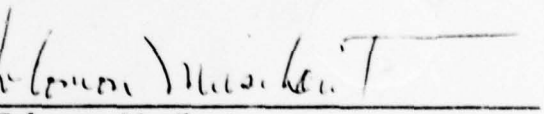

Dr. Solomon Musikant
Program Manager and Principal Investigator
General Electric Co.
Re-entry and Environmental Systems Division
Tel.: (215) 823-4942

Table of Contents

Table of Contents (Continued)

Table of Contents (Continued)

Table of Contents (Continued)

*References are numbered sequentially starting with Reference 1 in each Section. All references are listed by Section in Section 6.

List of Illustrations

List of Illustrations (Continued)

List of Illustrations (Continued)

List of Tables

SECTION 1

INTRODUCTION AND SUMMARY

SECTION 1

INTRODUCTION AND SUMMARY

1.1 Introduction

This Advanced Optical Ceramics Phase "O" Study was designed firstly to identify the advanced DoD missions which will impose performance requirements on electro optical/electromagnetic (EO/EM) windows beyond the state-of-the-art as it is currently progressing. The time frame being considered is for missions entering operational status in the 1985-1995 period. The second aspect of this study was to identify advanced EO/EM window materials and provide a program plan for the development of these advanced materials which will meet the projected system demands. Phase "O" is contemplated to be part of a more comprehensive program leading to the synthesis of advanced materials and application to advanced missile systems, as indicated in Figure 1.

The following paragraphs summarize the conclusions reached and reported in the classified report on Task 1.

1.2 Missions

Advanced ceramic materials are being considered as candidates for electro-optical and electro-magnetic window applications for future tactical and strategic systems. These systems include tactical and strategic missiles, aircraft, remotely piloted vehicles, spacecraft, battlefield optics, and high energy lasers. Since the performance criteria for some of these systems (particularly missiles) have been advancing rapidly, it has become increasingly clear that one of the limiting technologies for such advanced systems is the window material. Table 1-1 lists the desired qualities required for window materials as a function of their application. As seen in this table, the missiles have the broadest and, therefore, the most demanding requirements. For this reason, and because of the potentially large number of future missile applications, this study concentrated on the missile applications. It was felt that materials meeting the missile requirements would most likely meet the requirements for other

FIGURE 1. Advanced Optical Ceramics -- Program Objectives

PHASE "O"	● Establish sensor window requirements for advanced DoD missions* ● Establish candidate Advanced Optical Ceramic Materials to meet requirements. (ONR Contract No. N00014-77-C-0649 - DARPA Order No. 3387)
PHASE I	● Screen candidates by synthesis, characterization and analytical performance evaluations ● Establish most promising candidates (small number) for full development
PHASE II, III	● Optimization and Applications Development

*Advanced Optical Ceramics
Task 1 Report
Advanced Mission Survey and
Ceramic Window Performance
Requirements
by J. Greshock (GE-RESD) November 30, 1977
(ONR Contract No. N00014-77-C-0649
-DARPA Order No. 3387)

TABLE 1.1. Desirable Qualities for Advanced Electro-Optical and Electro-Magnetic Window Materials

Systems	Desired Qualities: Bandpass	All Weather	Particle Erosion	Aerothermal	Aerodynamic	Laser	Large FOV	Low Cost	Multi-Mode	Thermal-Chemical Recession	Captured Flight
Tactical Missiles	X	X	X	X	X	X	X	X	X	X	X
Strategic Missiles	X	X	X	X	X	X				X	
Aircraft	X	X	X	x	x	X					
RPV's	X	X	X	x	x	X		X			
Spacecraft	X					X					
Battlefield Optics	X	X				X		X			
High Energy Lasers	X			X		X					

x = These characteristics are required, but to a much lesser extent than those marked "X".

system applications. The high energy laser window application might be the one exception to this rule because of the large power transmission levels and low optical distortions required.

An extensive survey of advanced requirements for missiles from the existing literature and from involved government agencies was conducted and it was concluded that sufficient need exists for advanced high performance electro-optical (EO) or electro-magnetic (EM) transmitting ceramics for missile applications to warrant the major emphasis of this study placed in this area. The major driving forces for these needs have resulted from the anticipated superiority in Soviet force size, the liklihood of non-ideal weather conditions in both tactical and strategic battle environments, and the need for methods to accomplish missions for which solutions have yet to be found. These driving forces are summarized in Table 1-2 and include those associated with the natural environment, the defense induced environment, and the new mission areas.

From the natural environment, the EO and EM transmission and the temperature dependence of this transmission are primary drivers. The thermal, structural and chemical integrity of the domes (windows) in light of higher velocity flight profiles is next followed by all weather capability (including visibility and rain erosion retardation). Low cost is another driver particularly for tactical battlefield support missiles which will be used in great quantities, against relatively inexpensive targets, protecting relatively inexpensive assets. The defense induced environments include countermeasures, high energy laser irradiation, physical avoidance through evasion and large numbers of targets requiring a large field of view for the sensor and window. Some new missions which are acting as drivers for missile dome material developments are the need for a missile which can engage other tactical missiles; the potential need for a high accuracy non-nuclear, anti-ballistic missile should nuclear fuel become scarce; and high precision terminal homing intercontinental ballistic missiles (ICBM's).

TABLE 1-2. Fundamental Driving Forces for Window Material Development

NATURAL ENVIRONMENT	-	EO, EM Spectrum
	-	High Velocity
	-	Large Field of View ($\sim \pm 90^{o}$)
	-	All Weather
	-	Low Cost
DEFENSE ENVIRONMENTS	-	Jamming
	-	Laser
	-	Evasion
NEW MISSIONS	-	Tactical Anti-Missile Missile
	-	Non-Nuclear ABM
	-	Precision Guided ICBM's

An evaluation of the current trends has led to the conclusion that a missile with the following characteristics would be highly desirable:

1) High EO and/or EM transmissibility and non-degrading transmissibility at elevated temperatures
2) High thermal shock, thermal soak and thermo-chemical capabilities
3) "Fire and forget" missile capability which implies completely autonomous homing devices with wide field of view and sufficient maneuvering capability to combat the superiority of enemy force levels
4) Operating wavelengths conducive to all weather performance
5) Missile dome physical hardness sufficient to survive weather or particulate erosion at elevated temperatures and to provide sufficient transmission performance in the presence of the erosion environment
6) Homing techniques like multi-mode operation to defeat enemy countermeasures
7) Low or negligible self-emittance in the sensor's bandpass as a result of thermal heating;
8) High aerodynamic structural integrity to withstand pressure, axial acceleration and maneuvering loads
9) Low thermal expansion and expansion compatible with missile interface materials
10) Clean ablation and controlled ablation compatible with surrounding vehicle heat shield material (as in the case of a re-entry vehicle [RV]).

Table 1-3 summarizes the broad spectrum of missile applications and the interested military services. The missile applications are separated into tactical and strategic. In the tactical area, the following categories of missions are given:

1) Air-to-Air (A-A)
2) Air-to-Surface (A-S)
3) Surface-to-Air (S-A)
4) Surface-to-Surface (S-S)

TABLE 1-3. A Broad Spectrum of Missile System Missions are Being Considered

Mission	Categories	Army	Navy	Air Force
Tactical	Air-to-Air		o Dog Fight → o Self-Defense →	
	Air-to-Surface	Battlefield Support	o Battlefield Support → o High Priority Targets →	
	Surface-to-Air	Air Defense	Air Defense	
	Surface-to-Surface	o Battlefield Support o Intermediate Range High Priority Targets	o Anti-Shipping o Ship to Shore High Priority Targets	
Strategic	Surface-to-Air	ABM		
	Surface-to-Surface		ICBM →	
	Air-to-Surface			Cruise

In the tactical missions, the systems can be grouped into three general categories according to the operational flight range of the missiles. Basically, the short range systems will be single booster boost system rockets and will have high accelerations, short boost times, and be submitted to high thermal shock conditions. The medium range systems may be rocket or ramjet type systems, be subjected to high acceleration (thermal shock) and sustained heating during the longer free flight or cruise periods. The long range systems will be either cruise type or intermediate range ballistic missile (IRBM) and will be subjected to high temperatures for long durations.

A rather broad list of terminal homing concepts are currently being investigated for advanced systems, some of which are already in operational use. Passive 3-5 Micron IR imaging devices for hot target surface-to-air and air-to-air applications, passive 8-12 Micron IR imaging devices for air-to-surface cold target applications, active and passive applications for radars in all wavebands as well as TV devices are all being considered for a wide range of advanced missiles.

Therefore, the high performance ceramic window materials which this study is attempting to identify must cover the entire spectrum from visible to long wave radar and have the potential for operations in a thermal shock environment and/or a long heat soak environment without failure while performing the vital electro-optical tasks.

1.3 Materials

Missile systems now in use or contemplated for near term deployment which demand ceramic EO/EM enclosures due to thermal loads are limited by the very few materials available. These materials are summarized in Figure 2. In addition to those listed, ongoing development includes silicon nitride as an emerging material primarily for radar applications.

The paucity of suitable EO/EM materials limits future missions particularly when the combined thermal shock/rain erosion environments are considered. The (potential) laser threat superimposed on the natural environments amplifies the dilemma of the system planner. There are few, if any, obvious choices for advanced materials.

The current study has identified a number of materials systems which have the potential for meeting the more stringent performance requirements anticipated for future missile applications. These advanced material candidates are summarized in Figure 3. Note that the $BeSiN_2$ is expected to perform similarly to Si_3N_4. The advantage of $BeSiN_2$ is that it forms solid solutions with AlN and thus provides the possibility of a precipitation hardened "alloy", as noted on Figure 3.

Since thermal shock resistance is a key requirement in the development of these candidate materials, the thermal shock parameter, R, will have to be maximized where

$$R = K_{IC}/E \, \alpha\sqrt{2}$$

α = coefficient of thermal expansion

E = modulus of elasticity

K_{IC} = fracture toughness parameter

E and α are intrinsic properties. However, K_{IC} is an extrinsic property and can be enhanced by a variety of approaches. This issue is discussed at some length in Section 4.

1.4 Program Plan

Based on the results of the Advanced Optical Ceramics Phase "O" study, a program plan has been devised for development of the advanced materials in three additional phases. This plan is summarized in Figure 4. The plan provides for a

FIGURE 2. State-of-the-Art Sensor Enclosure Windows

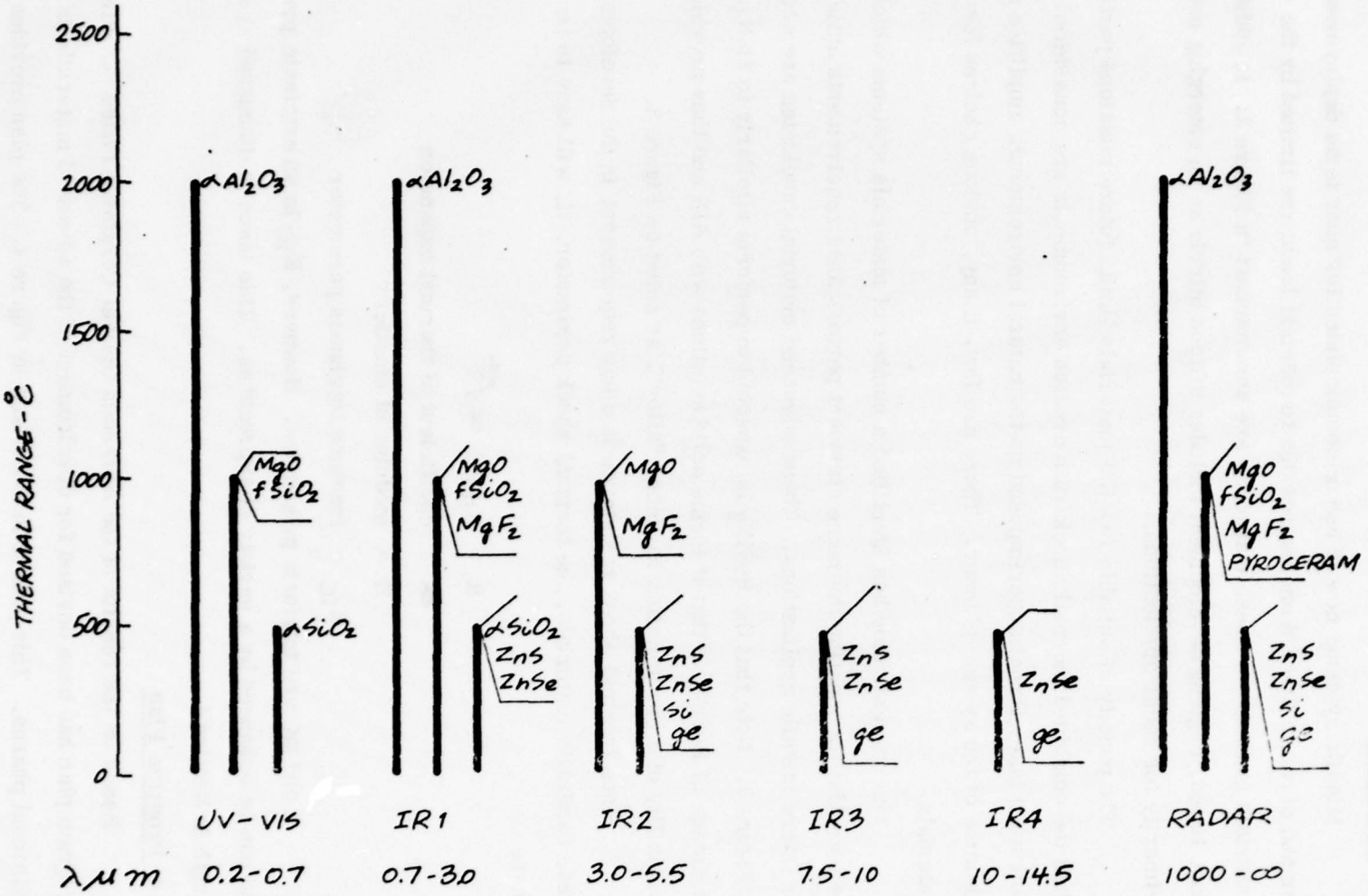

FIGURE 3. New Candidates to be Screened

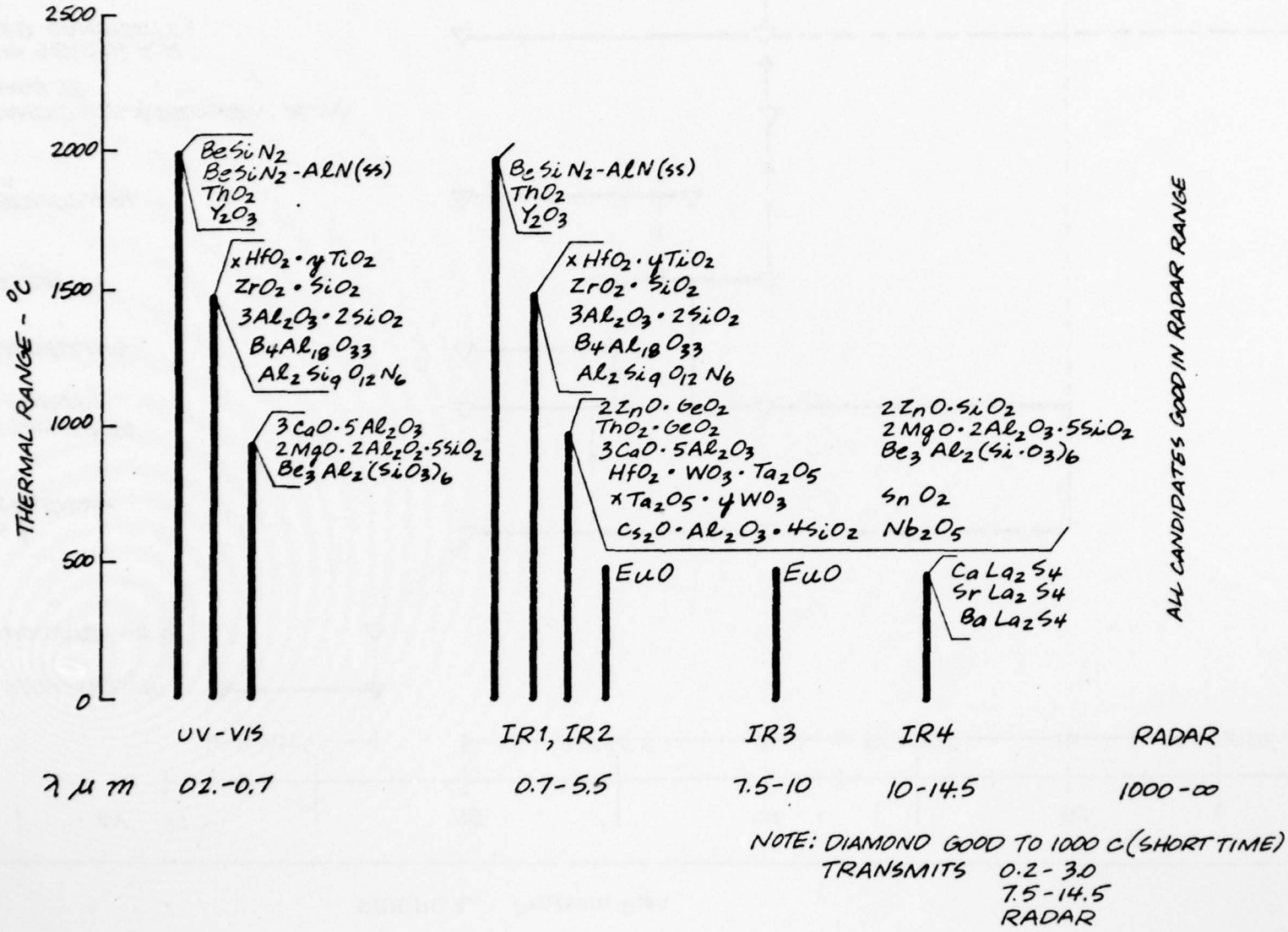

NOTE: DIAMOND GOOD TO 1000 C (SHORT TIME)
TRANSMITS 0.2-3.0
7.5-14.5
RADAR

FIGURE 4. Program Plan

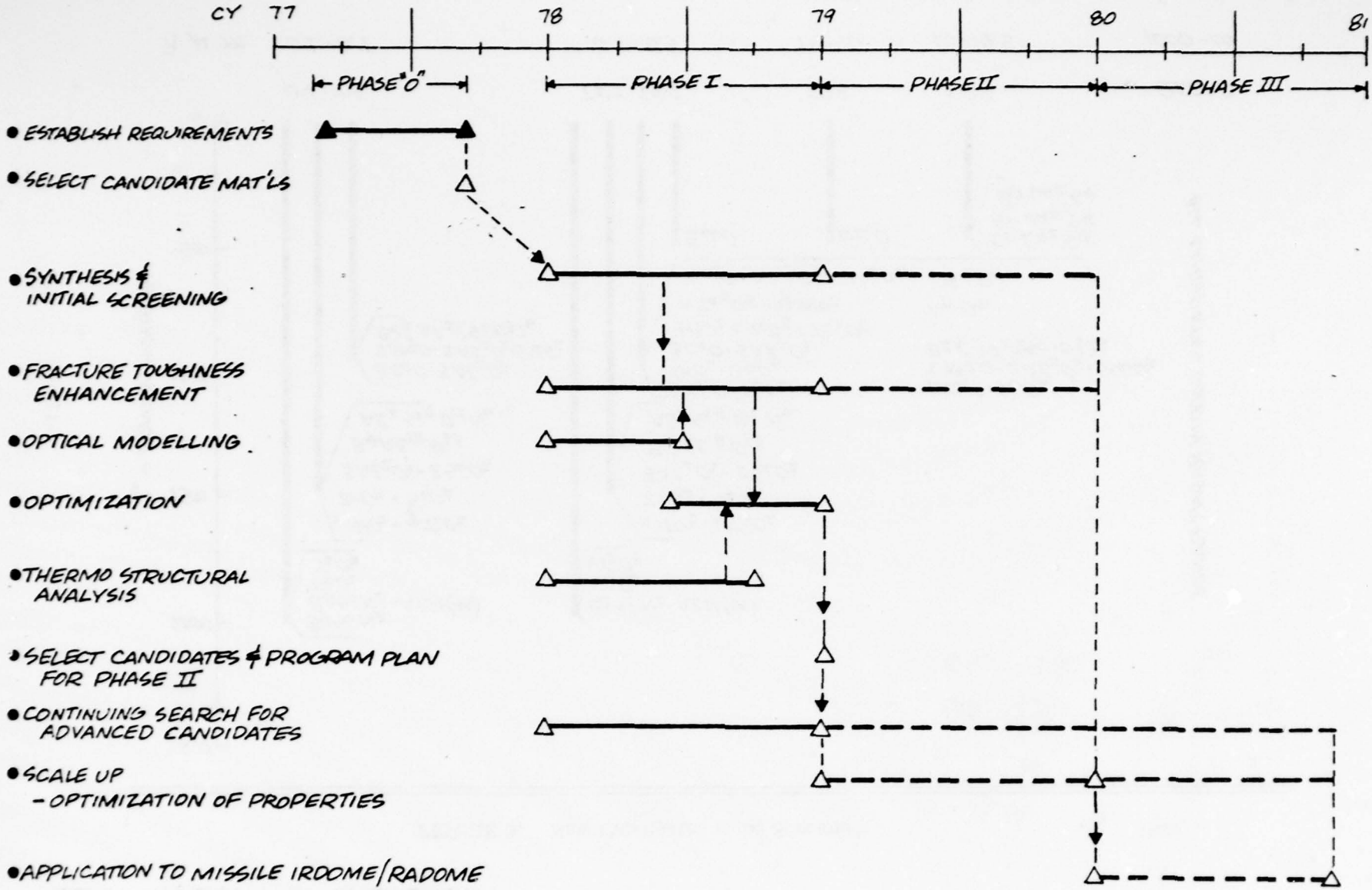

systematic development over a period of three years (three phases) leading to scale-up experiments and application studies for advanced missile irdomes and radomes. The recommended program plan is discussed in more detail in Section 5.

SECTION 2

REVIEW OF MATERIALS

SECTION 2

REVIEW OF MATERIALS

2.1 Wavenumbers and Temperatures

The major requirements for high performance materials for optical windows are optical transparency, low thermal expansion, high hardness and toughness, and high melting or decomposition temperatures. Not all of these requirements can be met simultaneously in any one material, hence some choices and compromises must be made. In order to systematize the selection process the spectral regions in which the atmosphere is transparent are first divided into several categories as follows:

Designation	Wavelength, microns	Wavenumber, cm^{-1}
UV	0.2 → 0.4	25,000 → 50,000
VIS	0.4 → 0.7	14,290 → 25,000
IR 1	0.7 → 3.0	3,330 → 14,290
IR 2	3 → 5.5	1,820 → 3,330
Atmos. Opaque	5.5 → 7.5	1,330 → 1,820
IR 3	7.5 → 10	1,000 → 1,330
IR 4	10 → 14.5	690 → 1,000
Atmos. Opaque	14.5 → 1,000	10 → 690
Radar	1000 → ∞	0 → 10

The second step is to divide the temperature range over which the material must operate into several ranges of 500 degree steps:

Temperature Range	Designation
$300^{o}K$ → $773^{o}K$	L = Low
$300^{o}K$ → $1273^{o}K$	M = Moderate
$300^{o}K$ → $1773^{o}K$	H = High
$300^{o}K$ → $2273^{o}K$	VH = Very High

In accord with these two divisions, a 4 x 7 matrix can be constructed with 28 different boxes as follows:

Thermal/ Optical	L	M	H	VH
UV				
VIS				
IR1				
IR2				
IR3				
IR4				
Radar				

Figure 5: Thermal/Optical Classification Format

The optical materials that are presently used can be entered in such a table as shown in Figure 5 if we know their optical pass-bands and their melting points or upper operating temperatures. Some of these current materials are single crystals of α -Al_2O_3, GaAs, Ge, MgO, Si, SiO_2; polycrystalline ceramic bodies of CdTe, MgF_2, pyroceram, ZnS, and ZnSe; and third, fused SiO_2 glass. A material has been designated as transparent if the optical absorption coefficient is less than 1 cm^{-1}. With respect to temperature divisions the upper operating temperature for α -Al_2O_3 is very high. The upper temperature for fused SiO_2 is limited to about 1500°K by softening, that of MgO by vaporization and reaction with H_2O to form $Mg(OH)_2$; the upper temperature limits on ZnS, and ZnSe are set by oxidation; the limits on CdTe, Ge, GaAs, and Si are set by the thermal generation of free carriers which make the windows opaque. The upper temperature limit for MgF_2 is unknown, but is clearly less than the melting point of 1536°K. Table 2-1 shows where the current materials fit in the classification format depicted by Figure 5.

TABLE 2-1 Operating Ranges of Current Window Materials Under Isothermal Conditions in Air.

OPTICAL RANGE	THERMAL RANGE			
	L	M	H	VH
UV	MgO α-Al_2O_3 α-SiO_2 f-SiO_2	MgO α-Al_2O_3 f-SiO_2	α-Al_2O_3	α-Al_2O_3
VIS	MgO α-Al_2O_3 α-SiO_2 f-SiO_2	MgO α-Al_2O_3 f-SiO_2	α-Al_2O_3	α-Al_2O_3
IR1	MgF_2 α-Al_2O_3 MgO α-SiO_2 ZnS ZnSe f-SiO_2	MgF_2 α-Al_2O_3 MgO f-SiO_2	α-Al_2O_3	α-Al_2O_3
IR2	MgF_2 MgO CdTe Si ZnS Ge GaAs ZnSe	MgF_2 MgO		
IR3	Ge ZnS GaAs CdTe ZnSe			
IR4	Ge CdTe ZnSe			
RADAR	Pyroc. α-Al_2O_3 MgF_2 α-SiO_2 ZnSe f-SiO_2 ZnS MgO Si CdTe Ge	Pyroc. α-Al_2O_3 MgF_2 α-SiO_2 MgO f-SiO_2	α-Al_2O_3 α-Si	α-Al_2O_3

The regions for which there are presently no fully acceptable materials are the IR2, IR3, and IR4 regions at temperatures of 773°K and above, even under isothermal conditions. In addition to the isothermal problem there is the problem of operation under conditions of high thermal stress where thermal shock is severe and many materials shatter. For example, the rather high thermal expansion coefficient of α -Al_2O_3 is mainly responsible for its low resistance to thermal stress. At 1000°K the directionally averaged thermal expansion coefficient of α -Al_2O_3 is $\bar{\beta} = 8.1 \times 10^{-6}$ / °K. Note that β is defined as $(dl / l_o dt)$, i.e., the slope of the length versus temperature curve at the particular temperature in question. The thermal shock resistance of fused SiO_2 is superior because $\bar{\beta} = 0.5 \times 10^{-6}$ / °K at 1000°K. Thus, for new window materials, oxides with thermal expansion coefficients approaching those of fused SiO_2 but with the upper temperature operating limits of α -Al_2O_3 and better infrared transparency than either are desired.

2.2 Chemical and Structural Guidelines to the Selection of Window Materials

Constraints on Window Materials

Figure 6 illustrates the optical properties that must be adjusted to produce a window. The short wavelength side is bounded by the optical absorption edge, a rough measure of the electronic band gap. The tail of the absorption edge is usually determined by extrinsic factors such as defects or impurities. The long wavelength boundary of the window is determined by the vibrational absorption edge. The position of the vibrational edge is determined by the highest frequency phonons but lies at somewhat higher frequency due to multiphonon processes. Overlapping absorption from multiphonon processes involving phonons from all parts of the Brillouin zone produces an exponential continuum of absorption of the form

$$\beta(\nu) = A e^{-\frac{\gamma \nu}{\nu_o}}$$

Where A and γ are fitting parameters.

The effective window bandpass is therefore determined by the application of the window material which dictates the permissable absorption coefficient at the

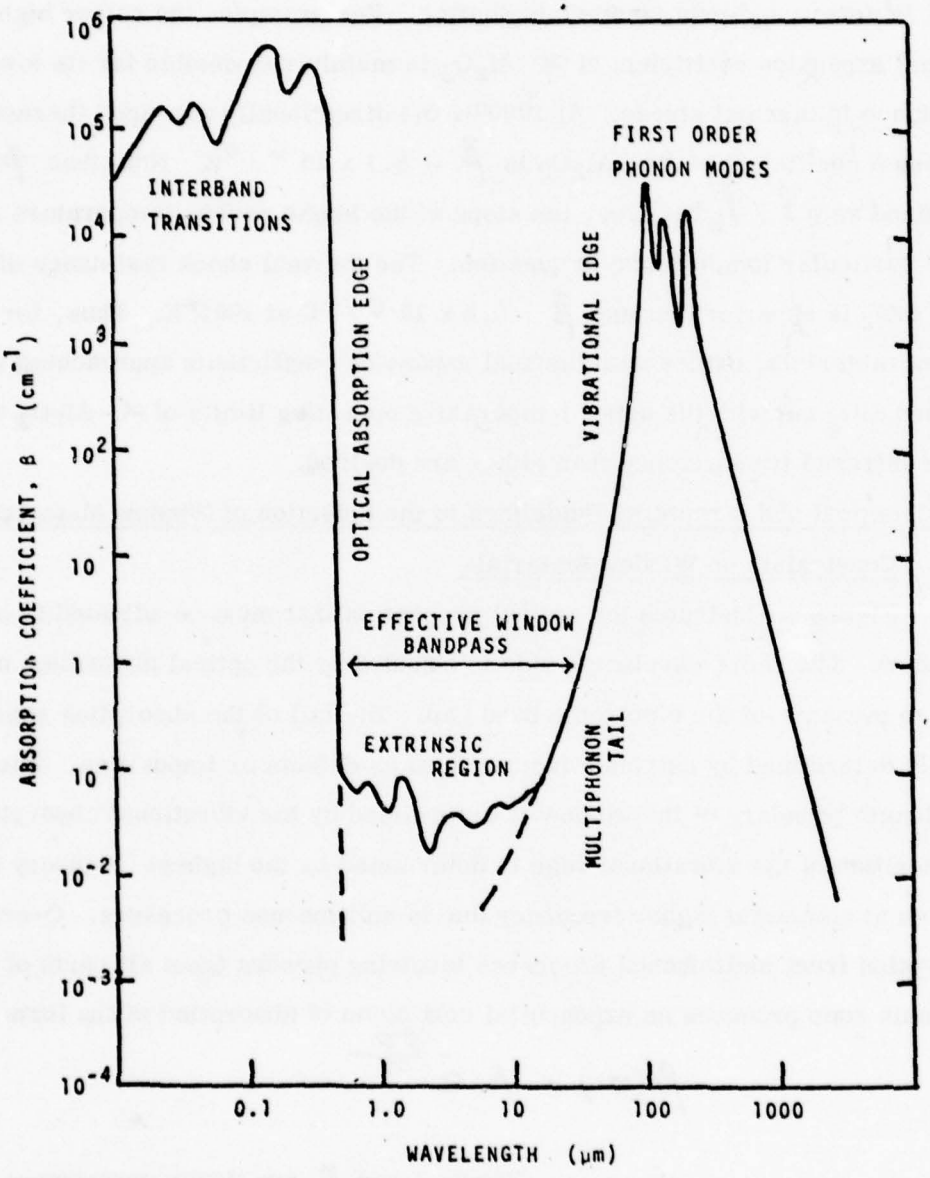

FIGURE 6. Window Optical Performance

wavelengths used by the device. The absorption in the window region is largely dictated by extrinsic factors (impurities, defects, free carriers, and electronic absorption within the atoms that make up the material).

The shape and position of the electronic band edge is critical for window materials that are expected to operate at high temperatures. At high temperatures the tail of the edge is extended to longer wavelengths decreasing the effective band-pass of the window. Likewise, high temperatures tend to ionize defect centers, increase free carrier concentrations and generally to raise the absorption background in the extrinsic region.

Screening for Candidate Window Materials

The first screening criterion is the position of the electronic absorption edge. Materials with a large band gap are insulators and these are constructed from anions found mainly in the upper right portion of the periodic table. These may be summarized:

--- The halides, especially those of the alkali metals have some of the band gaps and some of the best optical properties for window materials, very low absorption coefficients in the visable and infrared and moderate to low refractive indices. Mechanical and thermal properties, and resistance to chemical attack, of course are poor.

--- Oxides including complex oxides such as the silicates, have intermediate band gaps, 3 to 6 eV being common. Metallic oxides are rare, although a few oxides of the transition metals are metallic and many are semiconductors.

--- Chalcogenides (S, Se, and Te) have lower band gaps than oxides. Sulfides exist with band gaps as high as 3 eV but higher values are not common. Chalcogenides with semiconductor or metallic properties are common.

--- Nitrides are separated into a relatively limited family of the nitrides of the light elements that are insulators and a large family of nitrides of the heavier elements, especially transition elements that are metals. However, from the restricted group of light element nitrides are compounds with exceptionally favorable thermal and mechanical properties.

--- Carbides are nearly all metallic with a few obvious and outstanding exceptions such as diamond and SiC.

--- Borides are nearly all metallic or semiconductors.

From this very quick screening based only on the electronic behavior of the anions, and with the understanding that the halides have already been intensively investigated, it is concluded that a choice of entire families of compounds for investigation will occur only among the oxide and chalcogenide materials. A more limited number of nitride, phosphide, and carbide compounds exist.

Screening of cations can be done in general terms with respect to their contribution to absorption in the extrinsic region. The arrangement is by ions rather than by elements since it is the electronic structure of the individual ions that determines many of the absorption characteristics. Cations can be classified into five categories on the basis of their electronic structure (Table 2-2). The noble gas core ions have filled electronic shells and do not give rise to absorption features within the extrinsic regions. However, alkali metal compounds tend to be subject to chemical attack and are seldom very refractory. The rare earth ions La^{3+}, Gd^{3+}, Y^{3+} and Lu^{3+} are those that do not have mixed valence states which might give rise to absorption because of charge transfer, and do not have partly-filled f-shells with accompanying sharp band absorption in the extrinsic region due to f-f transitions. The filled d-shell cations generally form insulating oxides and sulfides. Mixing of the d and p orbitals is responsible for a higher degree of covalent bonding in compounds of these ions.

These sets of criteria define, in very general terms, the range of chemical compositions in which a search for new materials with useful optical properties might be productive.

Absorption Coefficients for Single Crystal Material

Appendix I contains absorption coefficient data as a function of photon wavenumber for a number of single crystal materials. This data has been assembled from a wide review of the literature and is reported in General Electric Company Technical Information Series, TIS No. 78-SDR-2199, May 15, 1978, by Dr. G. A. Slack.

TABLE 2-2: Electronic Structure of Cations

I. Noble Gas Core Ions	
Li^+ Na^+ K^+	Tend to form hygroscopic compounds
Be^{++} Mg^{++} Ca^{++} Sr^{++} Ba^{++}	Useful
Al^{3+} Si^{4+}	Useful, may be hygroscopic chalcogenides
II. Rare Earth Ions	
La^{3+}.....Lu^{3+}, Y^{3+}	La^{3+}, Gd^{3+}, Y^{3+} Lu^{3+} do not have absorption in the visible - near IR due to partly-filled f-shells.
III. Filled d-Shell Ions	
Cu^+, Ag^+, Zn^{2+}, Cd^{2+}	Possibly useful (?)
Ga^{3+}, In^{3+} Sn^{4+} Ge^{4+}	
IV. Transition Metal Ions	
Fe^{2+} Other iron-group	Partly filled d-orbitals (or bands) leads to semiconducting or metallic behavior. Useful windows unlikely.
4d and 5d ions	
V. Rydberg Ions	
Sn^{2+} As^{3+} Sb^{3+}	Complex bonding due to lone pair electrons leads to soft, low-melting materials although optical properties may be good.
Pb^{2+} Bi^{3+}	

Structural Controls of the Vibrational Absorption Edge

The position of vibrational absorption bands is critical for infrared window materials. Good infrared windows require a long wavelength vibrational cut-off . Low frequency modes are associated with long bonds, and high atomic masses. Such materials are unlikely to be refractory, tough, hard, and have good thermomechanical

properties. Below are considered some of the parameters that influence the frequencies of the fundamental phonon modes and thus the position of the vibrational edge and which can be used to guide the trade-offs in these materials.

Vibrational frequencies depend directly on the force constants of the bonds and inversely on the atomic masses. Heavy atoms vibrate with lower frequencies than light atoms and this can be used as a guideline. As a rough approximation the highest frequency modes are mainly of bond-stretching character. Regarding the cation-anion pair rather crudely as diatomic molecules, the dependence of the frequency on mass goes as $\nu = A\mu^{-1/2}$ where μ, the reduced mass of the cation-anion pair is $1/\mu = 1/m_c + 1/m_a$. The effect of varying cation mass on the vibrational frequency can be described by a scaling factor (Figure 7) which has been normalized to unity when the cation mass is equal to the mass of oxygen. For any given anion mass, Figure 7 shows that increasing the cation mass decreases the band frequencies up to about mass number 75. The shift in vibrational frequency obtained by substituting germanium for silicon due to mass effects alone is seen to be about 10%. Once the mass number is above 75, the frequency shift obtained by substituting still heavier ions rapidly becomes negligible. Substitution of hafnium (m_c = 178) for zirconium (m_c = 91) in an oxide should produce a frequency shift from the mass effect alone of less than 2%. Figure 7 does show that the frequency shift obtained by substituting a heavier anion is large. These curves allow the conclusion that it would be extremely difficult to find an oxide material suitable for far infrared windows whereas there may be a considerable number of chalcogenide materials that would satisfy at least the optical property requirements.

The high frequency vibrational modes vary directly as (force constant)$^{1/2}$. Bond force constants decrease rapidly with interatomic distances and also decrease with increasing cation coordination number. In purely ionic bonding this can be seen to follow directly from the Coulomb force in which the force constant would vary with the inverse cube of the interatomic distance. The coordination number effect arises because the effective charge must be shared among more ligands in structures with higher coordination numbers. In real systems where the bonding is

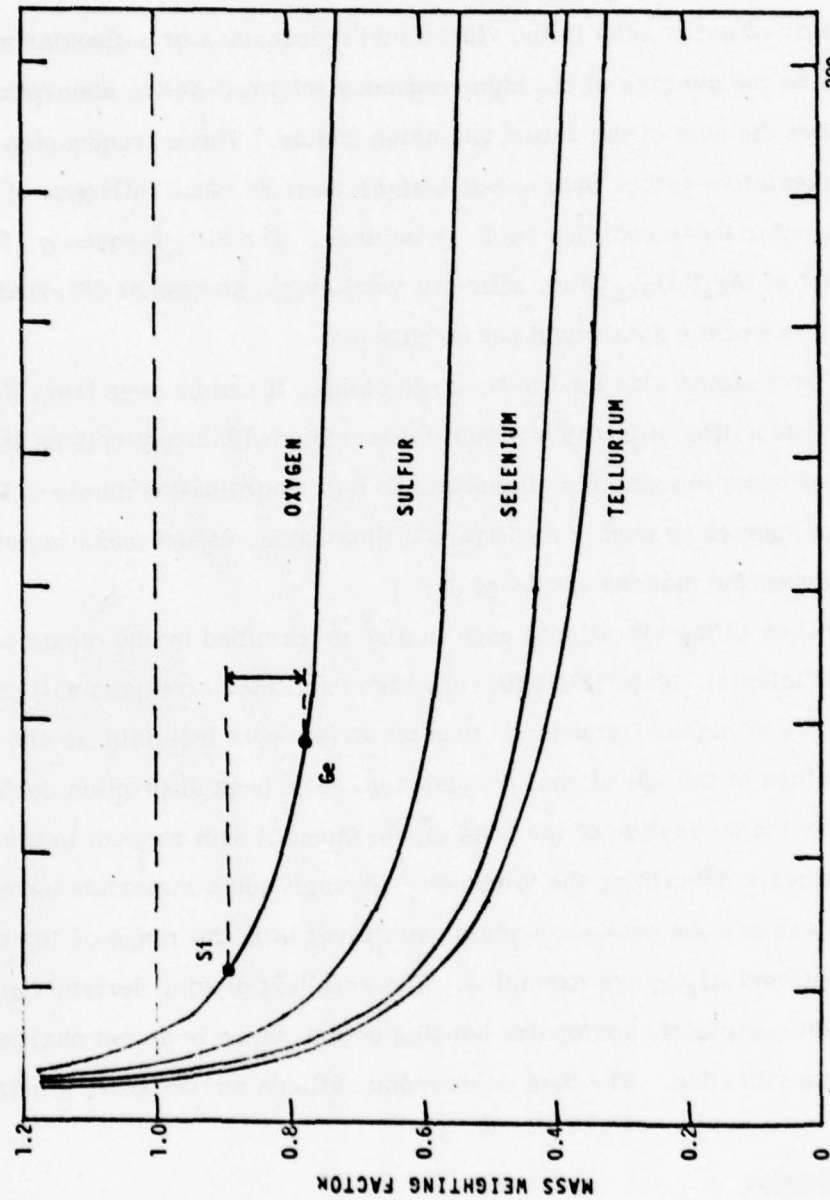

FIGURE 7. Mass Weighting Factors

of mixed covalent/ionic character, the force constant still decreases with increasing interatomic distance. These effects are illustrated in Figure 8 where is plotted the highest frequency mode of a number of simple crystal structures as a function of the cation-anion distance. With a few exceptions such as ZnO, the materials tend to fall into well-defined coordination groups.

A similar effect is seen in the vibrational frequencies of molecular anions (Figure 9). Here the average of the high frequency infrared-active absorption bands is plotted against the sum of the cation and anion radius. These frequencies must be taken as representative rather than specific since there is some influence of the other ions that enter these complex oxide structures. The SiO_4 frequency, for example, is that of Mg_2SiO_4. Other silicates would yield somewhat different values. However, the trend of the data would not be changed.

Since heavy atoms also tend to be large atoms, it can be seen from Figures 8 and 9 that the association of low vibrational frequencies with heavy cations is likely more a result of large interatomic distances and high coordination numbers than of the large cation masses as such. As Figure 7 illustrates, cation mass is not a strong control when the masses are large.

The position of the vibrational edge is also determined by the maximum absorption coefficients. Materials with very high oscillator strengths will have virbrational edges at higher frequencies than materials with less intense absorption for the same values of the vibrational frequencies. The peak absorption coefficient is determined by the derivative of the bond dipole moment with respect to the displacement coordinate describing the vibration. Strongly ionic materials have large dipolar derivatives and the peak absorption coefficient is in the range of 10^5 cm^{-1}. The data for MgO and Al_2O_3 are examples. The smallest dipolar derivatives occur in materials with completely homopolar bonding so that there is no net charge displacement during vibration. The data on diamond, silicon and β-boron provide examples.

2.3 Optical Behavior

Specular vs. Diffuse Transmittance

With regard to optical behavior, there is no question regarding the desirability for an optically isotropic material. Optical isotropy occurs only in cubic crystals

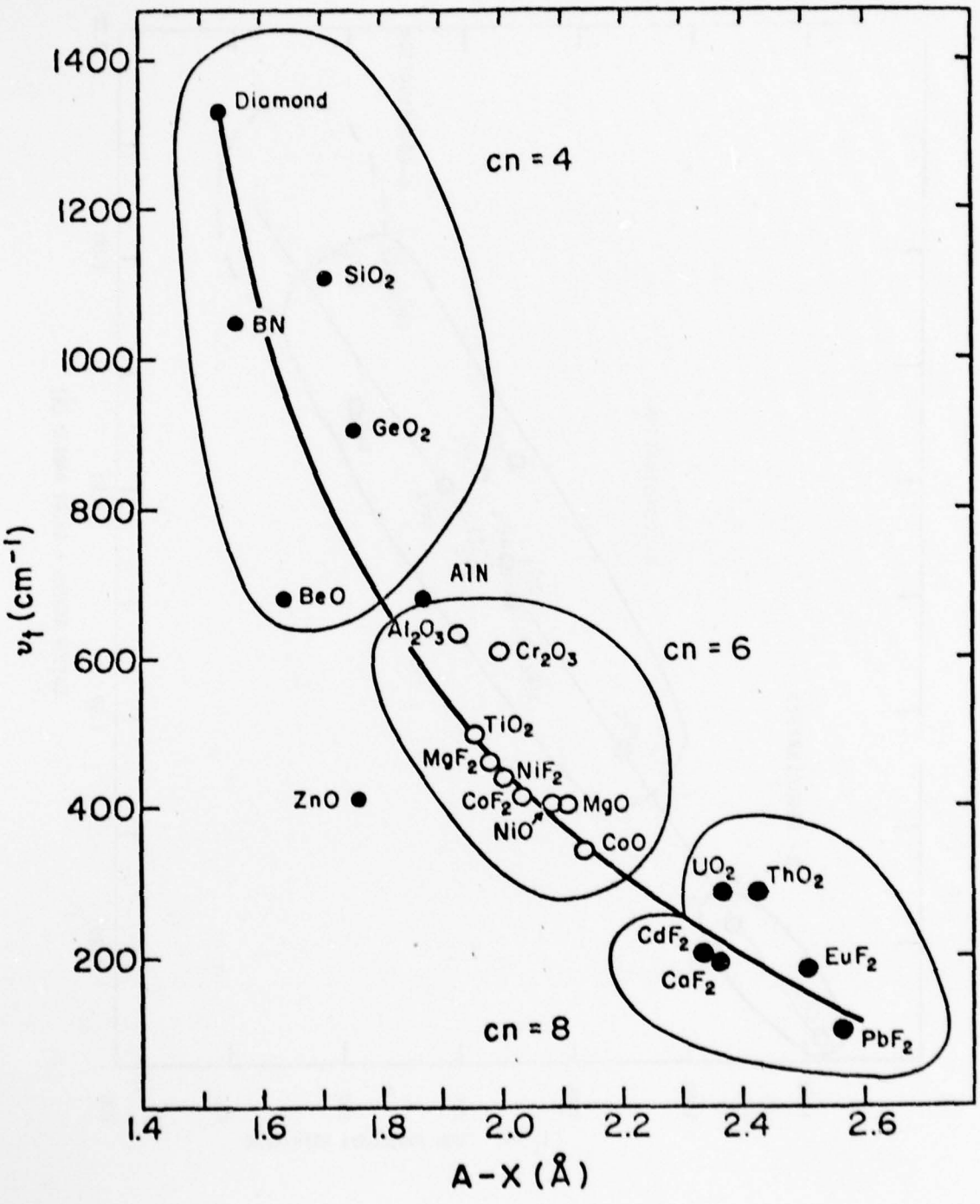

FIGURE 8. Highest Frequency Mode vs. Cation-Anion Distance for Crystals

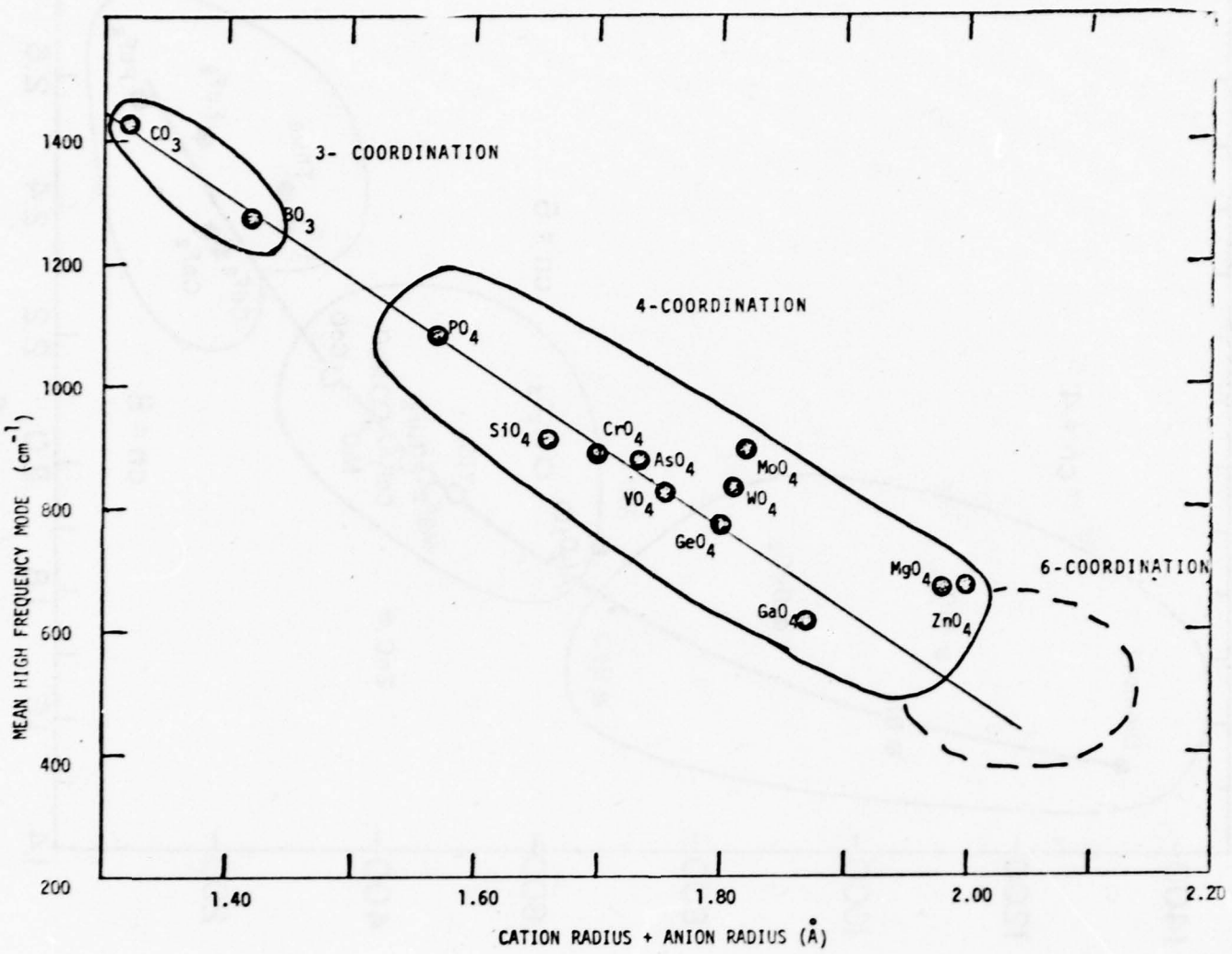

FIGURE 9. Vibration Frequency Molecular Anions

and "amorphous" materials (glasses, liquids and gases).

The velocity of light in non-cubic crystals varies with the direction of propagation. An allied property of anisotropic crystals is that of double refraction or birefringence. In uniaxial crystals (tetragonal, trigonal, and hexagonal) there is only one direction in which double refraction does not occur. This is called the optical axis. In biaxial crystals (orthorhombic, monoclinic and triclinic) there are two directions where double refraction does not occur. Within a polycrystalline aggregate, the phenomena of double refraction or birefringence (which represents the extremes in indices of refraction within a crystal, i.e., $n_E - n_O$ in uniaxial crystals or $n_Z - n_X$ in biaxial crystals) is an intrinsic property the degree of which must be assessed in terms of its contribution to scattering in a polycrystalline aggregate.

Harrison[1] has derived the following equation relating birefringence, grain morphology and scattering angle:

$$\theta \cong \frac{\Delta n}{n}\sqrt{N}$$

where Θ_s is the angular spread in radians of a pencil light beam after passing through a polycrystalline plate

Δn is the birefringence

n is the average index of refraction

N is the number of randomly oriented grain boundaries crossed by the light beam

The transparency or ability to see through a material is further related to geometrical factors as given by the following equation, also developed by Harrison[1]:

$$d = L\,\Theta_s$$

where d is the spacing between lines in a grid which can be resolved

L is the distance between sample and grid

Obviously, isotropic materials with zero birefringence are predicted to be specularly transparent even with randomly oriented grains. On the other hand, for anisotropic crystal aggregates having a randomly oriented grain structures, the transparency is decreased with increasing birefringence, decreasing grain size and with increasing window thickness.

It should be noted, however, that the use of single crystal growth techniques, or process methods for controlling crystal orientation eliminate or greatly reduce scattering problems in anisotropic crystals. A qualitative guide for ranking birefringence [2] is given below:

Birefringence Scale

Description	Assumed Value
Very weak	0.002
Low or weak	0.006
Moderate	0.014
Rather strong	0.023
Strong	0.032
Very strong	0.045
Extreme	> 0.050

In addition to intrinsic scattering effects, other extrinsic factors known to contribute to scattering (even in isotropic materials) include:

(i) residual strain } isotropic crystals in a state of strain acquire (to some extent) optical properties of anisotropic crystals

(ii) porosity
(iii) microcracks
(iv) grain boundary separations
(v) second phases of differing index of refraction
} index of refraction mismatching at interfaces results in radomwalk Fresnel reflection effects

These latter defects (i.e., ii-v) must be eliminated or controlled to the extent that their size is small compared to the wavelength of radiation being transmitted.

Transmittance Band-Pass

As discussed in Section 2.2, the crystal chemistry factors which define the useful window bandpass have been extensively reviewed. It has been pointed out that the shape and position of the optical and vibrational boundaries (Figure 6) are temperature dependent generally causing a shortening of the window's bandpass as temperature increases. High temperatures also tend to ionize defect centers, increase free carrier concentrations and generally raise the absorption background in the extrinsic region. A secondary factor which will be important at higher use temperatures is the window self-emission problem. The infrared transmittance cut-off ideally should be located in the far infrared (approaching 10μm for oxides) to minimize the effect of window emittance.

A brief perusal of transmittance cut-off data in Tables 2-3, 2-4, and 2-5 for single and mixed oxides indicates that transmittance windows for oxides generally extend from 4.0 microns to 9.5 microns. System requirements for infrared homing missiles appear to be requiring at least 5.0 micron cut-off. It is unfortunate that such a requirement has evolved since, from a materials viewpoint, silicate-based materials, which have cut-offs in the 4 to 5 um range, present many opportunities for low thermal expansion and hardness levels superior to state-of-the-art materials (Table 2-3). As will be discussed in a subsequent section, possibilities exist in the isolated tetrahedra-type silicates for nearly meeting the 5 micron cut-off requirement. Thus, it is desirable to further investigate the potential for achieving slight shifts (0.2-0.5 um) in the infrared cut-off (i.e., reducing the absorption coefficient at 5.0 microns) through partial substitution of heavier cations. Of course, such substitutions must not significantly degrade the primary favorable property of selected silicates, viz. their low intrinsic thermal expansion.

2.4 Thermo-Structural Factors

Thermal Stress Resistance

With regard to resistance to thermal stress, there is no question regarding the desirability for low thermal expansion. The question remains, "how low?."

TABLE 2-3: State-of-the-Art

Material	MgF_2 (Irtran 1)	SiO_2 (Corning 7940)	$CaO-Al_2O_3-SiO_2$ (Corning 9753)
Optical Behavior			
o Crystal Structure	Tetragonal	Amorphous	Amorphous
o Index of Refraction (n_o, n_e or n_z, n_x)	1.389, 1.377	1.46	1.60
o Birefringence, Δn	0.011	0	0
o Infrared Transmittance			
- cut-off (μm)	8.0	4.5	4.8
- absorption coeff. @5μm (cm^{-1})	0.25		22.4
Thermal Stress Resistance			
o Thermal Expan. Coeff. ($^1/^oC$)	11×10^{-6}	0.56×10^{-6}	7.2×10^{-6}
o Young's Modulus (psi)	16.6×10^6	10.5×10^6	14.3×10^6
Erosion Resistance			
o Hardness (Moh)	5 - 6	-	-
(Knoop)	415 - 576	560	658 (100 g)
Chemical			
o Density (g/cc)	3.18	2.20	2.80
o Melting Pt. (^oC)	1312	1242 (softening pt.)	981 (softening pt.)

TABLE 2-4: Advanced Materials Candidates

Material	Al_2O_3 (Sapphire)	$MgO.Al_2O_3$ (Spinel)	MgO (Irtran 5)	β -SiC (CVD-GE)	α -Si_3N_4 (CVD-GE)	$CaO-Al_2O_3-GeO_2$ (Corning 9754)
Optical Behavior						
o Crystal Structure	Hexagonal	Cubic	Cubic	Cubic	Hexagonal	Amorphous
o Index of Refraction (n_o, n_e or n_z, n_x)	1.769, 1.757	1.716	1.75	2.48	2.00	1.66
o Birefringence, Δn	0.012	0	0	0	-	0
o Infrared Transmittance						
- cut-off μm	6.5	6.5	9.5	5.5	4.5	5.7
- absorption coeff. @5 μm (cm^{-1})	0.05	0.50	0.16	6.0	74.4	1.5
Thermal Stress Resistance						
o Thermal Expan. Coeff. ($^1/^oC$)	7.7×10^{-6}	7.6×10^{-6}	12.0×10^{-6}	4.2×10^{-6}	2.5×10^{-6}	6.2×10^{-6}
o Young's Modulus (psi)	56.0×10^6	34.5×10^6	48.2×10^6	60×10^6	45.3×10^6	12.2×10^6
Erosion Resistance						
o Hardness (Moh)	9.0	8.0	6.5	9.0	9.0	-
(Knoop)	1600-2200	1230-1500	640	2000 (500g) est.	2400 (500g)	560 (100g)
Chemical						
o Density (g/cc)	3.98	3.55	3.58	3.21	3.18	3.58
o Melting Pt. (^oC)	2040	2135	2853	3400 (dissoc.)	-	735 (Anneal pt.)

TABLE 2-5: DARPA Optical Ceramic Mixed Oxides Whi

MATERIAL	$2ZnO.GeO_2$	$ThO_2.GeO_2$	$3CaO.5Al_2O_3$	Low Aggregate Expansion F (and other possible $HfO_2.WO_3.Ta_2O_5$	"x" Ta_2O
	Category I				Cat
Phase 1 candidates	X	X	X	X	X
Optical Behavior					
o Crystal Structure	Hexagonal	Tetragonal	Orthorhombic	Tetragonal	
o Index of Refraction (n_o, n_e or n_z;n_x)	1.769, 1.802		1.635		
o Birefringence, Δn	0.033		0.035		
o Infrared Transmittance					
- cut-off μm	5.5	6.3	6.5 (est.)	5.0	5.
- absorption coeff. @5 μm (cm^{-1})					
Thermal Stress Resistance					
o Thermal Expan. Coeff. ($^1/^oC$)	$2.3x10^{-6}$	$3.2x10^{-6}$	$2-4x10^{-6}$	0	neg
o Young's Modulus (psi)					
Erosion Resistance					
o Hardness (Moh) (Knoop)					
Chemical					
o Density (g/cc)	4.82				3.
o Melting Pt. (^oC)	1490		1720		118

LE 2-5: DARPA Optical Ceramic Mixed Oxides Which are Potential Candidates

GeO_2	$3CaO.5Al_2O_3$	Low Aggregate Expansion Result of High Crystal Expansion Anisotropy (and other possible crystallographic phenomena) $HfO_2.WO_3.Ta_2O_5$	"x" Ta_2O_5. "y" WO_3	"x" HtO_2. "y" TiO_2	"x" HfO_2. "y" Nb_2O_5
I		Category II			
X	X	X	X	X	X
gonal	Orthorhombic	Tetragonal		Orthorhombic	
	1.635				
	0.035				
3	6.5 (est.)	5.0	5.0	5.0	5.0
10^{-6}	$2-4x10^{-6}$	0	neg 0	0	neg 0
			3.16		
	1720		1185		

TABLE 2-5: DARPA Optical Ceramic Mixed Oxides

MATERIAL	Silicates Requiring Tuning to Shift Cut-off 0.2 - 0.5 μm to 5 μm						
	$CaO.CuO.4SiO_2$	$SrO.CuO.4SiO_2$	(Pollucite) $Cs_2O.Al_2O_3.4SiO_2$	(Eucryptite) $Li_2O.Al_2O_3.SiO_2$	(Zircon) $(Zr,Hf)O_2.SiO_2$	(Willimite) $2ZnO.SiO_2$	(To $Al_2(F,$
	Category III				Category III		
			X		X	X	
Optical Behavior							
o Crystal Structure	(Layers of Tetrahedra Tetragonal)	(Layers of Tetrahedra Tetragonal)	(Frameworks of Tetrahedra Cubic)	(Frameworks of Tetrahedra Hexagonal (β)	(Isolated Tetrahedra) Tetragonal (Zr)	(Isolated Tetrahedra Hexagonal)	(Isolat hedra ho
o Index of Refraction (n_o, n_e or n_z, n_x)	1.635, 1.605		1.53	1.573, 1.583	1.92, 1.96 (Zr)	1.695, 1.715	1. 1.
o Birefringence, Δn	0.030		0	0.010	0.040	0.020	0.
o Infrared Transmittance - cut-off (μm) - absorption coeff. @ 5μm (cm^{-1})	4.8-5.1 (est.)	4.8-5.1 (est.)	4.5 (est.)	4.3 (est.)	4.8-5.0 (Zr)	5.0	5
Thermal Stress Resistance							
o Thermal Expan. Coeff. ($^1/^oC$)	3.3×10^{-6}	2.8×10^{-6}	2.0×10^{-6}	9.0×10^{-6}	$3.8-4.0 \times 10^{-6}$	3.0×10^{-6}	6.67x1
o Young's Modulus (psi)					3.0×10^6		
Erosion Resistance							
o Hardness (Moh) (Knoop)					7.5(Zr)	5.5	8.
Chemical							
o Density (g/cc)	3.04		2.94		4.66(Zr)	4.24	3.5
o Melting Pt. (^oC)							

ked Oxides Which are Potential Candidates (continued)

te) O_2	(Topaz) $Al_2(F,OH)_2SiO_4$	(Mullite) $3Al_2O.2SiO_2$	(Spodumene) $Li_2O.Al_2O_3.4SiO_2$	(Cordierite) $2MgO.2Al_2O_3.5SiO_2$	Silicates Requiring Tuning to Shift Cut-Off 1 um to 5 um $3BeO.Al_2O_3.6SiO_2$	Non-silicates Requiring Tuning to Shift Cut-Off 1 um to 5 um $2ZrO_2.P_2O_5$
	X			X		
dra al)	(Isolated Tetrahedra Orthorhombic)	Single Chain of Tetrahedra Orthorhombic	Single Chain of Tetrahedra Tetragonal (β)	(Rings of Tetrahedra) Orthorhombic)	(Rings of Tetrahedra) Hexagonal	Cubic
	1.618, 1.607	1.654, 1.642	1.516, 1.522	1.52, 1.53	1.568, 1.564	1.657
	0.011	0.012	0.006	0.010	0.004	0
	5.0	4.8	4.5	5.0	4.0	4.0
6	6.67×10^{-6} (0-400°)	5.6×10^{-6} 32×10^{6}	1.0×10^{-6}	2.0×10^{-6}	0.8×10^{-6}	1.0×10^{-6}
	8.0	1750 (100g)	6.7	7 - 7.5	7.5 - 8.0	
	3.57	3.16	3-3.2	2.60	2.7 - 2.9	
		1880	1380	1471	1420	1700 (Dissoc.)

An initial criterion has been established for selecting Phase 1 candidate systems from Table 2-5, viz., the thermal expansion coefficient should be approximately one half that of candidate oxides currently under advanced development by DoD (i.e., Al_2O_3: $\sim 7.7 \times 10^{-6}/^oC$; $MgO \cdot Al_2O_3$: $\sim 7.6 \times 10^{-6}/^oC$.

With regard to Young's moduli and its intimate relationship to strength potential and hardness (as well as the development of thermal stress, i.e., $E \propto \Delta T$), no criterion has been established at this time. Once, the appropriate system or systems are identified, based upon meeting minimum optical, thermal expansion, and hardness criteria, many opportunities exist for optimization of mechanical properties.

Erosion Resistance

Correlations by Evans [3] have established the importance of hardness and fracture toughness in determining a brittle materials resistance to erosion. Little data exists regarding the intrinsic hardness of oxides since the motivation for achieving theoretical x-ray density has previously not existed. Fortunately in some instances candidates were found which were naturally occurring minerals where some data on hardness existed (defined in terms of the Moh scale). It should be noted that hardness of a material may be determined by its ability to abrade or indent one another. Two scales of hardness are used: the Moh scale, which rates materials according to their ability to scratch one another, and the Knoop scale (or Vicker's), which is based on the extent to which a diamond point is pressed into a material with a known force. Listed below is a table of minerals illustrating a correlation between the Moh and Knoop scales:

Material	Moh	Knoop (kg/mm^2)
Gypsum	2	32
Calcite	3	135
Fluorite	4	163
Apatite	5	430
Orthoclase	6	560
Quartz	7	820
Topaz	8	1340
Corundum	9	1800
Diamond	10	7000

Since there is a captive-flight erosion problem with MgF_2 whose hardness is 5-6 Mho, or 415-576 kg/mm^2, candidates must exhibit at least improvements in hardness over this state-of-the-art material. Also, if one establishes criteria based upon advanced materials under development within DoD such as sapphire (Al_2O_3) and spinel ($MgO \cdot Al_2O_3$) then the following data must be matched or exceeded

Al_2O_3:	9.0 Mho,	1600-200 kg/mm^2
$MgO \cdot Al_2O_3$:	8.0 Mho,	1230-1500 kg/mm^2

by DARPA candidates. For many mixed-oxide candidates, this data is not available and must be generated early in Phase 1 to insure achievement of meaningful goals. It should be noted that fracture toughness is also of importance in the final judgement of impact resistance as defined in the Evans correlations for brittle materials. The issue of fracture toughness and erosion resistance are discussed at greater length in Section 4.

Chemical Stability

Candidates obviously must be able to withstand ground and flight environments. For the infrared homing missile, operational environments up to $1000^{o}C$ in an oxidizing environment are anticipated for relatively short times. Hygroscopic tendencies must be avoided in selecting candidates. Some insights into selection of materials in this regard have already been discussed in terms of screening criteria based upon the electronic structure of cations (see Section 2, 2.2). Solid-state chemical stability criteria will be used extensively during Phase 1 to guide against unwise choices in this regard.

SECTION 3

MATERIALS SELECTIONS

SECTION 3

MATERIALS SELECTIONS

3.1 Low Thermal Expansion Oxides

Some idea of which oxides might be suitable can be obtained from the calculations of Minko et al[1]. They show that the Si-O bond is the one with the lowest thermal expansion coefficient of all. The next in line are Ti-O, V-O, and Nb-O bonds The highest expansion bonds are those of Li-O and Ba-O. We note that the Si-O bond is a directed, covalent bond while those of Li-O and Ba-O are ionic. One requires covalent bonds to obtain low thermal expansion coefficients. The thermal expansion of the framework silicates[2] indicates what possibilities exist with respect to low expansion coefficients.

Silicates are structures whose basic building block is the SiO_4 tetrahedron. The silica tetrahedra can be polymerized by sharing corners with adjacent tetrahedra. Structures vary from the orthosilicates (O/Si = 4) where no corners are shared through structures made of $(SiO_4)_n$ infinite chains with two out of four corners shared (O/Si = 3) and sheet structures (O/Si = 2.5) to three-dimensional frameworks in which all corners are shared and the SiO_4 tetrahedra are completely cross-linked (O/Si = 2). Of the structures considered in this report, mullite, zircon, olivine, and willemite are orthosilicates, cordierite is a ring silicate (of sorts) and pollucite is a three-dimensional framework silicate.

The infrared cut-off of anhydrous silicate structures is determined by the stretching modes of the SiO_4 tetrahedra. These frequencies are lowest, 850 to 905 cm^{-1} in the orthosilicates. They increase with the degree of silicate polymerization reaching values of 1150 to 1200 cm^{-1} in the framework silicates (of which quartz is an important example). Substitution of aluminum to form the aluminosilicate structures generally introduces new infrared bands at lower frequencies but has only a perturbing effect on the Si-O absorption bands.

In fully-expanded framework silicates, the thermal expansion coefficient approaches that of fused quartz. The total expansion is a combination of rotation of SiO_4 tetrahedra and Si-O bond expansion. When the temperature is sufficiently high or the framework is sufficiently expanded the tetrahedra no longer rotate and one obtains expansion coefficients characteristic of the Si-O bonds. In beta-cristobalite[3] at high temperatures above 700°K and up to the melting point the linear expansion coefficient is $\beta = +1.75 \times 10^{-6}/^{\circ}C$. For quartz[2] the high temperature expansion is even negative. Thus one seeks to find framework silicates that are fully-expanded, stable to high temperatures, and not so open in structure that they absorb moisture and gases as do the zeolites. The three best candidates for these specifications are:

Cordierite:	$Al_3Mg_2Si_5AlO_{18}$
Beryl:	$Be_3Al_2Si_6O_{18}$
Scandium beryl:	$Be_3Sc_2Si_6O_{18}$

The directional thermal expansion of beryl has been measured[4-9] as well as the average thermal expansion of ceramic beryl[10]. The average expansion of cordierite ceramics has also been measured[11-14]. No expansion data on scandium beryl[15] are known. There is some variation in the expansion of beryl depending on its composition[6,8]; representative values are shown in Figures 10 and 11. Figure 11 shows how these two materials compare with betacristobalite. Beryl and cordierite have essentially the same crystal structure[16] and can be classed as either ring or framework silicates. Note that, although the thermal expansion coefficient of beryl is anisotropic because the crystal structure is anisotropic, the magnitude of the anistropy, in Figure 10, i.e., $\beta_{\perp} - \beta_{\parallel}$, is small. One has approximately $\beta_{\perp} - \beta_{\parallel} = 2 \times 10^{-6}/^{\circ}K$. A small anisotropy in β is needed if a good ceramic body is to be made from the compound. The upper limit on a tolerable anistropy depends on the ceramic grain size[17], but a maximum value of $\Delta\beta = 3 \times 10^{-6}/^{\circ}K$ seems desirable. It is important to notice that this anisotropy limit rules out many other materials which have low average β values but large anisotropies[18]. Such materials

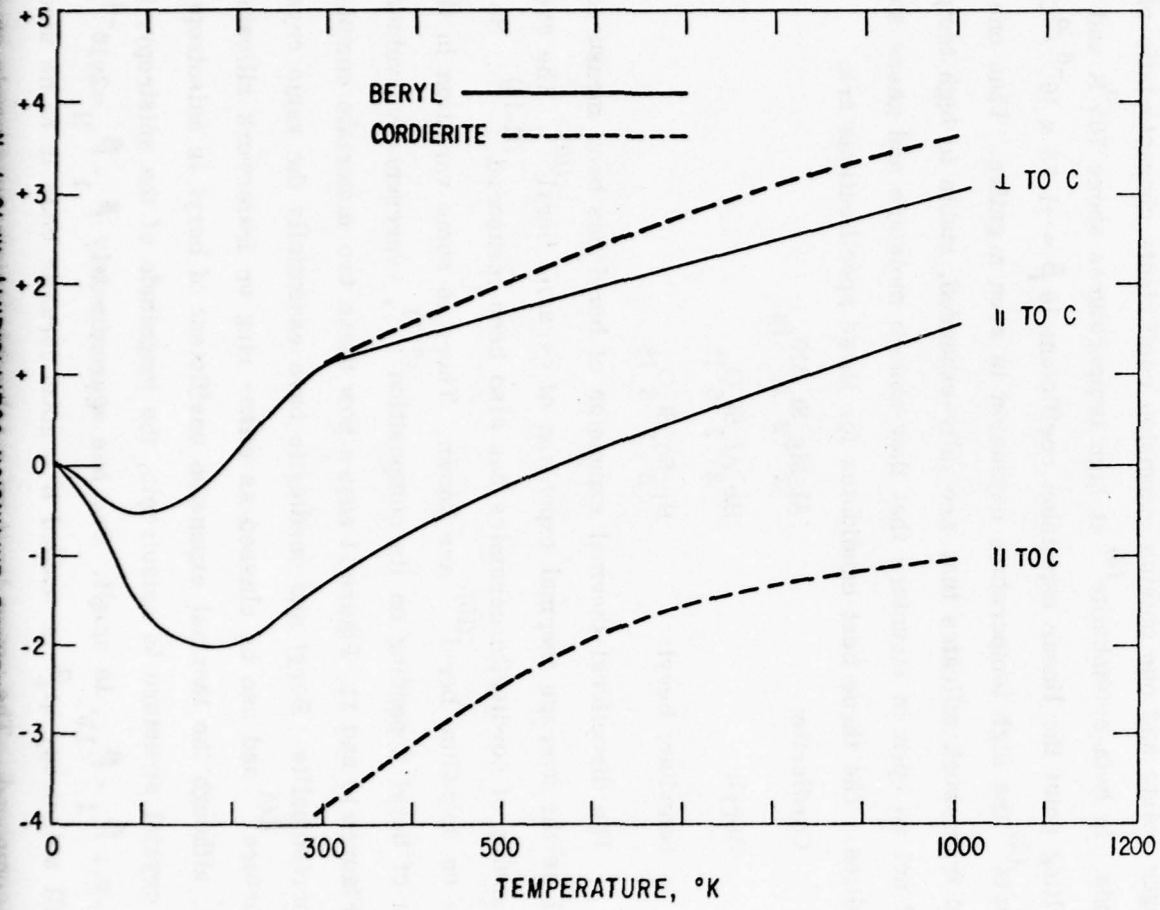

FIGURE 10. Thermal Expansion Coefficients of Beryl and Cordierite

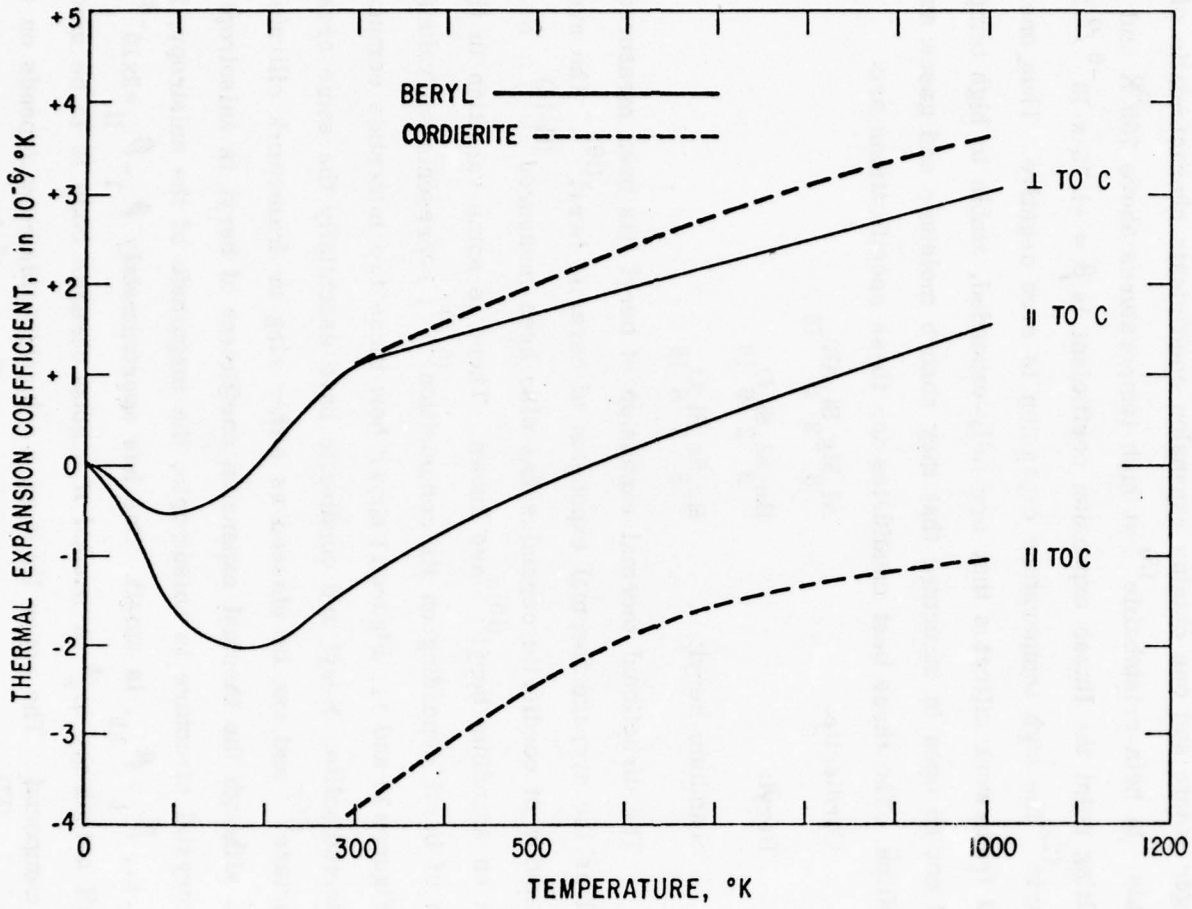

FIGURE 10. Thermal Expansion Coefficients of Beryl and Cordierite

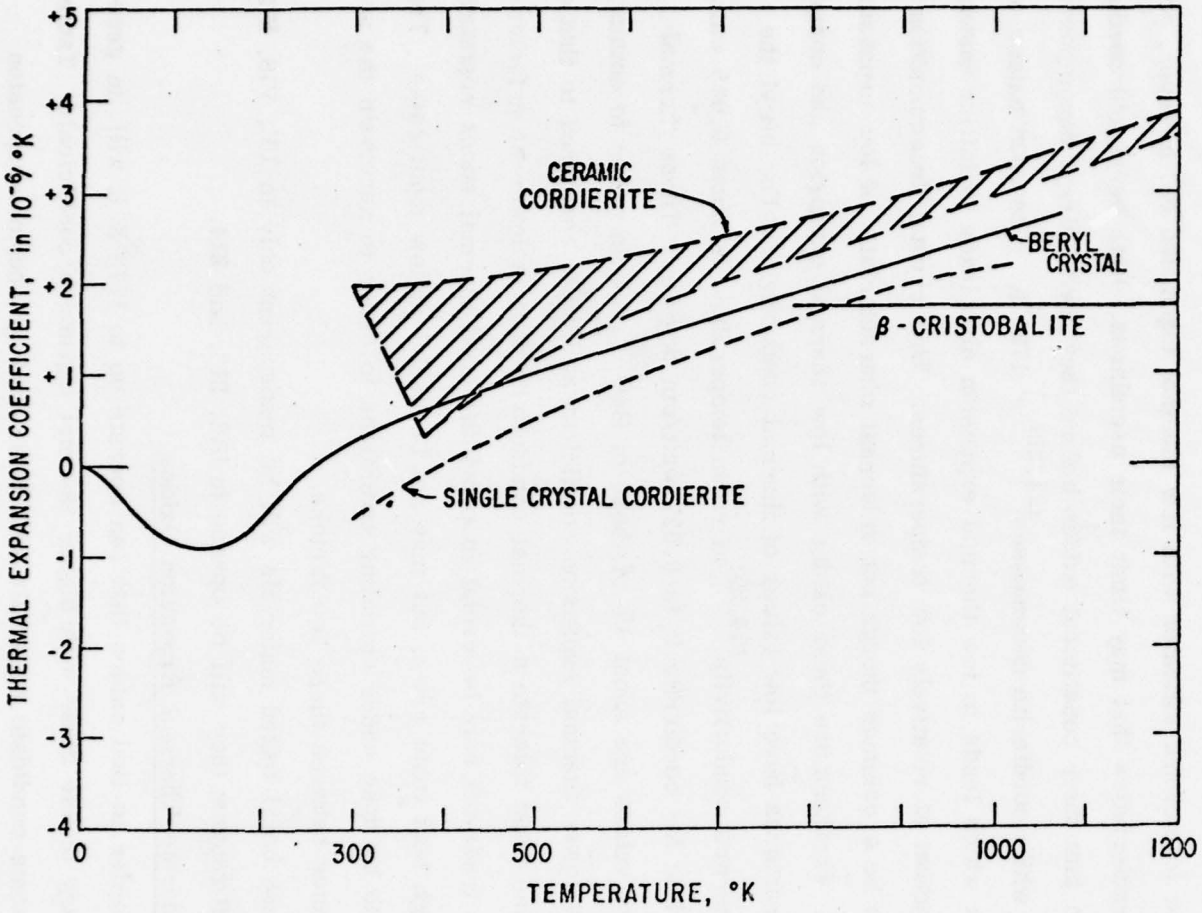

FIGURE 11. Thermal Expansion Coefficients of Cordierite Beryl and β-Cristobalite

are Al_2TiO_5, Sc_2TiO_5, α-SiO_2, $LiAlSiO_4$, $MgTiO_3$, and $LiNbO_3$. High anistropies are also found[19, 20, 21] in $CaMgSi_2O_8$, (diopside), $LiAlSi_2O_6$ (β-spodumene), $CaAl_2Si_2O_8$ (anorthite). The existence of a tightly-bonded, three-dimensional framework is needed to obtain small anisotropy; these latter materials do not possess this characteristic.

The framework silicates with low thermal expansion do, however, possess some characteristics that may limit their usefulness. Both beryl and cordierite decompose into their constituent oxides before they melt. Beryl decomposes[22] at 1750°K while cordierite decomposes[11, 23] at 1720°K. The open nature of the framework which leads to low thermal expansion also leads to lattice instability and destruction at relatively low temperatures. This crystal decomposition appears to be a common though not universal characteristic of low expansion materials. Furthermore these oxides with low thermal expansion and complex crystal structures have low values of thermal conductivity. For beryl the average thermal conductivity[24, 25] at room temperature is about 0.045 watt/cm degrees while for cordierite it is 0.027 watt/cm degrees. These thermal conductivity values are about 1% of those of BeO[26]. So in order to obtain a factor of 4 lower thermal expansion coefficient at 1000°K compared to that of BeO[27], one must tolerate a thermal conductivity that is lower by a factor of 100. This trade-off may be useful in providing good thermal shock resistance at very high heat input rates, but may not be useful at low input rates. Testing will have to be done under operating conditions in order to ascertain the appropriate balance between these two factors.

These beryl based materials will be transparent only in UV, VIS, IR1, and RADAR ranges; they will be opaque in IR2, IR3, and IR4.

3.2 Moderate Thermal Expansion Oxides

In order to find oxides that can operate up to 1773°K it will, in general, be necessary to use those with higher thermal expansion coefficients. Table 3-1 lists some candidate materials with their average thermal expansion coefficients, $\bar{\beta}$, at 1000°K, the maximum anisotropy in expansion, $\Delta\beta$, and their decomposition or melting temperatures. In the thermal expansion

TABLE 3-1. Properties at 1000°K of Some Oxides: Low, Intermediate, and High Thermal Expansion Coefficient

Mho Hardness	Material	Max.Temp. °K	$\bar{\beta}$ 10^{-6}/°K	$\Delta\beta$ 10^{-6}/°K	Structure	Ref. for β
6.5	β-Cristobalite	1970-M	1.8	0	C	
7.7	$Be_3Al_2Si_6O_{18}$	1750-D	2.5	1.5	H	
6.5	$AlPO_4$*	2300-M	2.9	0	C	28
∿6	$AlNbO_4$	1800-D	2.9	?	M	29,10
∿5	Zn_2GeO_4	1760-M	3.4	0.5	R	
7.5	$HfSiO_4$	2020-D	3.8	2.0	T	18,30,31
5.5	Zn_2SiO_4	1790-M	4.0	0.8	R	31
7.5	$ZrSiO_4$	1950-D	4.1	1.5	T	18,37
∿8	$B_4Al_{18}O_{33}$	2220-D	4.7	?	O	31
∿6	$AlTaP_4$	1950-M	5.3	?	M	29
6.5	$Al_6Si_2O_{13}$	2200-M	5.5	2.2	O	31,32
7.0	$BAl_7Si_3O_{18}$	1800-D	?	?	O	
?	$HfGeO_4$	?	5.6	2.9	T	10
?	$ThSiO_4$	2250-M	6.2	?	T	31
∿6	$MgTa_2O_6$	2040-M	6.5	?	T	29
7.7	Be_2SiO_4	1830-D	7.2	0.8	R	31,33
8.5	$BeAl_2O_4$	2140-M	7.4	0.9	O	31,33,34
8.0	$MgAl_2O_4$	2400-M	10	0	C	31,36,38
6.5	Mg_2SiO_4	2160-M	12	?	O	31
9.0	α-Al_2O_3	2323-M	9.0	0.9	R	39
6.5	ThO_2	3490-M	8.7	0	C	39
9.0	BeO	2350-X	10.6	1.1	H	40
6.0	MgO	3070-M	14.3	0	C	31

Column 1 *Cristobalite structure
Column 2 M=melting, D=decomposition, X=structure change
Column 5 C=cubic, H=hexagonal, M=monoclinic, O=orthorhombic, T=tetragonal

coefficient range of 3 to $6x10^{-6}/^{o}K$ there are a number of possible candidates for temperatures in the high range up to $1773^{o}K$. The materials like Zn_2GeO_4 and Zn_2SiO_4 will not operate well near $1700^{o}K$ because of low melting points and ZnO evaporation. They should be restricted to the moderate temperature range up to $1273^{o}K$. None of these intermediate expansion materials will operate in the very high temperature range to $2273^{o}K$. Many decompose into simpler oxides before they melt. For $2273^{o}K$ one has to rely, at best, on the simple oxides such as α-Al_2O_3, ThO_2, BeO, or MgO as shown in Table 3-1.

The regions of useful infrared transparency in these binary oxides will be determined by the high-wavenumber edge of the Reststrahlen band This will be governed by the Si-O, Be-O, Ge-O, or Al-O, vibrations and the corresponding photon energies. For these four the respective cut-off energies are approximately 3600 cm^{-1}, 2600 cm^{-1}, 2300 cm^{-1}, and 1900 cm^{-1}. Thus, some of these moderate expansion materials will be useful in the IR1 and IR2 ranges as well as in the radar, VIS and UV ranges. None of them will operate in IR3 or IR4 ranges.

The hardest materials in this group is chrysoberyl, $BeAl_2O_4$, with a Mho's hardness of 8.5; while the lowest is germanium willemite, Zn_2GeO_4 at about 5. The low thermal expansion materials tend to be softer than the high expansion ones. In terms of environmental toughness, Zn_2GeO_4 appears to be too soft and would be of value only if its optical properties are particularly useful. It would seem that the better choices from the central section of Table 3-1 are probably:

First:	$HfSiO_4$, $ZrSiO_4$
Second:	$B_4Al_{18}O33$
Third:	$Al_6Si_2O_{13}$ and the related $BAl_7Si_3O_{18}$ (mullite and dumortierite)
Fourth:	$AlNbO_4$ and $AlTaO_4$ (simpsonite group)

The hafnium-zircon group is placed first because of the low expansion, high decomposition temperatures, high hardness, and the availability of a

considerable amount of ceramic experience with these compounds. The second choice, $B_4Al_{18}O_{33}$, might rank first if the thermal expansion anisotropy were known. The chemistry will be much like that of the well known α-Al_2O_3. Mullite is placed third because of the higher values of $\bar{\beta}$ than the first and second choices. The low expansion $AlNbO_4$ is very interesting if the available expansion data are indeed correct. However, the expansion anisotropy and chemistry are poorly known. There may be considerable problems with keeping all of the niobium in the Nb^{+5} state. This high charge state will be needed to ensure high electrical resistivity and good optical transparency.

The four choices from $HfSiO_4$ to $AlTaO_4$ will be transparent in the UV, VIS, IR1 and RADAR ranges. The ones without Si will probably also operate in IR2. None will be transparent in IR3 and IR4.

The following section discusses mixed oxides which will perform in the IR2 (3-5.5 μm) band-pass.

3.3 Mixed Oxide Candidates For IR2 (3-5.5μm)

Category I - Non-Silicates With Intrinsic Low Expansion $< 4.0\times10^{-6}/^{o}C$ and IR Cut-offs Beyond 5 Microns

Three (3) mixed oxides have been identified in Category I, viz.,:

(i) $2ZnO\cdot GeO_2$

(ii) $ThO_2\cdot GeO_2$

(iii) $3CaO\cdot 5Al_2O_3$

A brief review of known properties for each system is given below.

a. The System $2ZnO\cdot GeO_2$

Axial and aggregate thermal expansion measurements on zinc germanate have been made by Wen, Brown, and Hummel [41]. Figure 12 shows both sets of data over the temperature range from 20°C to 1000°C. Computed average coefficients of expansion are listed below:

Temp (°C)	$\bar{\beta}$ ($^1/^{o}C$ = (β_c + 2β_a)/3
310	0.4×10^{-6}
583	1.21×10^{-6}
688	1.34×10^{-6}
1030	2.56×10^{-6}

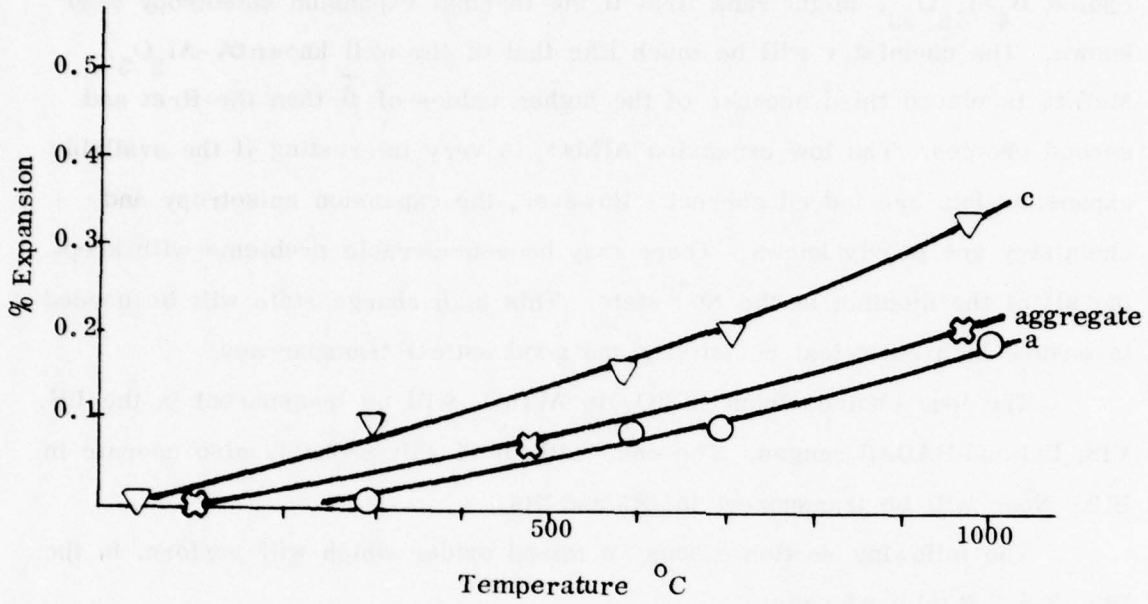

FIGURE 12. Comparison of Axial and Dilatometric Thermal Expansion Behavior of Zinc Germanate ($2ZnO \cdot GeO_2$) [41]

Infrared absorbance data obtained from transmittance measurements of dilute $2ZnO \cdot GeO_2$/KCl pellets, (shown in Figure 13), indicate that the infrared cut-off of theoretically dense material will occur at 5.5 microns. Intrinsic transmittance levels after surface reflection losses will be about 84 percent. Application of a rear surface antireflection coating would increase transmittance to about 92 percent. Critical property data not available for zinc germanate include hardness and Young's modulus. Also, the effect of a rather strong birefringence factor on scattering in a polycrystalline aggregate form must be assessed during Phase 1.

b. The System $ThO_2 \cdot GeO_2$

The axial thermal expansion coefficients of thorium germanate have been determined by Bayer[42] and are given below:

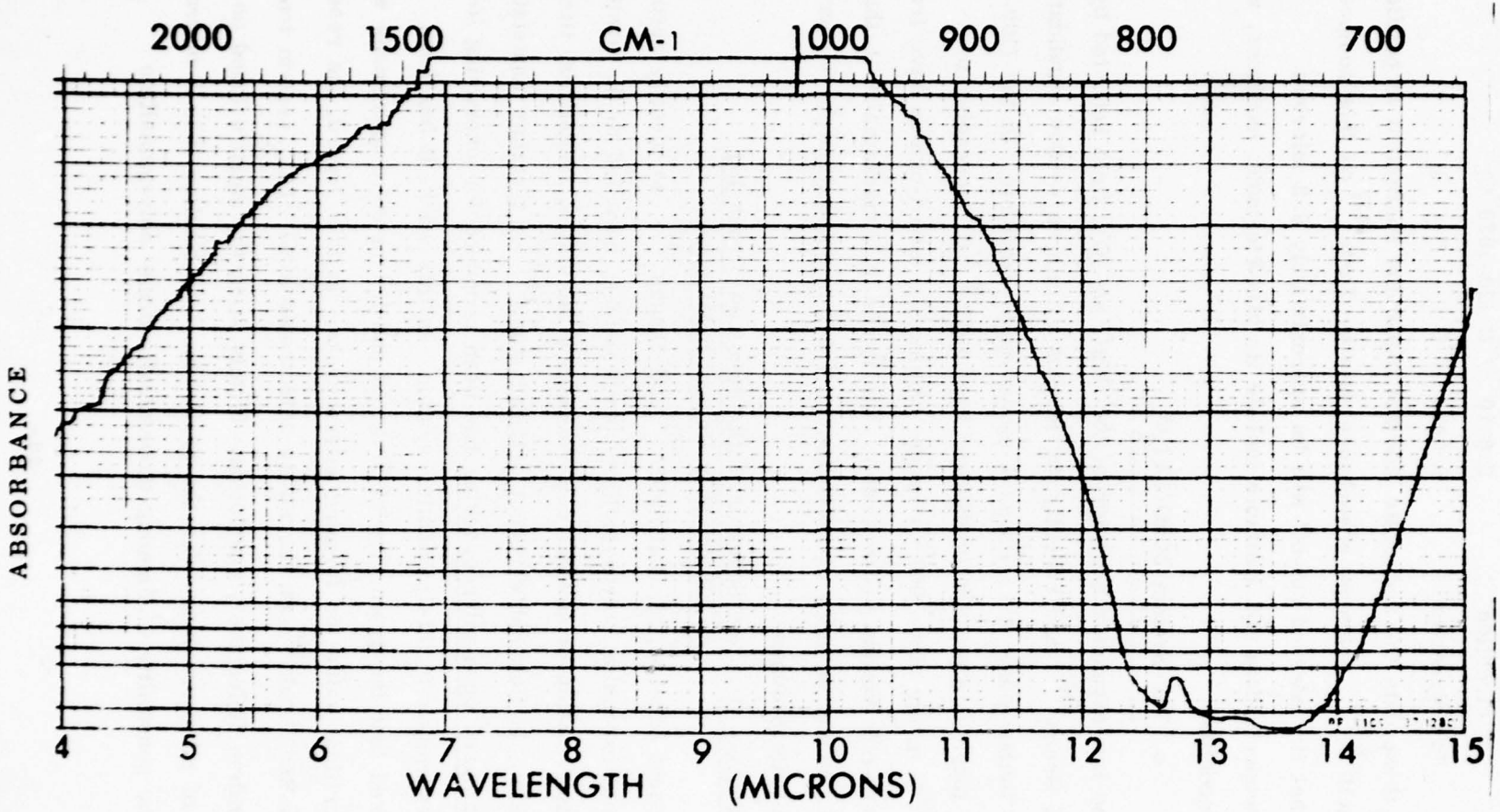

FIGURE 13 Infrared Transmittance of a Dilute Mixture of Zinc Germanate and Potassium Chloride. Predicted Infrared Cut-Off is Approximately 1/2 the Wavelength of the Short-Wavelength Absorbance Trough Boundary.

"a" direction $2.3 \times 10^{-6}/^{o}C$ (20-1020°C)

"c" direction $5.0 \times 10^{-6}/^{o}C$ (")

Based on these data the aggregate thermal expansion coefficient is predicted to be $3.2 \times 10^{-6}/^{o}C$. Infrared absorbance data by Tarte[43] on this compound indicate that its infrared cut-off will be approximately 6.3 microns. Critical property data not available include its birefringence, hardness, and Young's modulus.

c. The System $3CaO \cdot 5Al_2O_3$

The low expansion behavior of the $3CaO \cdot 5Al_2O_3$, first reported by Rigby and Green[44], and recently, by Rice as a 5 micron window candidate[45], warrants further study as a Phase 1 mixed oxide candidate. In the (100-500°C) range its thermal expansion coefficient is $1.2 \times 10^{-6}/^{o}C$, increasing to $4.0 \times 10^{-6}/^{o}C$ in the (100-1000°C) range. Aluminate mixed-oxides have transmittance cut-offs beyond 6.0 microns. The intrinsic transmittance of this compound, having an index of refraction of 1.64, is approximately 88 percent in its optimum bandpass.

Category II - Non Silicates With Ultra-Low Expansion and IR Cut-Offs Beyond 5 Microns

Recent surveys, by Holcombe[46] and Skaggs[47], to identify zero and low thermal expansion polycrystalline mixed oxides, have led to the synthesis and characterization of several new refractory tantalates, tungstates, titanates, and niobates. In Holcomb'e recent detailed study[48] of tantalum tungstates, a model not based upon microcracking has been proposed for explaining low thermal expansion in this particular system In this work, it has been hypothesized that the grain size of sintered and hot pressed specimens were below a critical value for forming microcracks. In this regard, the research of Kyszyk and Bradt[49] on the highly anisotropic $MgO \cdot 2TiO_2$ system tends to partly confirm Holcombe's contention. In this work the authors found no evidence of microcracking when the grain size was smaller than 3 microns.

The possibility of forming theoretically-dense polycrystalline

aggregates of crystals exhibiting significant thermal expansion anistropy is particularly interesting with these systems since both the cut-off and thermal stress requirements would be unquestionably satisfied for the most demanding infrared homing missile systems.

During Phase 1, the following four systems (Table 2-5) should be further studied to identify a model system to perform fine-diameter powder synthesis and consolidation studies:

(i) $HfO_2 \cdot WO_3 \cdot Ta_2O_5$

(ii) $x\ Ta_2O_5 \cdot yWO_3$

(iii) $x\ HfO_2 \cdot yTiO_2$

(iv) $x\ HfO_2 \cdot yNb_2O_5$

In addition, selected rare earth niobates and tantalates should be considered. As with other Phase 1 systems, screening data on birefringence and hardness should be obtained early in the program and ranked against other potential candidates. In addition, screening data should include an assessment of residual strains (not relieved by microcracking) which could introduce scattering due to strain induced birefringence.

Category III - Silicates With Low Expansion ($< 5.6 \times 10^{-6}/^{o}C$) and IR Cut-Offs Near 5 Microns

a. Silicate With Isolated Tetrahedra Structures

A review of infrared absorption spectra of silicate minerals by Launer[50] has established a correlation between wavelength ranges for strong infrared absorption and silicon-oxygen groups. Figure 14 summarizes the results of this study; regions of strong bands are shown by a horizontal line to the left of each group. As the Si:O ratio progresses from 0.50 in silica to 0.25 in the isolated SiO_4 tetrahedra, the region of strong absorption shifts to longer wavelengths, and the wavelength ranges tend to expand. Since the infrared transmittance cut-off is approximately one half the wavelength which bounds the short wavelength side of the absorbance spectra, isolated-tetrahedra silicates offered the potential for nearly meeting the 5 micron cut-off requirement. A further

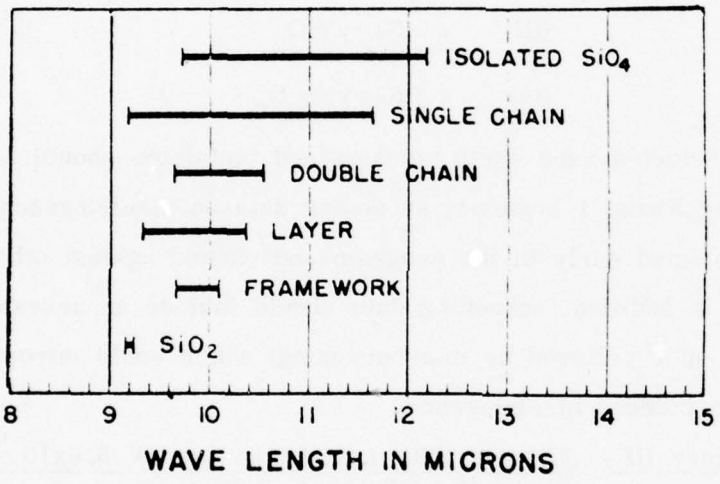

FIGURE 14. Wavelength Ranges of Strong Infrared Absorption Bands of Silicon-Oxygen Groups. (Ref. 50)

investigation of silicates with an isolated tetrahedra structure uncovered three systems (there are probably more to be identified) which had relatively low thermal expansion, moderate to high hardness, and which were naturally occurring in gem quality. It was also hypothesized at this time, that possible partial substitutions of heavier cations could enable slight (but necessary) shifts in the cut-off to occur without adversely effecting (or possibly improving) other desired properties.

As listed in Table 2-5 the systems found were:

(i) $Al_2(F,OH)_2SiO_4$ (Topaz)

(ii) $ZrO_2 \cdot SiO_2$ or $ZrSiO_4$ (Zircon)

(iii) $2ZnO \cdot SiO_2$ or Zn_2SiO_4 (Willemite)

Figures 15 through 21 show both the specular transmittance and reflectance of each system. The naturally-occurring mineral specimens were obtained from the Philadelphia Academy of Natural Sciences[51] and provided an opportunity to obtain actual specular transmittance and reflection data on theoretically dense forms. It should be noted that a substantial effort is normally involved in developed processes for synthesizing transparent ceramics so that the availability of naturally occurring minerals represents an expedient screening capability. As predicted from the infrared absorbance spectra, the infrared cut-off for this class of silicates is near 5 microns. Also, it is noted that the short wavelength boundary of the reflectance spectra approximately locates the cut-off boundary (approximately 1/2 the wavelength for the onset of the Reststrahlen reflection band). In the case of the willemite crystal, since it forms a complete series of solid solutions with Zn_2GeO_4, the effect of partial substitution of Ge^{+4} for Si^{+4} was briefly explored. A 50:50 solid solution was synthesized and the shift in reflectance spectra measured. Figure 21 compares the reflectance spectra for Zn_2SiO_4 (willemite) with the $Zn_2(SiO_{0.5}GeO_{0.5})O_4$ solid solution. Based upon this data, a shift of approximately 0.4 microns should be predicted in the infrared cut-off of Zn_2SiO_4 when the $Zn_2(Si_{0.5}Ge_{0.5})O_4$ solid solution was synthesized in transparent

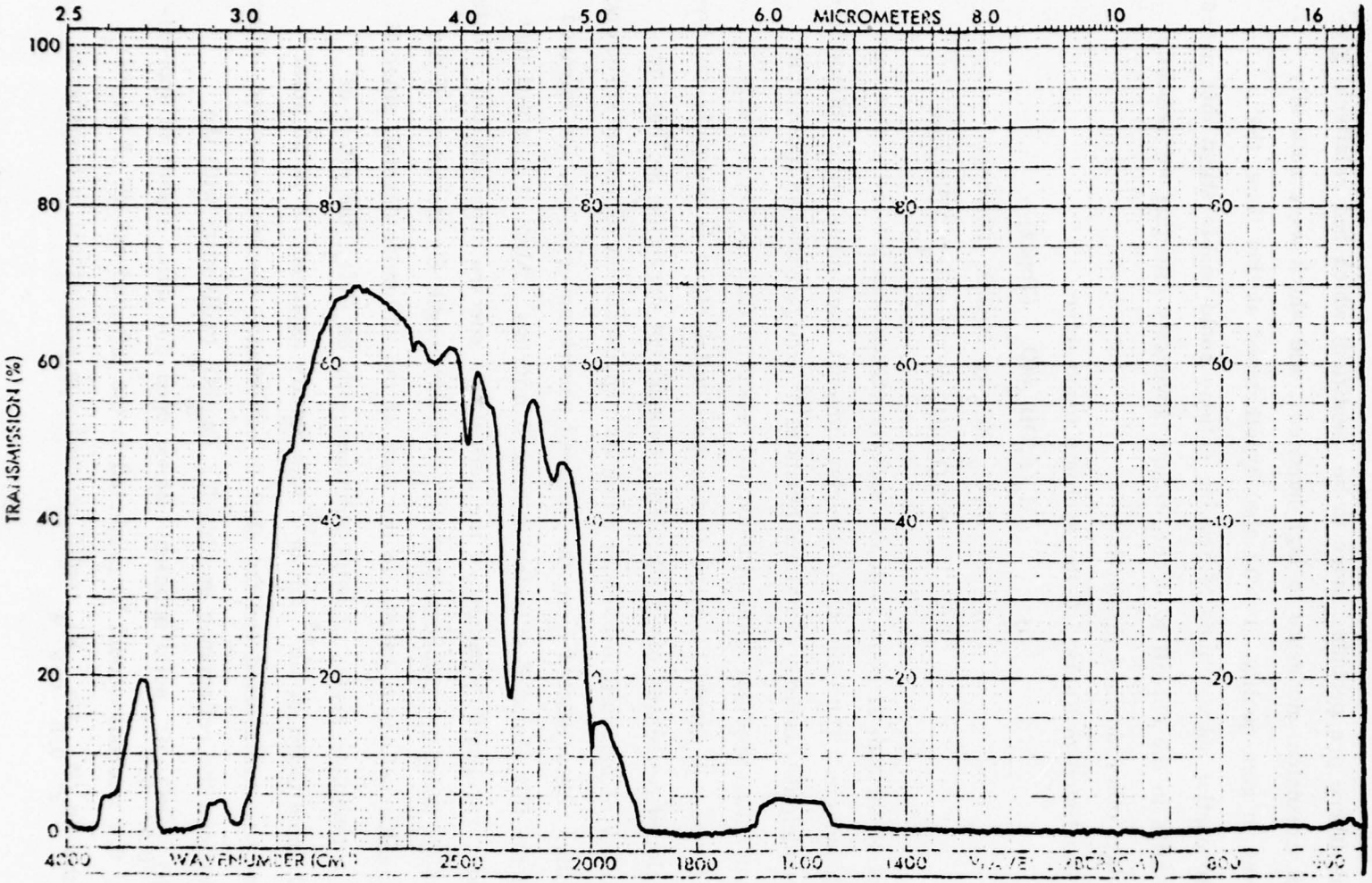

FIGURE 15. Specular Transmittance of $Al_2 (F,OH)_2 SiO_4$ (Topaz). Specimen Thickness = 0.0427 in.

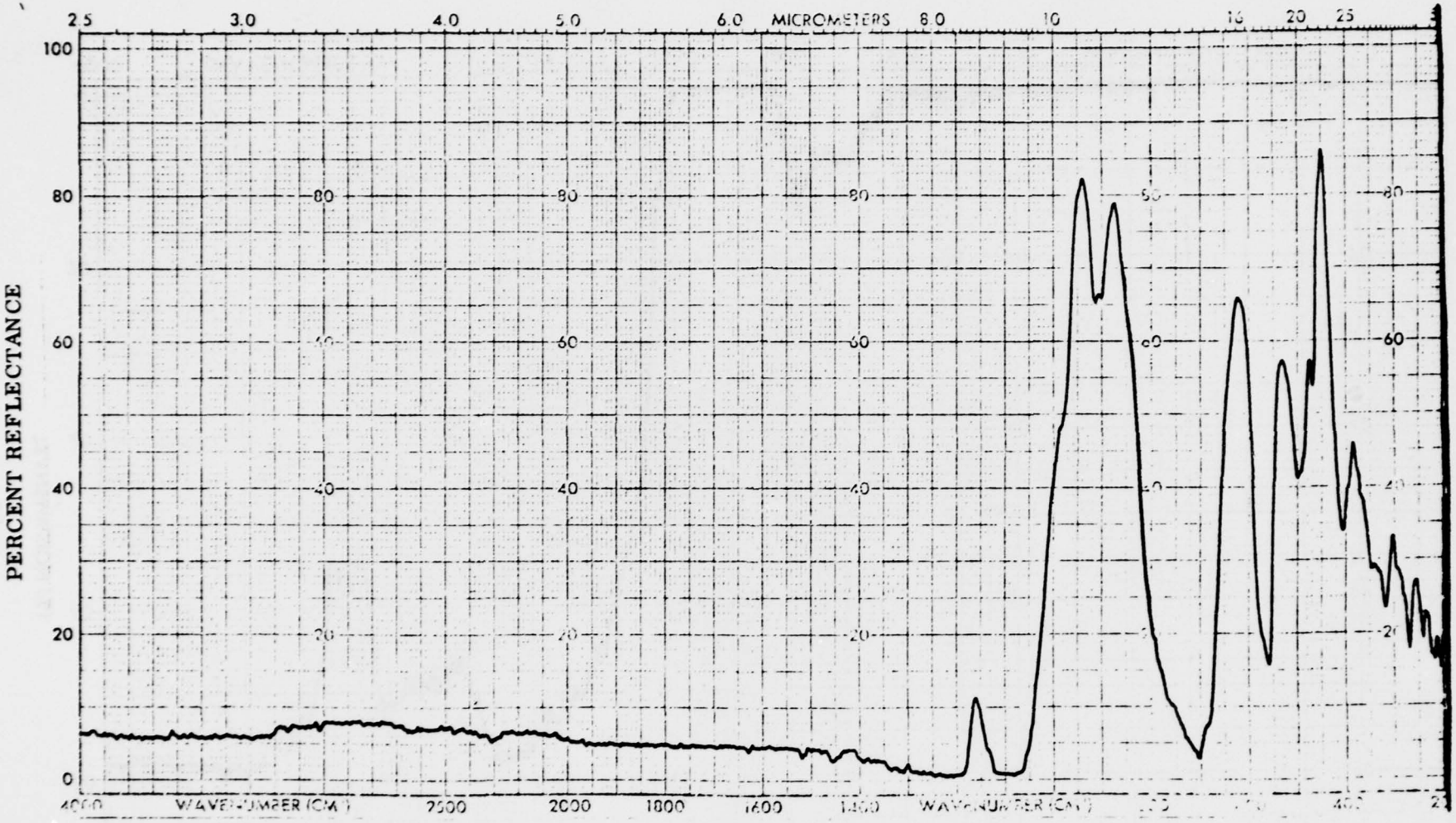

FIGURE 16. Specular Reflectance of Al_2 (F, OH)$_2$ SiO_4 (Topaz). Specimen Thickness = 0.0427 in.

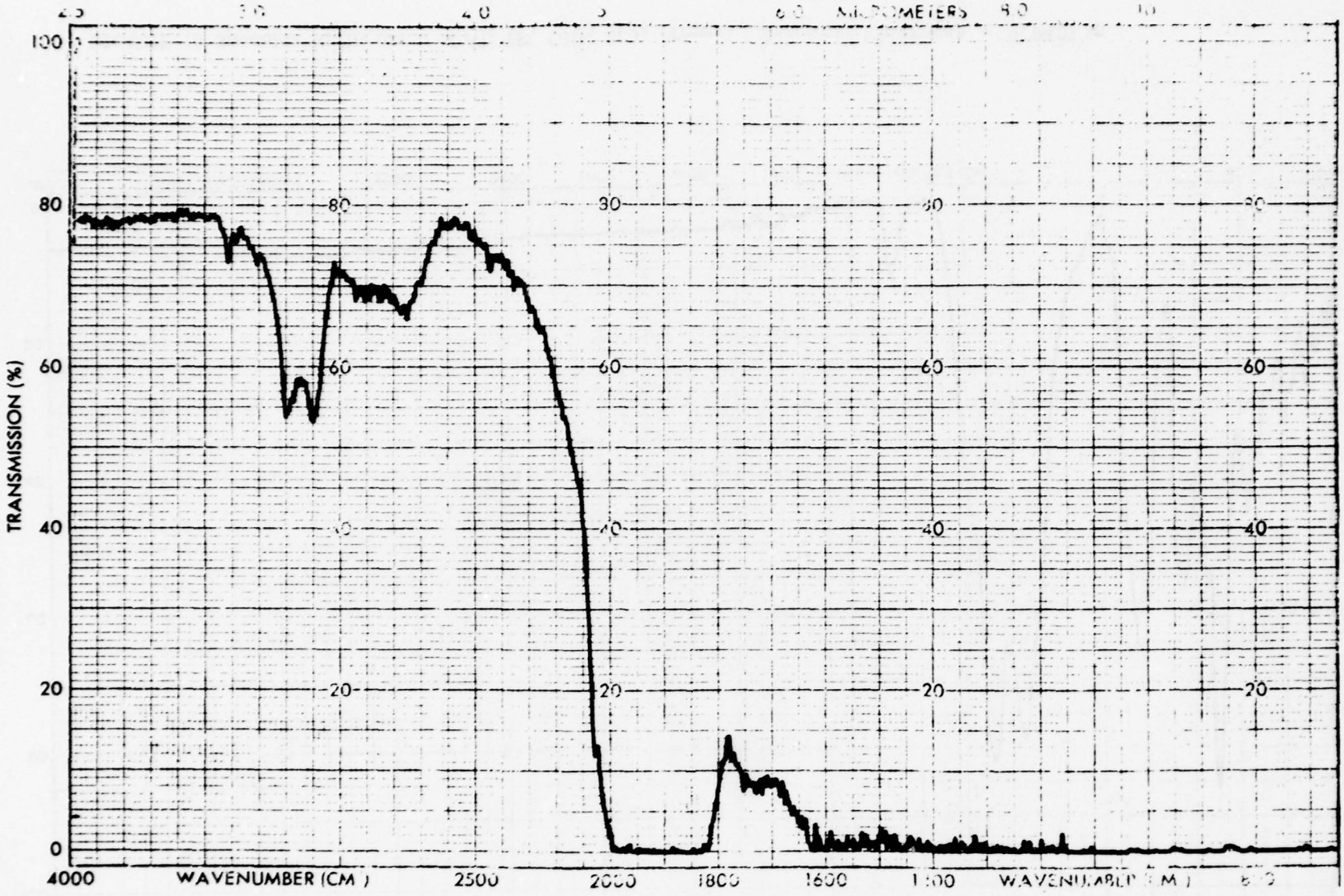

FIGURE 17. Specular Transmittance of $ZrSiO_4$ (Zircon). Specimen Thickness - 0.0732 in.

FIGURE 18. Specular Reflectance of $ZrSiO_4$ (Zircon). Specimen Thickness = 0.0732 in.

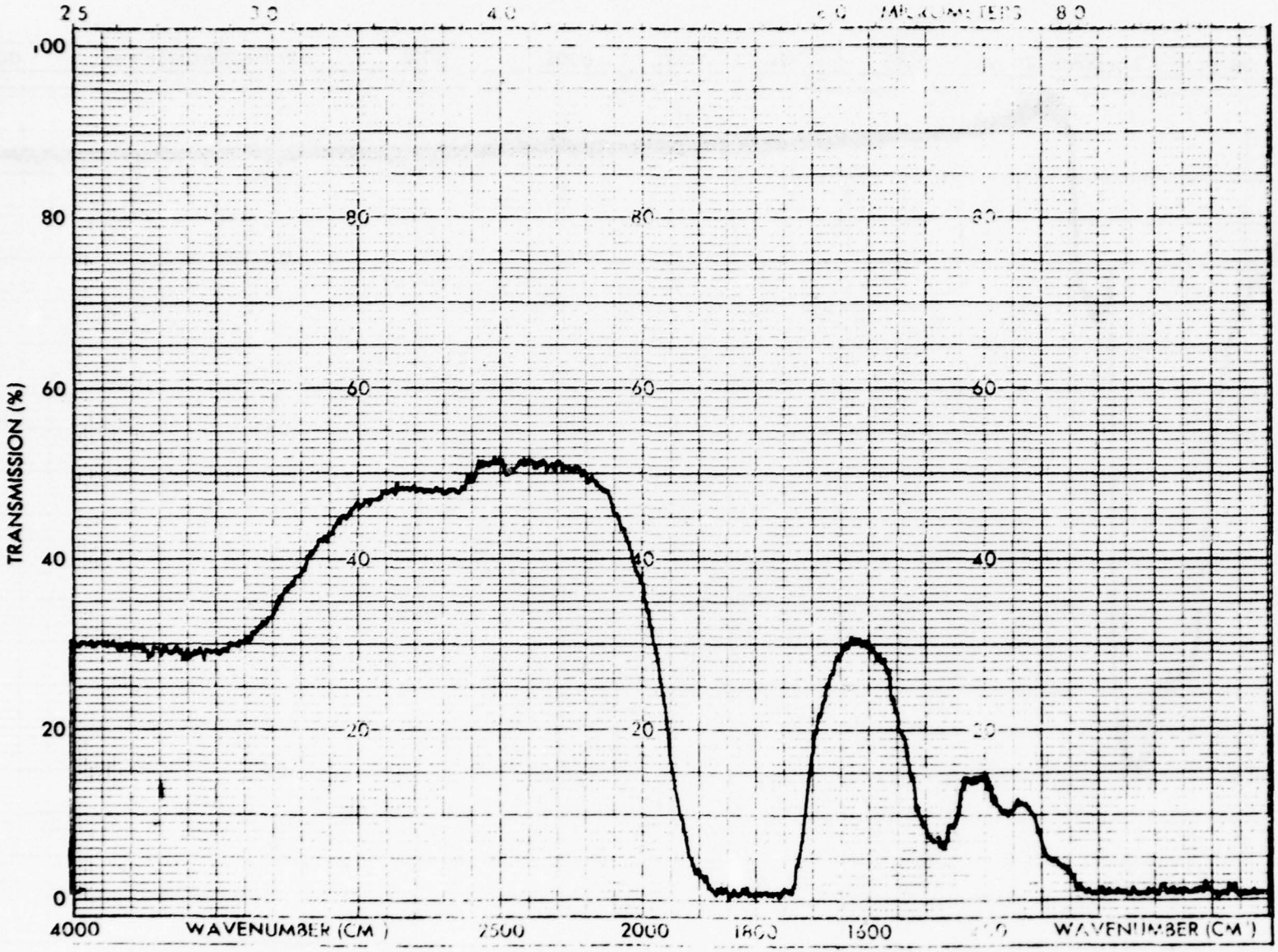

FIGURE 19. Specular Transmittance of Zn_2SiO_4 (Willemite). Specimen Thickness = 0.038 in.

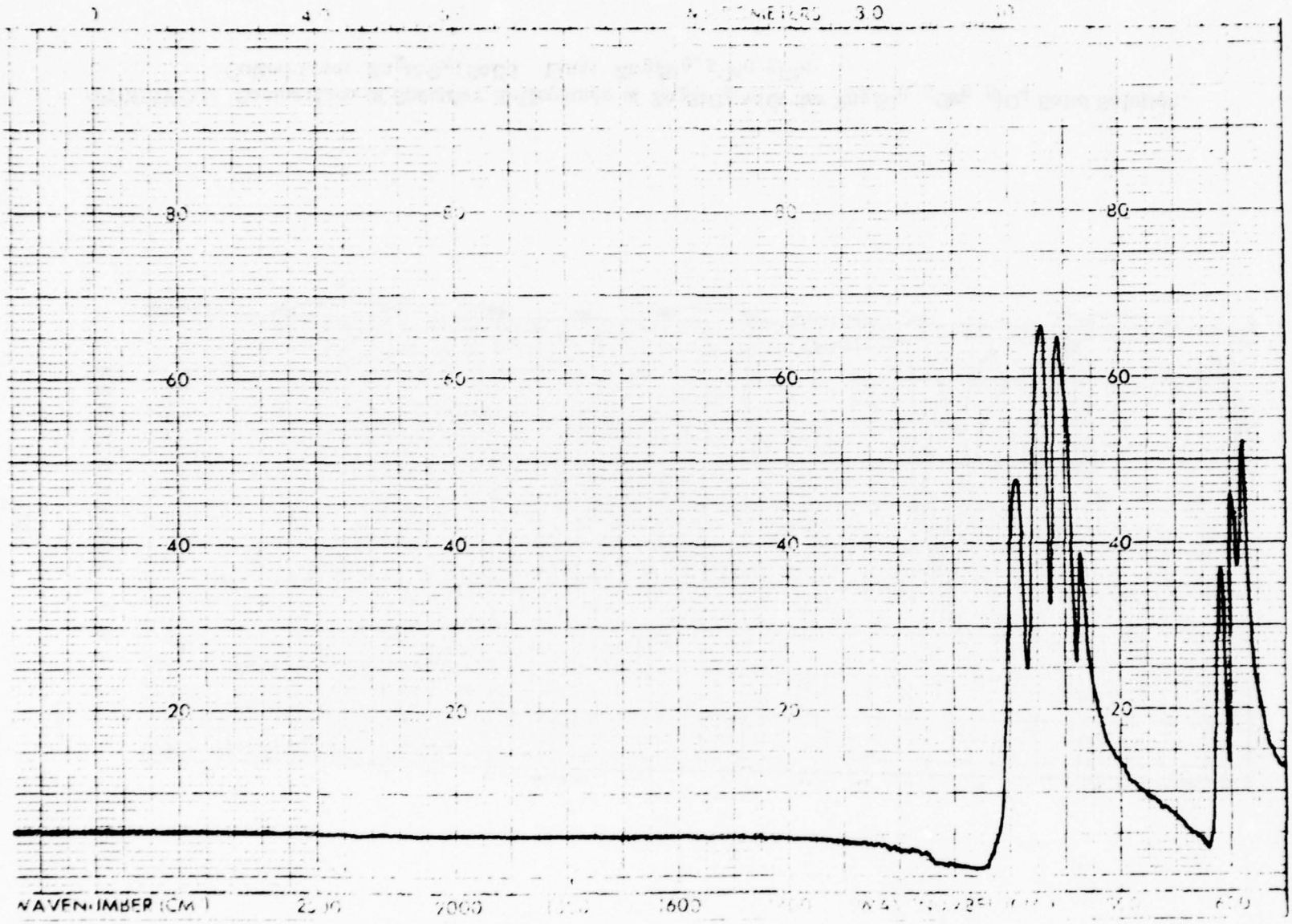

FIGURE 20. Specular Reflectance of Zn_2SiO_4 (Willemite). Specimen Thickness = 0.038 in.

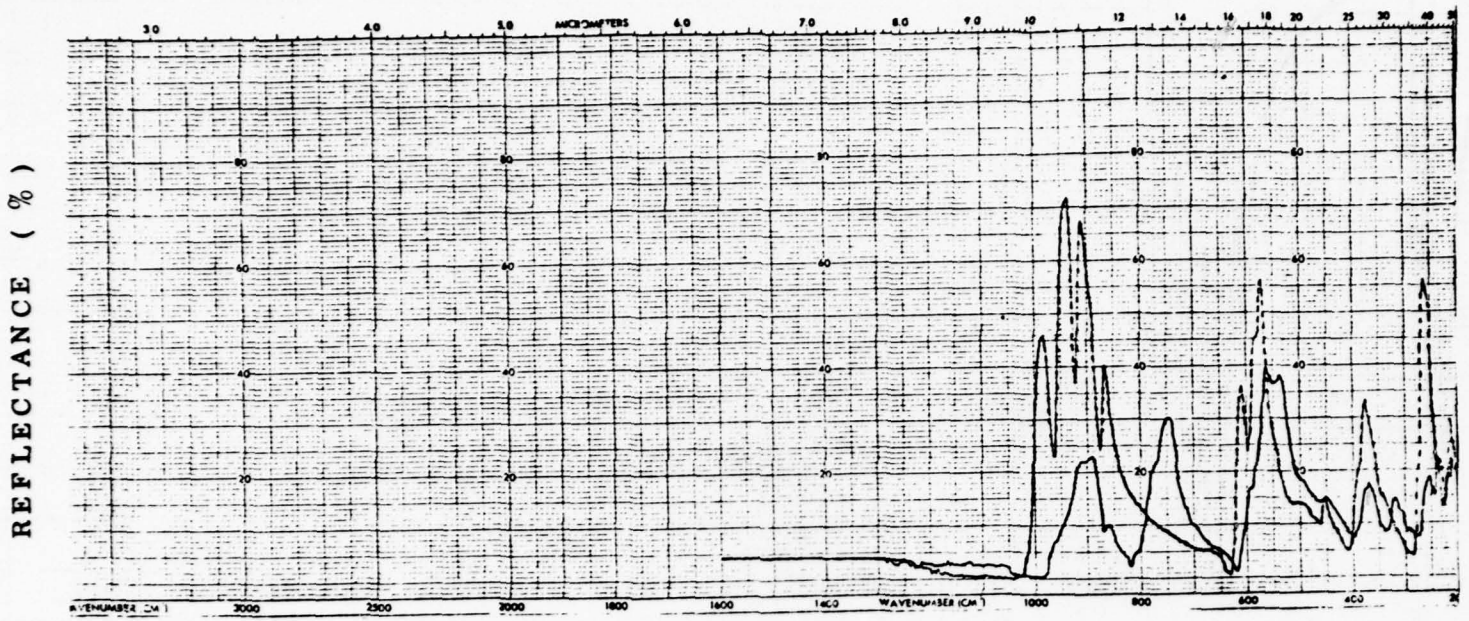

FIGURE 21: Comparison of Specular Reflectance of Zn_2SiO_4 with the $Zn_2(Si_{0.5}Ge_{0.5})O_4$ Solid Solution. Dotted Line: Zn_2SiO_4; Solid Line: $Zn_2(Si_{0.5}Ge_{0.5})O_4$.

form. In this system, the partial substitution provides a slight benefit in thermal shock resistance (note: thermal expansion coefficient of $Zn_2(Si_{.5}Ge_{.5})O_4$ is $2.9 \times 10^{-6}/^{o}C$ compared to $3.0 \times 10^{-6}/^{o}C$ for Zn_2SiO_4[4]. A similar shift in the infrared absorbance spectra (which is a mirror image of the reflectance spectra) was also found, as shown in Figure 22. This work confirms similar studies conducted by Tarte[43] on the Zn_2SiO_4-Zn_2GeO_4 system as discussed earlier.

The conclusion reached at this point is that isolated tetrahedra silicates such as $ZrO_2 \cdot SiO_2$ and $2ZnO \cdot SiO_2$ (mixed oxide designations) offer significant improvements in thermal shock resistance compared to sapphire and spinel; however, their cut-offs are marginal. Partial substitutions could offer increases in cut-off.

Of course, questions regarding birefringence scattering, hardness and magnitude of thermal shock resistance improvements must be addressed.

Other Types of Silicates

A review of other silicate structures uncovered other systems with low thermal expansion but with varying degrees of potential for satisfying the 5 micron cut-off requirement. Some candidates are listed below:

Type Tetrahedra	System	Crystal Structure
Layer	$SrO \cdot CuO \cdot 4SiO_2$	Tetragonal
Framework	$Cs_2O \cdot Al_2O_3 4SiO_2$	Cubic
Single Chain	$3Al_2O_3 \cdot 2SiO_2$	Orthorhombic
	$Li_2O \cdot Al_2O_3 \cdot 4SiO_2$	Tetragonal
Ring	$2MgO \cdot 2Al_2O_3 \cdot 5SiO_2$	Orthorhombic

Additional property data is listed in Table 2-5. Transmittance spectra illustrating the cut-off characteristics of naturally-occurring mineral forms are given in the following illustrations:

Figure 23 : Pollucite ($Cs_2O \cdot Al_2O_3 \cdot 4SiO_2$)

Figure 24 : Spodumene ($Li_2O \cdot Al_2O_3 \cdot 4SiO_2$)

Figure 25 : Cordierite ($2MgO \cdot 2Al_2O_3 \cdot 5SiO_2$)

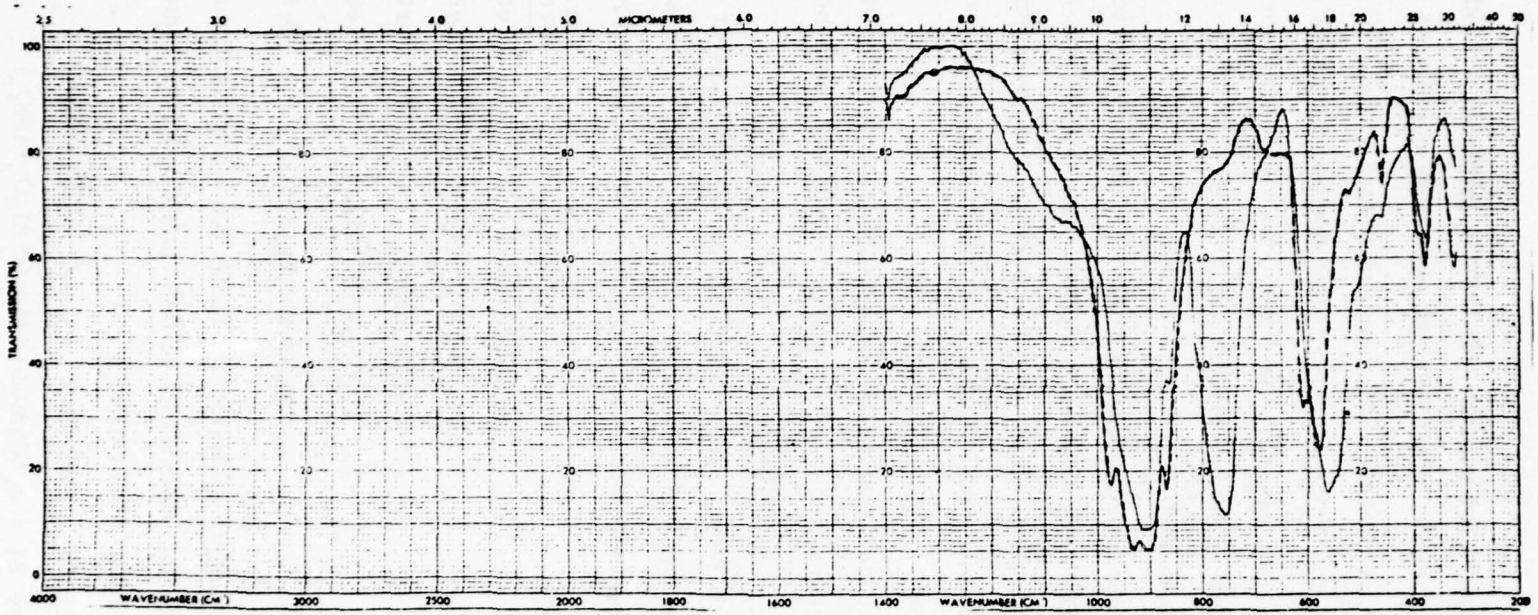

FIGURE 22. Comparison of the Infrared Absorbance Spectra of Zn_2SiO_4 with the $Zn_2(Si_{0.5}Ge_{0.5})O_4$. Dotted Line : Zn_2SiO_4 ; Solid Line: $Zn_2(Si_{0.5}Ge_{0.5})O_4$

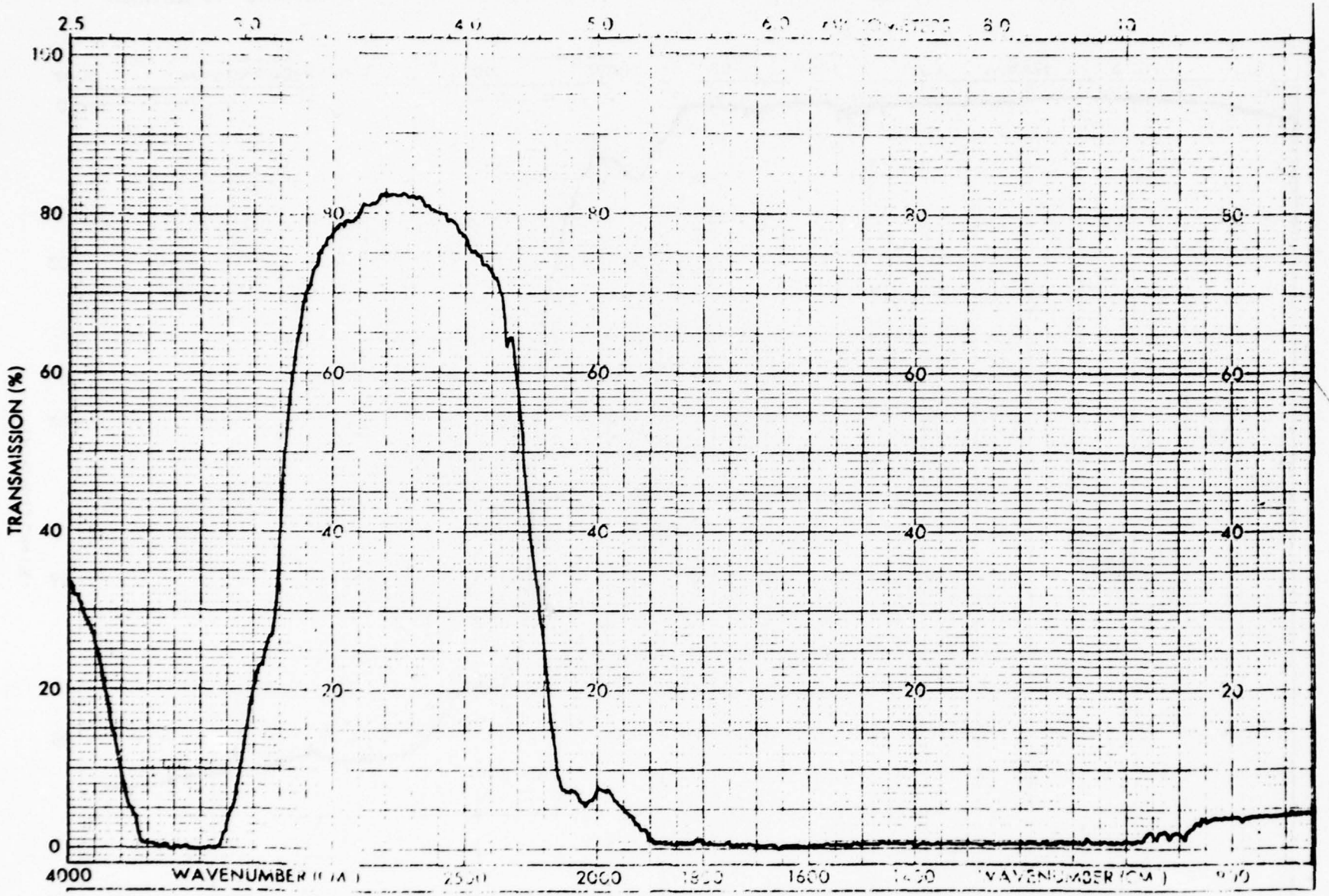

FIGURE 23: Specular Transmittance of $Cs_2O.Al_2O_3.4SiO_2$ (Pollucite). Thickness = 0.0456 in.

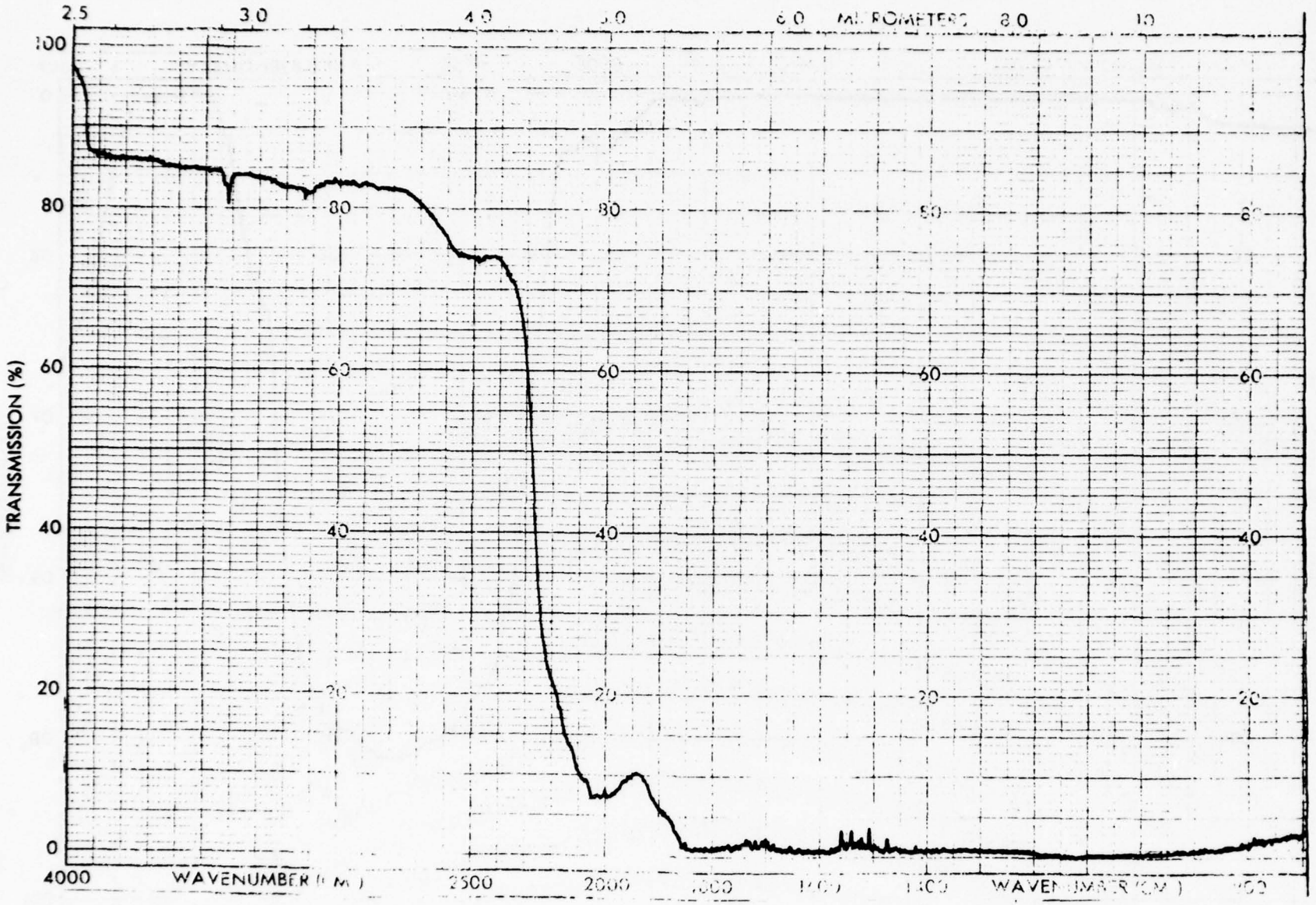

FIGURE 24: Specular Transmittance of $Li_2O.Al_2O_3.4SiO_2$ (Spodumene). Thickness = 0.0335 in.

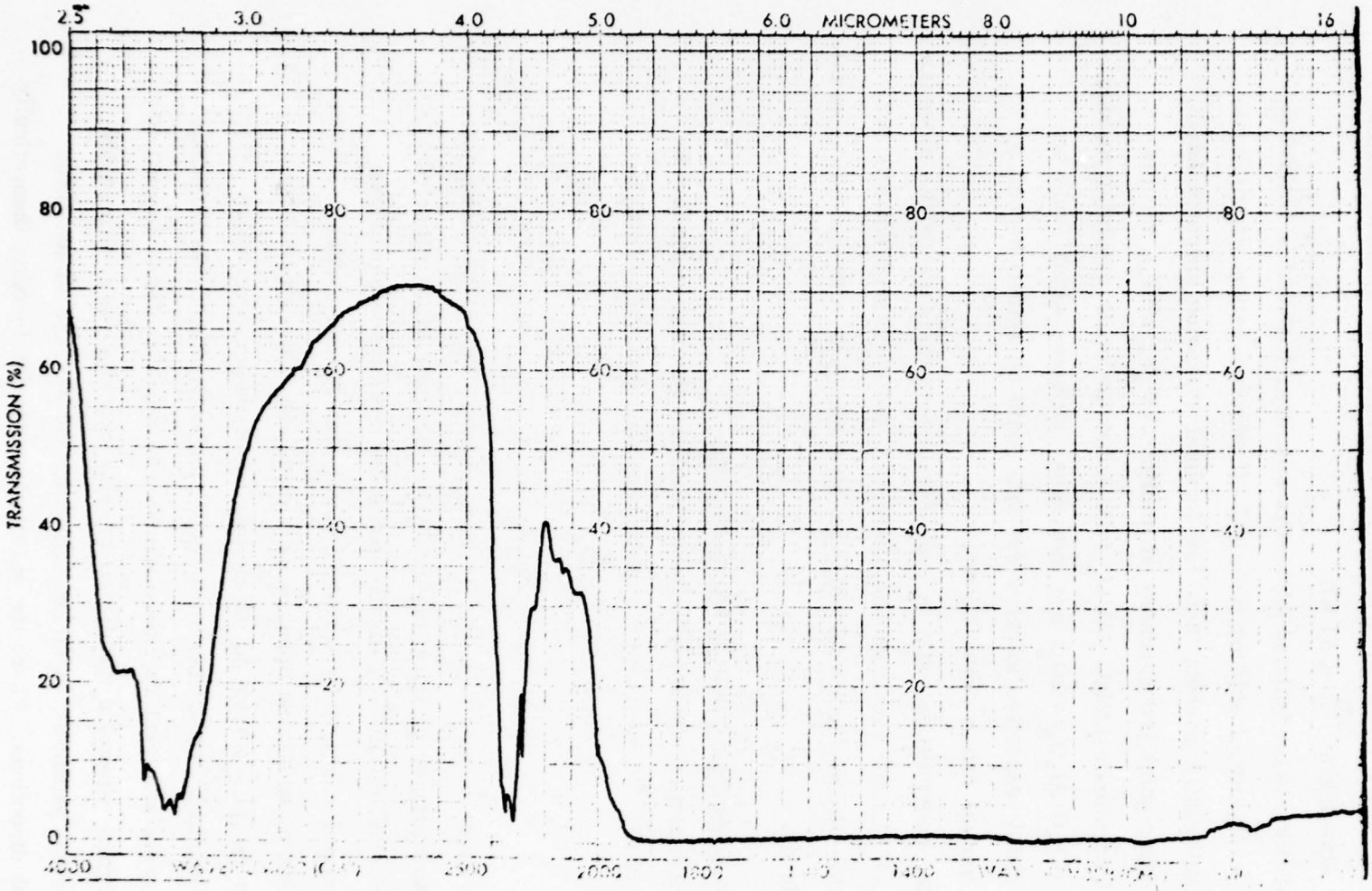

FIGURE 25: Specular Transmittance of $2MgO.2Al_2O_3.5SiO_2$ (Corderite). Thickness = 0.030 in.

Also shown in Figure 26 is the transmittance spectra for synthetic mullite prepared by Mazdiyasni[52] of AFML.

In addition to the isolated tetrahedra silicates, it should be fruitful to explore the feasibility of shifting their cut-off (through cation substitutions) while not significantly altering their low thermal expansion characteristics. The high melting point and hardness of mullite ($3Al_2O_3 \cdot 2SiO_2$), the low expansion of cordierite ($2MgO \cdot 2Al_2O_5 \cdot 5SiO_2$) and the cubic crystal structure of pollucite ($Cs_2O \cdot Al_2O_3 \cdot 4SiO_2$) are individual attributes which could be exploited if their respective infrared cut-offs could be shifted beyond 5 microns by partial cation substitutions.

Other possibilities exist in non-silicate systems such as the phosphates (e.g. $2ZrO_2 \cdot P_2O_5$) for low expansion; however, their infrared cut-offs are similar to the silicates and would also require tuning to shift cut-offs approximately 1 micron.

3.4 Low Expansion Single Oxide Candidates

Based upon a screening criterion that the thermal expansion be less than $4.0 \times 10^{-6}/^{o}C$ two single oxides have been found (Table 3-2):

(i) SnO_2

(ii) Nb_2O_5

Tin oxide occurs naturally in gem quality. Figure 27 shows the specular transmittance of Cassiterite (SnO_2). Because of its reported high thermal conductivity[53], its thermal shock resistance parameter including thermal conductivity would be similar to silicon carbide.

Niobium oxide also appears as a possiblity although its low expansion is directly related to anisotropic axial thermal expansion behavior. Manning[55] has shown, however, for hot-pressed modifications with small grain size that thermal expansion hysteresis effects leading to negative thermal expansion (attributed to microcracking) were eliminated, yielding thermal expansion behavior reflecting the average of the three axial crystal directions. Thus, the potential exists for forming theoretically

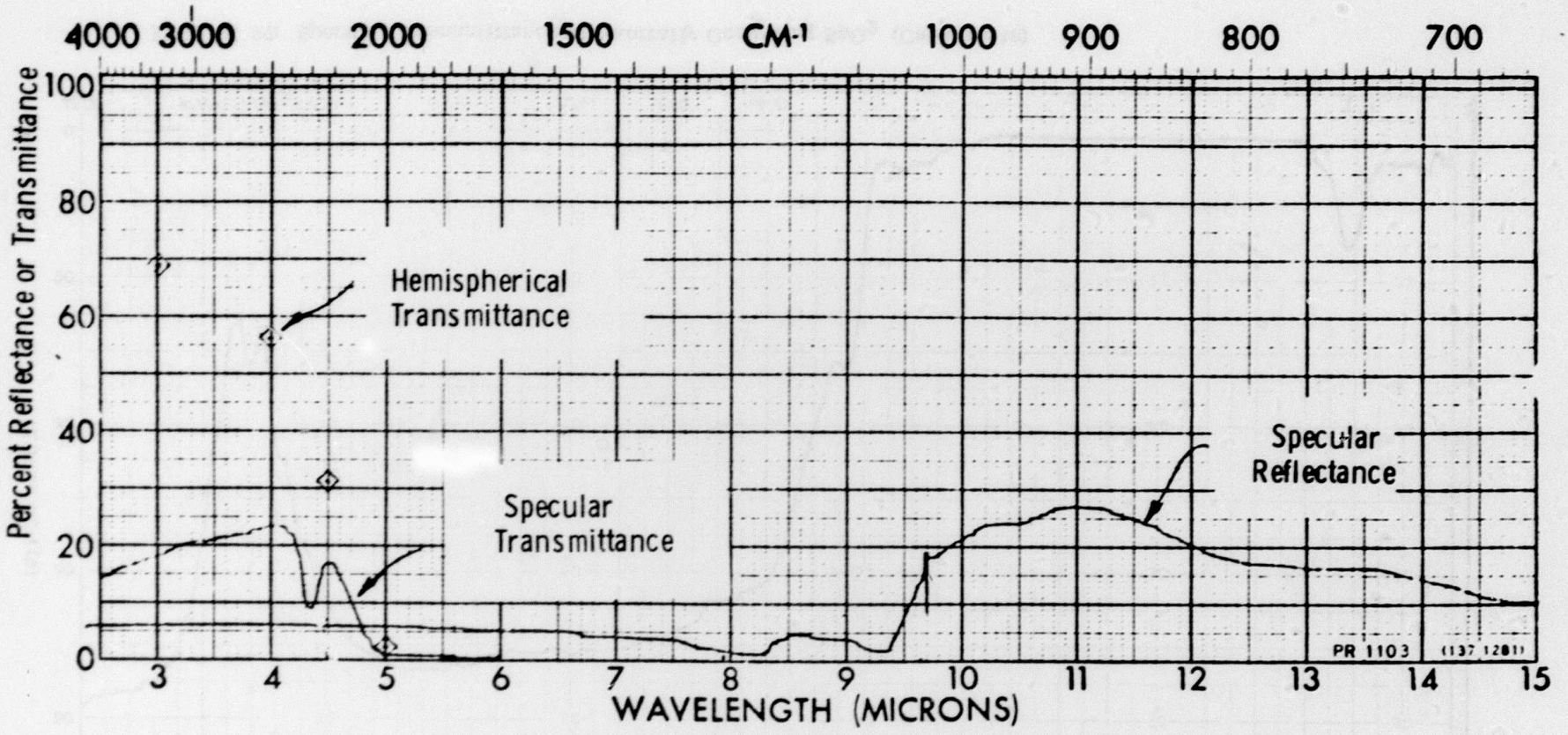

FIGURE 26. Reflectance (Specular) and Transmittance (Specular, Hemispherical) Properties of Transparent Mullite ($3Al_2O_3.2SiO_2$).

Thickness = 0.129 in.

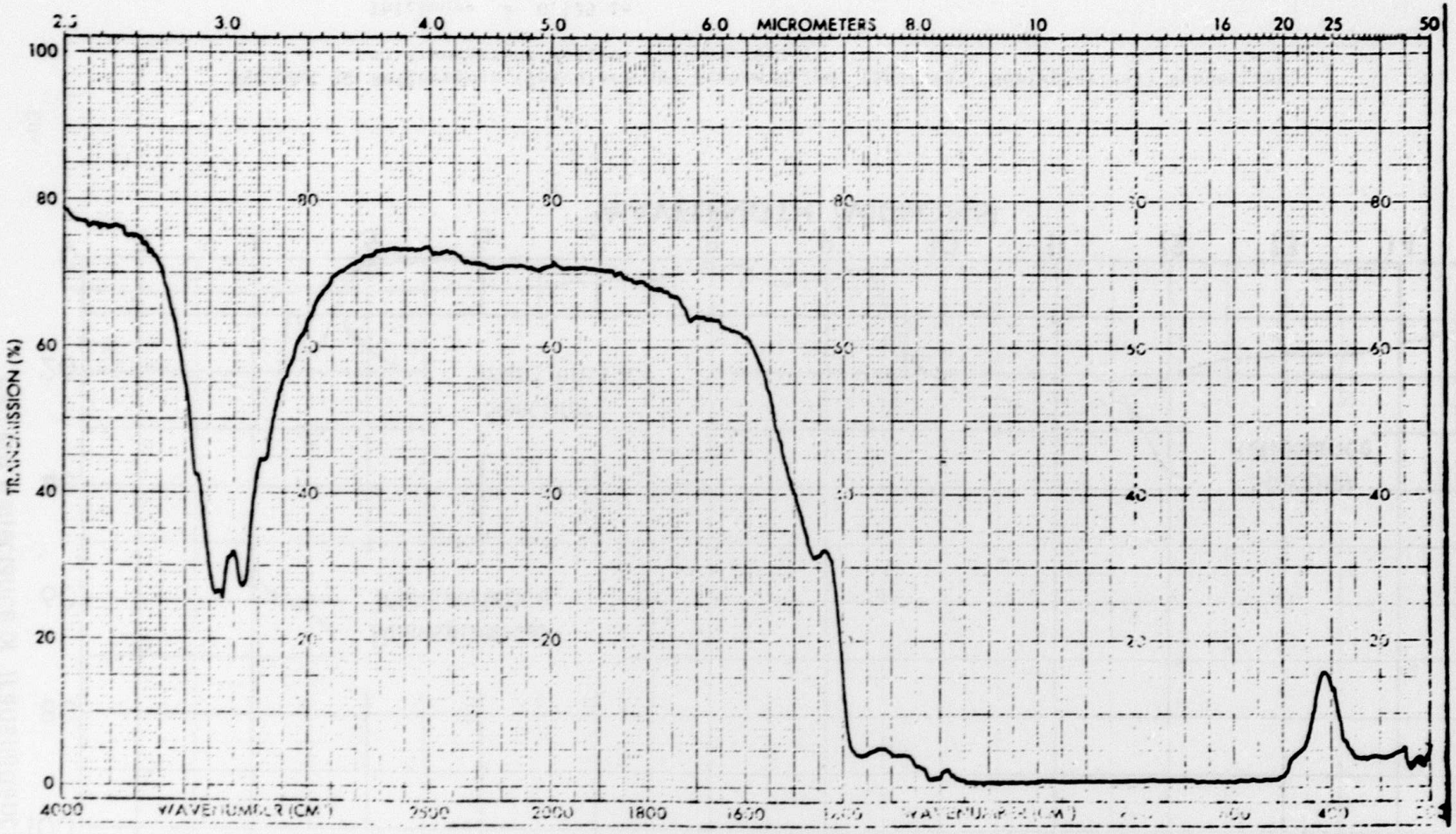

FIGURE 27: Specular Transmittance of Naturally Occurring SnO_2 (Cassiterite)

TABLE 3.2. Single Oxide Candidates

MATERIAL	(Cassiterite)[53] SnO_2	ZrO_2[54]	Y_2O_3	HfO_2[54]	Nb_2O_5
Optical Behavior					
o Crystal Structure	Tetragonal	Cubic (Y_2O_3- stabilized)	Cubic (ThO_2 SS)	Cubic(Ref. 2) (Y_2O_3 stabilized)	Monoclinic
o Index of Refraction (n_o, n_e or n_z, n_x)	2.024, 2.119	2.15			
o Birefringence, Δn	0.095	0	0		
o Infrared Transmittance					
- cut-off (μm)	7.1	7.0	9.0	7.0	7.0
- absorption coeff. @5 μm (cm^{-1})	-	-	-		
Thermal Stress Resistance					
o Thermal Expan. Coeff. ($^1/^oC$)	3.76×10^{-6}	7.3×10^{-6}	7.9×10^{-6}	$5.6 - 6.5 \times 10^{-6}$	2.19×10^{-6}
o Young's Modulus (psi)	33.8×10^{6}	26×10^{6}	25×10^{6}		
Erosion Resistance					
o Hardness (Moh)	6-7	7.5-8.5	7.2		
(Knoop)	-	-	875		
Chemical					
o Density (g/cc)	6.99	5.64	5.30		
o Melting Pt. (^oC)	1850	2677	2227	2790	1512

dense Nb_2O_5 which is free of microcracks. Whether the fine grain size required leads to aggravated birefringence effects or induced residuals strain remains to be determined through careful experimentation.

3.5 High Expansion Heavy-Metal Oxides For The IR3 (7.5 to 10 μm) And IR4 (10-14 5 um)

There may not be exceptional oxide candidates of low thermal expansion for the IR3 and IR4 ranges. The simple heavy metal oxides all have thermal expansion coefficients at $1000^{o}K$ of about $10x10^{-6}/^{o}C$. Some of these, for example, are ThO_2, BaO, and EuO with transparency cut-off energies of 1300 cm^{-1}, 1300 cm^{-1}, and 1000 cm^{-1} respectively. Consequently, EuO might possibly operate in IR3; the other two will not. Some properties of the heavy metal oxides are shown in Table 3-3. Except for EuO they are probably all optically transparent in the UV, VIS, IR1, IR2, and RADAR ranges. The small band gap of EuO makes it non-transparent in the UV and VIS ranges These oxides should only be employed when their very high melting temperatures are needed since their intrinsic high thermal expansion coefficients produce poor thermal shock resistance. The thermal shock resistance of the garnet, bixbyite, and pyrochlore structures, however, may produce ceramic or single crystal bodies with better shock resistance than others in the list since their complex structures prevent crystal cleavage.

3.6 Rare Earth Niobates and Tantalates

The rare earth niobates and rare earth tantalates are mixed oxides with the monoclinic fergusonite structure. Both cations are in 6-coordination and this is reflected in the relatively low vibrational frequencies (Figure 28). Phase diagrams for the lanthanum compounds (Phase Diagrams for Ceramists, Figures 4423 and 4424) shows these compounds to be congruently melting and with no phase transitions listed. The lanthanum and yttrium compounds should not exhibit absorption from f-f transitions in the visable and near IR.

TABLE 3-3: Properties of Some Heavy-Metal Oxides

Material	Melts °K	IR Cutoff cm^{-1}	Structure (all cubic)	β at 1000°K $10^{-6}/°k$	Ref. for β
MgO	3070	1450	Rocksalt	14.3	31
BaO	2190	1300	"	18	56
EuO	2249	1000	"	∿12	57, 58
$Y_2Al_5O_{12}$	2200	1650	Garnet	9.6	18, 59
Y_2O_3	2653	1400	Bixbyite	8.9	31
$CaHfO_3$	2740	∿1300	Perovskite	9.5	60
$BaThO_3$	?	∿1300	"	11.5	18
$La_2Zr_2O_7$	2470	∿1300	Pyrochlore	∿9	-
$LaSn_2O_7$	?	∿1300	"	8.6	18
$La_2Hf_2O_7$	2570	∿1300	"	∿9	-
ThO_2	3490	1300	Fluorite	8.7	31

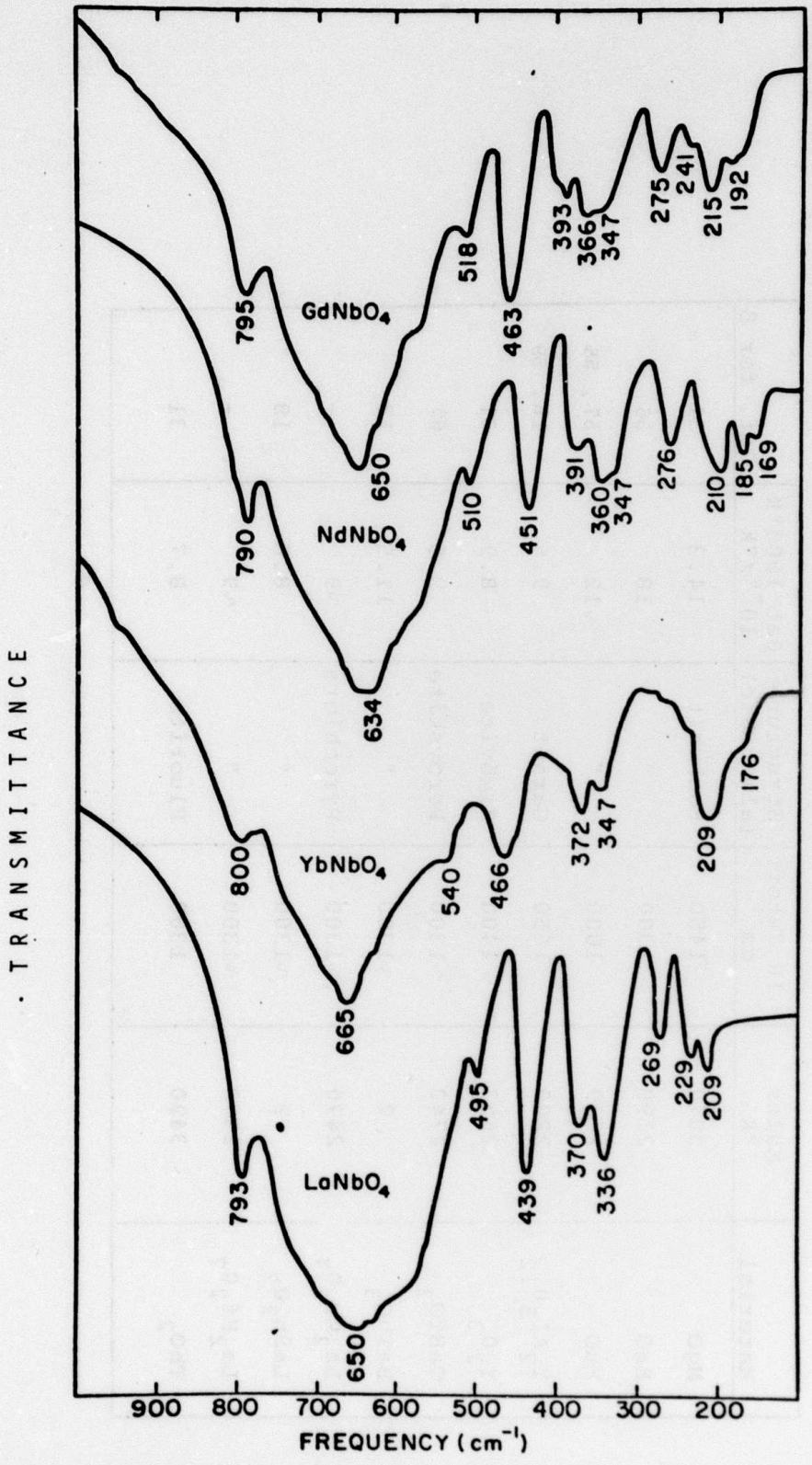

FIGURE 28: Transmittance - Rue Earth Niobates and Tantalates

The compounds that might be of some interest with their melting are:

$LaNbO_4$	1620°C
$LaTaO_4$	1930°C
$YNbO_4$	?
$YTaO_4$	?

3.7 Non-Oxides

None of the metal oxides or nitrides are sufficiently transparent in the IR4 range and only EuO might perform in IR3. Other types of solids are needed. Table 3-4 lists some possible candidates among the elements, sulfides, selenides, phosphides, and antimonides. The metal sulfide with the lowest energy IR cut-off is EuS at $\nu = 535\ cm^{-1}$. This cut-off energy is calculated from 3TO (Γ), where TO (Γ) is the energy of the transverse optic mode at the zone center[61-63]. The multiphonon optical absorption coefficient is approximately 1 cm^{-1} at 3TO(Γ). The mechanical properties of $SrLa_2S_4$ may be superior to those of EuS, and its reststrahl band is also sufficiently low in energy[65] to make it transparent in IR3 and IR4. The two standard materials ZnS (Irtran2) and ZnSe (Irtran 4) are listed for comparison. Among the 3-5 compounds GaP is useful for IR3 (as is GaAs) while only GaSb (and InSb) can be used in IR4. The high temperature thermal stress and oxidation resistance of these materials from EuS to GaSb are, however, not high.

The last three entries in Table 3-4 are possible candidates among the high temperature refractory materials. The infrared optical absorption of β-boron has been measured and is plotted in the present collection of curves. The average absorption coefficient is $\alpha \sim 3000\ cm^{-1}$ in the IR3 and IR4 ranges. If a sufficiently sensitive detector is used and if the window does not become so hot that it produces emission in this wavenumber range, then β-boron might be useful. However, BP appears to be a much better candidate, especially for IR3. The optical absorption curve for BP has been estimated by taking the results for SiC and shifting them slightly to take account of the slight difference in

TABLE 3-4: Non-Oxides for IR3 and IR4 Ranges

Material	Melt °K	β at 1000°K 10^{-6}/°K	IR Cutoff cm^{-1}	Eg cm^{-1}	α cm^{-1} IR3	α cm^{-1} IR4	References
EuS	2831	14	535	13,300	<1	<1	47, 61-64
$SrLa_2S_4$	∿2400	10 to 25	600	∿24,000	<1	<1	65
ZnS	2100	7	800	25,000	<1	∿30	66, 67
ZnSe	1780	8	630	20,000	<1	<1	67
GaP	1740	6.0	1000	18,000	<1	∿30	27, 68-70
GaSb	980	∿6	690	6,000	<1	<1	68, 71
β-Boron	2330	7.6	3300	12,900	∿3000	∿3000	
BP	3000	5.4	2000	18,000	10	∿1000	
Diamond	4000	4.5	3630	48,400	<1	<1	

values of TO(Γ) and by reducing the intensity of the SiC absorption to an assumed Szigeti effective charge of 0.1 electron. This is about correct for BP which possesses very little ionic bonding. The absorption coefficient of BP in IR4 is estimated to be a $\sim$ 1000 cm^{-1}. Hence BP is not recommended for this range.

Diamond is a special case in comparison to all of the other materials. As the optical absorption curve shows, the main lattice absorption of diamond occurs in the IR2 range and diamond becomes transparent in IR3 and IR4. Thus it is a good candidate for windows in these ranges. There is a size limitation on transparent diamonds at 1 to 10 mm in size. Thus larger windows may have to be made of mosaics or honeycomb structures or of a lattice work of metal holding the diamond elements together. The upper temperature limit on diamond is fixed by the graphitization temperature somewhere above 1300^{o}K and by oxidation if the surface is not protected.

In conclusion the best candidate for IR3 and IR4 are $SrLa_2S_4$, BP, and diamond.

The following section discusses the possibilities in the $SrLa_2S_4$ family of candidates.

3.8 IR3 (7.5-10 μm) And IR4 (10-14.5 μm) Chalcogenide Windows Screening the Chalcogenide Compounds

The total number of ternary chalcogenide compounds is very large. Selecting mainly the sulfides, and only those compounds that contain noble gas core, filled d-shell, or rare earth cations, still provides more than a thousand materials (Muller, 1972)[72] which have at least been synthesized and for which some crystallographic data exist. Phase equilibria have been determined for very few of these chalcogenide systems. Data on the optical properties, infrared absorption spectra, hardness, mechanical properties, thermal expansion coefficients, and thermal conductivities are for most compounds, non-existent.

The sections that follow screen the ternary sulfides rather quickly and identify several families of compounds where materials with the correct optical properties for IR window application might be found.

If the ternary compounds are plotted as a function of the ionic radii of the two kinds of cations, it is found that compounds with the same structure appear in the same part of the plot forming a sort of map on which the various types of structures may be identified. Figure 29 shows such a map for ternary sulfides with the cation ratio A_2BS_4. These maps allow the prediction of the structures of unknown compounds since any combination of cations can be plotted by means of their radii. The names given to the structures are those commonly used in the literature and usually refer to the type compound for which the structure was originally determined. Thus the listing of a "$CaFe_2O_4$" structure implies that this group of ternary sulfides have the same structural arrangement of atoms as the oxide compound $CaFe_2O_4$.

The structures that appear in Figure 29 are tabulated with some comments (Table 3-5) on their suitability as IR window materials. Of greatest interest are those with the higher coordination numbers and these are shown in more detail for the sulfide compounds and the selenide compounds in Figures 30 and 31. Each point on these plots represents a known compound and some of these with the Th_3P_4 structure are specifically indicated. Many of these ternary sulfides and selenides have the same structure except that the MnY_2S_4 structure appears only among the sulfides and the $CaHo_2Se_4$ structure appears only among the selenides.

Ternary Sulfides with the Th_3P_4 Structure

The alkaline earth - rare earth sulfides of the formula $A(RE)_2S_4$ (where A = Ca, Sr, or Ba; RE - La, Pr, Nd, Sm) belong to the cubic Th_3P_4 structure type. Both cations are in 8-fold coordination on the same crystallographic site. Optical band gaps are in the range of 2.5 to 2.9 eV, as indicated below:

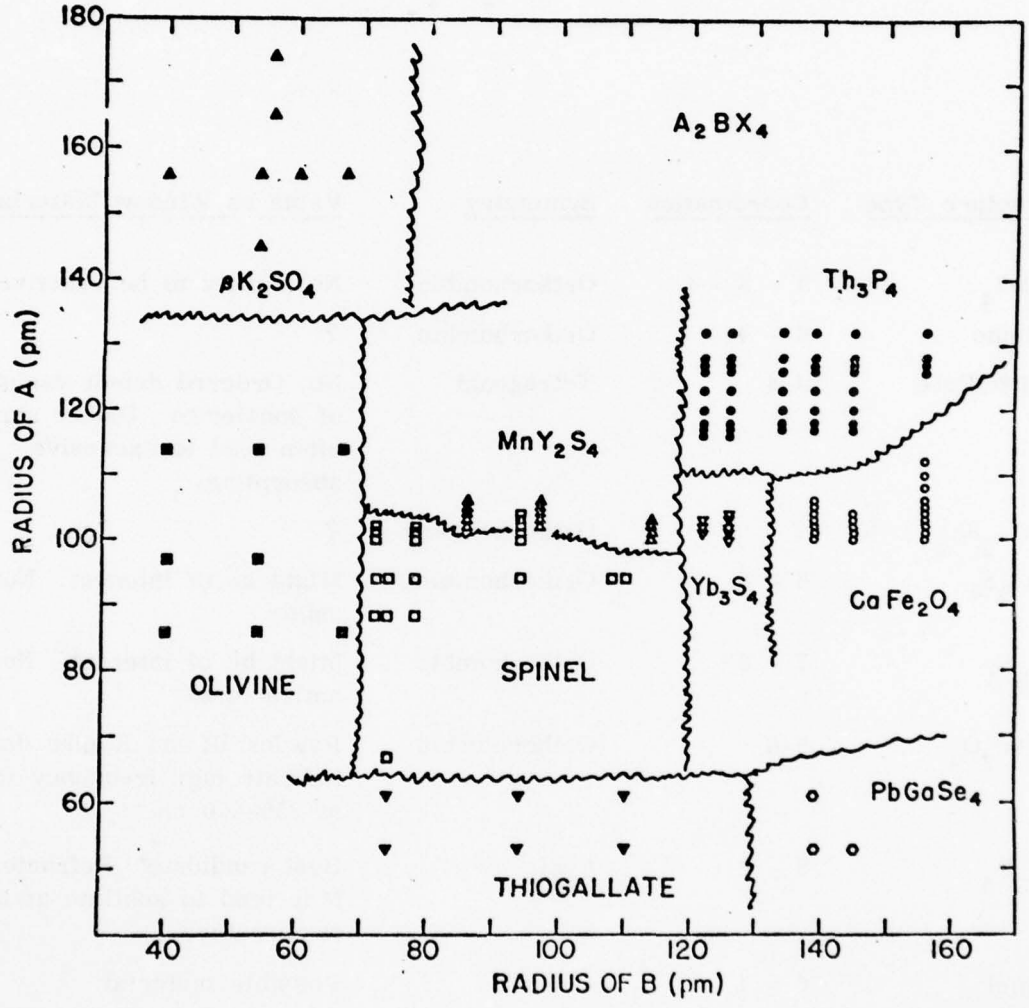

FIGURE 29. Structures of the Ternary and Chalcogenides

TABLE 3-5. The Main A_2BX_4 Structural Families

Structure Type	Coordination	Symmetry	Value as Window Material
K_2SO_4	9 - 8 - 4	Orthorhombic	No. Likely to be reactive
Olivine	6 - 4	Orthorhombic	?
Thiogallate	4-4	Tetragonal	No. Ordered defect variant of sphalerite. Defect states often lead to excessive absorption.
$PbGa_2Se_4$	?	Orthorhombic	?
MnY_2S_4	6 - 6	Orthorhombic	Might be of interest. Not cubic.
Yb_3S_4	7 - 6	Orthorhombic	Might be of interest. No. optical data.
$CaFe_2O_4$	8-6	Orthorhombic	Powder IR and Raman data indicate high frequency modes at 350-400 cm^{-1}.
Th_3P_4	8 - 8	Cubic	Best candidate. Refractory May tend to sublime at high temperatures.
Spinel	6 - 4	Cubic	Possible material.
$CaHo_2Se_4$	6 - 6	Rhombohedral	No. Ordered defect NaCl structure. Defects likely to lead to extrinsic absorption.

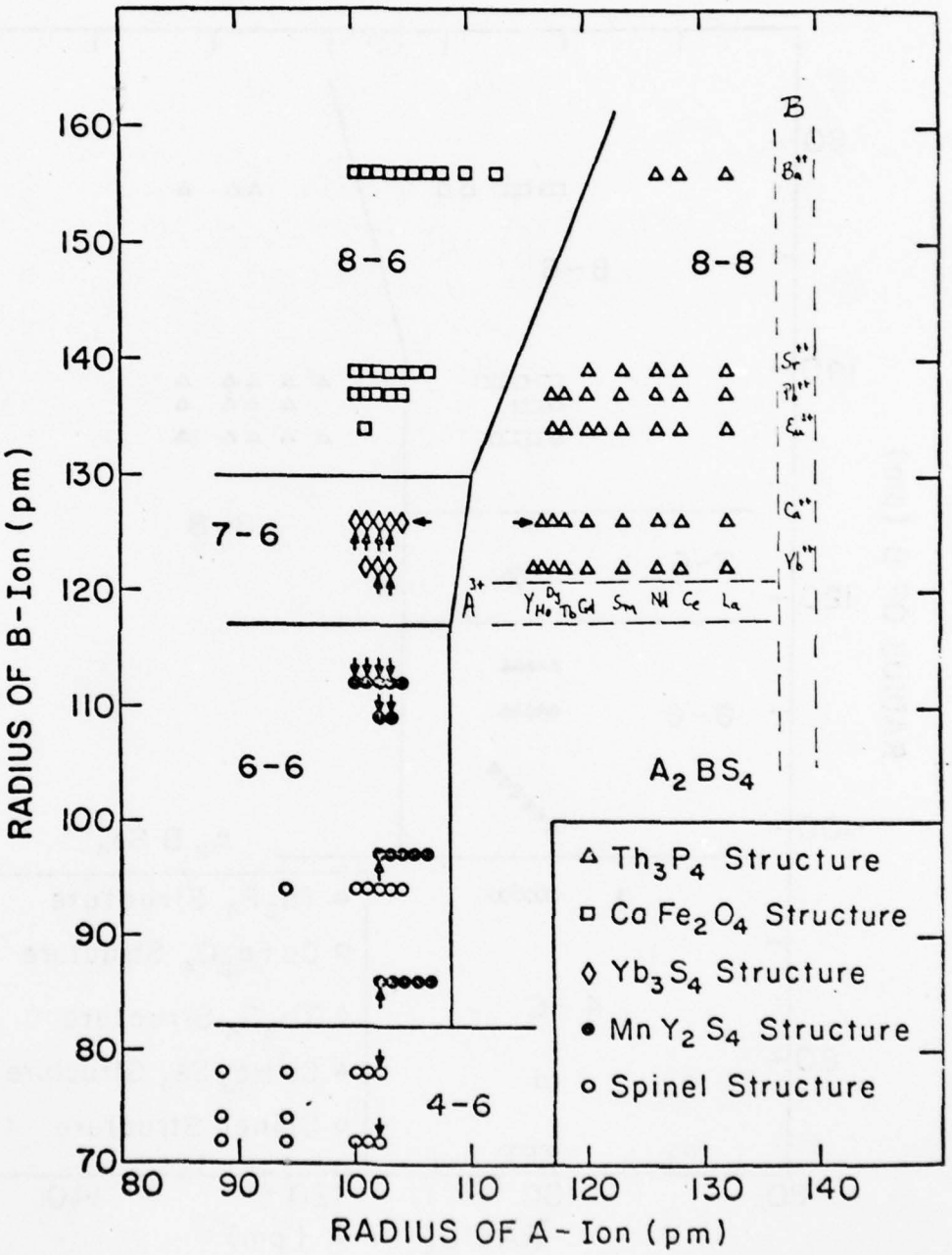

FIGURE 30. Structures of the Ternary Chalcogenides - Detail 1.

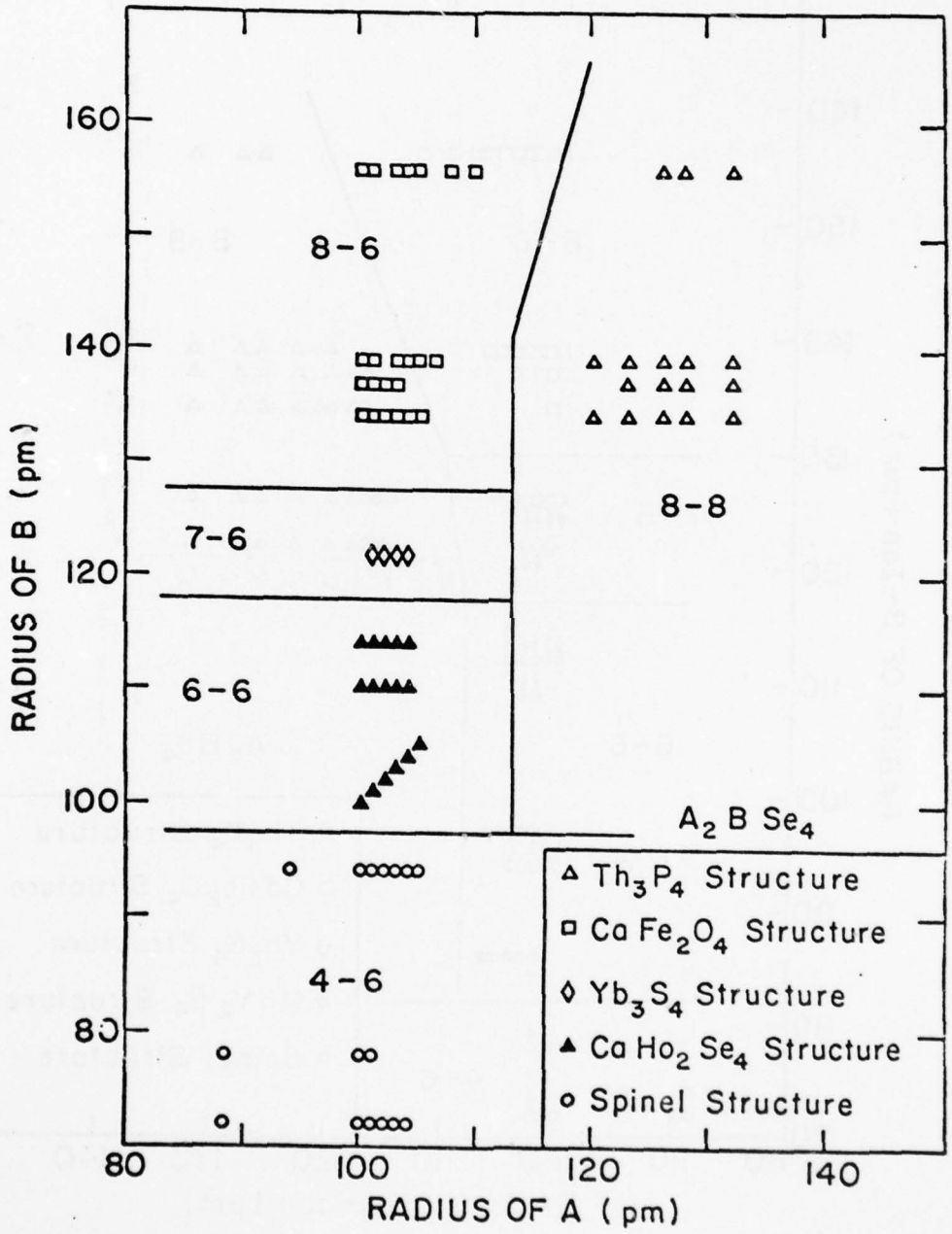

FIGURE 31. Structures of the Ternary Chalcogenides - Detail 2.

Measured Electronic Band Gaps of Some Ternary Sulfides With the Th_3P_4 Structure, $A(RE)_2S_4$

A	La	Pr	Nd	Sm
Ca	2.70	2.88	2.70	2.17
Sr	2.82	2.70	2.58	2.48
Ba	2.88	2.82	--	--

Gap energies in electron volts

Infrared spectra have been measured on a hot-pressed specimen of $SrNd_2S_4$ (Provenzano et al., 1977)[74]. Figure 32 shows that the main absorption peaks are in the range of 100 to 300 cm^{-1} and that the material appears to have good infrared transmission characteristics in the infrared. The high transmission region is estimated and these data would need to be verified by better experimental measurements.

The Th_3P_4 structure sulfides are said to be moderately refractory with melting points in the range of 1800°C. These data need to be verified because the materials have not been melted. Some of them appear to have high vapor pressures at temperatures close to the melting point. They are known to be stable to temperatures at least as high as 1400°C (Provenzano and White, 1974[73].

There are few data on the hardness, thermal conductivity, thermal expansion or other related thermomechanical properties of these compounds. Most of the available literature data comes from the laboratory of Professor Jean Flahout at the University of Paris and this group has as its primary interest the crystal structure and crystal chemistry of sulfide compounds, not their physical properties.

Other Chalcogenide Materials

On the map of ternary structural families are several others which might be of some interest as window materials except that the available data are too fragmentary for evaluation.

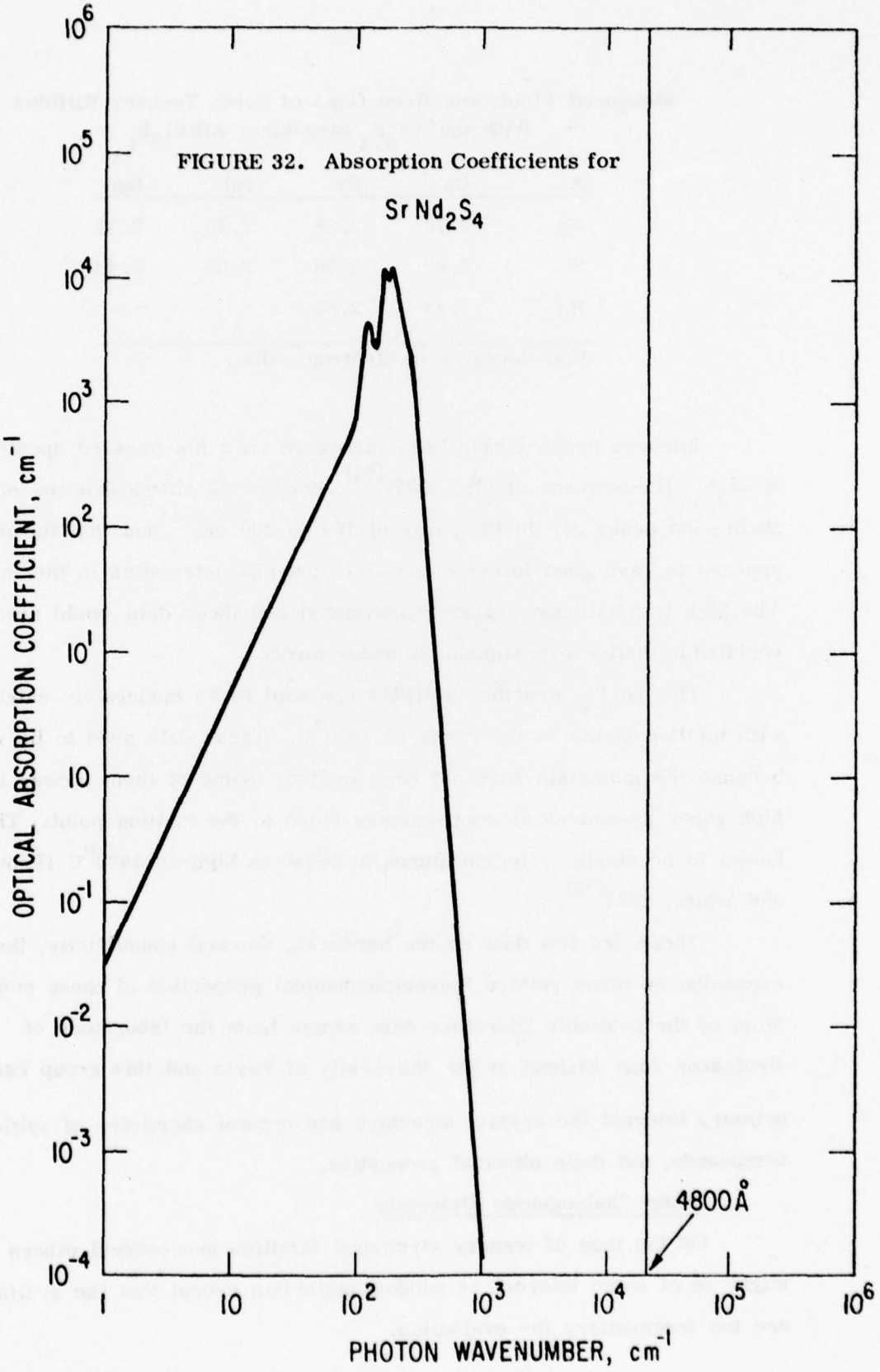

FIGURE 32. Absorption Coefficients for $SrNd_2S_4$

Sulfides with the spinel structure are cubic and so could be used in CVD or hot-pressed forms. The vibrational frequencies are somewhat higher, but the materials are transparent to beyond 15 micrometers. These materials are less refractory than the Th_3P_4 structure materials.

Sulfides with the $CaFe_2O_4$ structure are orthorhombic so that use of polycrystalline pieces would be difficult. The infrared spectra (Figure 33) shows a complex pattern of absorption bands. With its 8-6 coordination scheme, the highest frequency modes of the $CaFe_2O_4$ structure sulfides fall between those of the 4-6 coordinated spinels and the 8-8 coordinated Th_3P_4 structures.

The sulfide materials with the MnY_2S_4 structure fall into the right part of the structure field map to be interesting but there appear to be no spectral data at all.

3.9 Nitrides

The interest in structural nitride ceramics comes from their very high operating temperatures, their high strengths, and their low thermal expansion coefficients. In general their regions of optical transparency will be about the same as those of other nitrides. The optical absorption curves for AIN, cubic BN, and Si_3N_4 are shown in the collection. A short list of the possibly interesting nitrides is given in Table 3-6. Boron nitride has been omitted because in the graphitic form it is too soft and in the cubic form, made under high pressure, it does not seem to have optical properties sufficently better than AIN to justify using the small sample sizes that are available.

The thermal expansion coefficient of the Si-N bond is[75] $3.7 \times 10^{-6}/^{o}K$ compared to $1.3 \times 10^{-6}/^{o}K$ for the Si-O bond[75]. Hence the nitrides do have thermal expansion coefficients as low as those of the oxides. The expansion coefficient of the Si-N bond at high temperatures is $4.4 \times 10^{-6}/^{o}C$ while at high temperatures in AIN it is $6.5 \times 10^{-6}/^{o}K$[26]. There are no published values

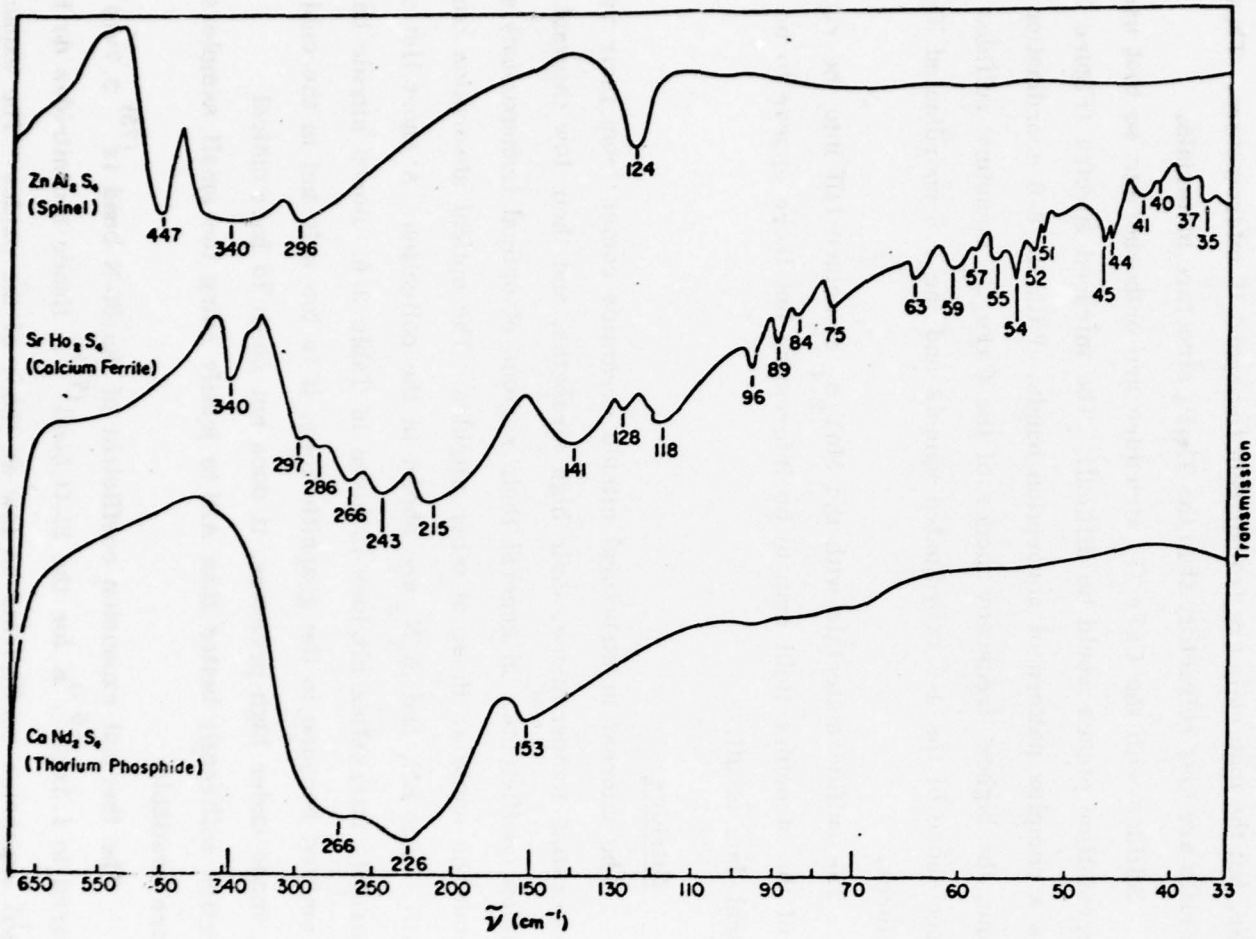

FIGURE 33. Infrared Spectra - Sulfides with the $CaFe_2O_4$

TABLE 3-6: Nitrides for Optical Windows

Material	β at 1000°K 10^{-6}/°K	$\Delta\beta$ 10^{-6}/°K	Sublimation T°K	Micro-hardness kg/mm^2	Bulk Modulus 10^{13} dyn/cm^2
β-Be_3N_2	?	?	2750		
AlN	6.2	0.9	2700	1200	22
β-Si_3N_4	4.4	0.4	2160	3400	22.5
$BeSiN_2$	7.3	0.5	~2500		
Mg_3N_2					
Cubic BN	6.0	0	2670*	4600	29

* over hex. BN

for the Be-N bond. However, this has recently been measured[76] approximately by studying the thermal expansion of $BeSiN_2$ at high temperatures. At 1000°K the results were $\beta_c = 7.0 \times 10^{-6}/^{o}K$ and $\beta_a = 7.5 \times 10^{-6}/^{o}K$ for $BeSiN_2$ (pseudo-hexagonal). Thus the Be-N bond expansion coefficient is higher than that of the Si-N bond. For comparison the B-N bond in cubic BN has an expansion coefficient[26] of $6.0 \times 10^{-6}/^{o}K$. The average thermal expansion coefficients and anisotropies for some nitrides are given in Table 3-6. The values for cubic BN and Mg_3N_2 are given for comparison.

The moderate thermal expansion values, the small thermal expansion anisotropies, and the high hardness values in Table 3-6 make these nitrides look useful. The upper operating temperature is limited by the dissociation into metal plus nitrogen. The sublimation temperatures in Table 3-6 are the temperatures at which the total dissociation pressure[77-81] equals one atmosphere. It is clear that Mg_3N_2 is not very stable at high temperatures, and offers no advantages over oxides. The Si_3N_4 will probably be stable to 1773°K, particularly with a thin surface coating of silicon oxynitride glass. The same will be true of $BeSiN_2$, but the surface may be Be_2SiO_4 plus SiO_2. The AlN and Be_3N_2 may be useful to almost 2273°K with surface coatings of Al_2O_3 or BeO. The four nitride compounds β-Be_3N_2, AlN, β-Si_3N_4, and $BeSiN_2$ have intrinsic optical transparency in the UV, VIS, IR1, and RADAR regions. AlN may have some possibilities in IR2. They will all be strongly absorbing in IR3 and IR4.

3.10 Oxy-Nitrides

It is possible to make many different metal oxynitride compounds of Be, Si, Al, Y, etc. One of the simplest is Si_2ON_2. Ceramic bodies[82] of Si_2ON_2 have been made which show that its average thermal expansion coefficient is small[75, 82]. Its operating temperature limit is about like that of Si_3N_4, as is its optical transparency. The great disadvantage of Si_2ON_2 is the anisotropy of the thermal expansion coefficient[75] $\Delta\beta \simeq 2.8 \times 10^{-6}/^{o}K$ over the range 300°K to 1300°K. Thus transparent,

polycrystalline ceramic bodies may be difficult to fabricate and may crack internally on thermal cycling.

There are a wide range of mixed crystals between Si_3N_4 and Al_3O_3N called beta-prime sialons. These may or may not have advantages over pure Si_3N_4 for optical windows. For example oxidation resistance may be improved[83] without appreciably changing the thermal expansion coefficients. The optical transmission spectra will be similar to Si_3N_4.

There are other possibilities in the oxynitrides[83]. The clue to obtaining low thermal expansion coefficients appears to be in modifying the SiO_2 structures in such a way that the SiO_4 tetrahedra cannot rotate as the temperature is changed. This prevention of rotation is rather successful in beryl. It might be possible to make a beryl structure without Be by replacing the Be with Al or Si and replacing O with N to maintain charge neutrality. These new compounds would be:

$$Al_5Si_6O_{15}N_3$$

$$Al_2Si_9O_{12}N_6$$

A scandium or yttrium analog might be:

$$Sc_2Si_9O_{12}N_6$$

Here the Sc is in octahedral sites; the Si in tetrahedral sites. Such compounds are not yet known but there are many possibilities. For some such compounds, the thermal expansion anistropy and magnitude might be less than in beryl and the upper temperature limit might be greater. This may be an area of fruitful research.

McCauley at Army Mechanics and Materials Research Center (AMMRC) has successfully synthesized a transparent $xAl_2O_3 \cdot yAlN$ with a cubic structure and a high congruent melting point. This material is similar to Al_2O_3 in its thermostructural characteristics with the important advantage of the cubic structure.

3.11 Highly Anisotropic Materials For Radar

There are a number of oxides whose average thermal expansion in a polycrystalline body is small but exhibit a large anisotropy in the thermal expansion coefficient. Some of these, such as Al_2TiO_5 and others, were mentioned earlier. Such ceramic bodies might be quite transparent at RADAR wavelengths but not in the UV, VIS, or IR. Microcracking would tend to make them opaque at these shorter wavelengths. If transparency only for RADAR is desirable, then these ceramics might perform. If multirange optical pass bands are desired, then they should probably be avoided.

3.12 Conclusions - Selection of New Candidate Materials For Windows

The foregoing comprehensive analysis has identified a variety of materials which have the potential of being developed to meet the advancing needs of the DoD. Some of these materials could operate in optical/thermal regions for which no materials are currently available. In addition, this analysis indicates that many of these new materials should exhibit thermal shock and stress resistances superior to those of the conventional materials used for these purposes.

A problem exists on deciding which of these new materials should receive emphasis and this decision must be weighed heavily with respect to the identification of critical applications. The list in Table 3-7, however, covers the major portion of the optical spectrum required for the overall range of possible applications and includes, within the range, candidates presently considered to be of highest overall potential for performance. It should be noted that Table 3-7 is the current estimate of potential performance level of each candidate including cation substitution or optimization of the bandpass in the case of solid solution candidates. Figure 34 depicts these candidates on a bandpass versus use temperature map.

For the very high temperature regime and up to the IR2 band, the simple oxides, Y_2O_3 and ThO_2, should be selected as back up to nitrides and would be top candidates for experimentation studies of "toughening" mechanisms. The results of such studies may lead to improved thermal stress

TABLE 3-7 Summary of New Candidate Materials for Windows

Class	Materials	Max. Temp. °K	Band Pass*					
			UV	VIS	IR1	IR2	IR3	IR4
A	$2ZnO \cdot GeO_2$	1273		o	o	o		
B	$ThO_2 \cdot GeO_2$	1273		o	o	o		
C	$3CaO \cdot 5Al_2O_3$	1273	o	o	o	o		
D	$HfO_2 \cdot WO_3 \cdot Ta_2O_5$	1273		o	o	o		
E	$xTa_2O_5 \cdot yWO_3$	1273			o	o		
F	$xHfO_2 \cdot yTiO_2$	1773		o	o	o		
G	$Cs_2O \cdot Al_2O_3 \cdot 4SiO_2$	1273		o	o	o		
H	$ZrO_2 \cdot SiO_2$	1773	o	o	o	o		
I	$2ZnO \cdot SiO_2$	1273			o	o		
J	$3Al_2O_3 \cdot 2SiO_2$	1773	o	o	o	o		
K	$2MgO \cdot 2Al_2O_3 \cdot 5SiO_2$	1273	o	o	o	o		
L	$B_4Al_{18}O_{33}$	1773	o	o	o	o		
M	$Be_3Al_2(SiO_3)_6$	1273	o	o	o	o		
N	SnO_2	1273			o	o		
O	Nb_2O_5	1273			o	o		
P	ThO_2	2273	o	o	o	o		
Q	Y_2O_3	2273	o	o	o	o		
R	EuO	773			o	o	o	
S	$BeSiN_2$	2273	o	o	o			
T	$BeSiN_2$ - AlN (SS)	2273	o	o	o	o		

*All candidates good in RADAR range.

TABLE 3-7. Summary of New Candidate Materials for Windows
(continued)

Class	Materials	Max. Temp. °K	Band Pass*					
			UV	VIS	IR1	IR2	IR3	IR4
U	$Al_5Si_6O_{15}N_3$ $Al_2Si_9O_{12}N_6$ $Sc_2Si_9O_{12}N_6$	1773	o	o	o	o		
V	$CaLa_2S_4$ $SrLa_2S_4$ $BaLa_2S_4$	773		o	o	o	o	o
W	Diamond	1273	o	o	o		o	o

*All candidates good in RADAR range.

UV 0.2 - 0.4 microns
VIS 0.4 - 0.7
IR 1 0.7 - 3.0
IR 2 3.0 - 5.5
IR 3 7.5 - 10.0
IR 4 10.0 - 14.5

THERMAL / OPTICAL	300 - 773°K (LOW)	300 - 1273°K (MODERATE)	300 - 1773°K (HIGH)	300 - 2273°K (VERY HIGH)
UV 0.2-0.4 μm	C H J K L M P Q S T U W	C H J K L M P Q S T U W	H J L P Q S T U	P Q S T
VIS 0.4 - 0.7	A B C D E F G H J K L M P Q S T U V W	A B C D F G H J K L M P Q S T U W	F H J L P Q S T U	P Q S T
IR1 0.7 - 3.0	A B C D E F G H I J K L M N O P Q R S T U V	A B C D E F G H I J K L M N O P Q S T U	F H J L P Q S T U	P Q S T
IR2 3.0 - 5.5	A B C D E F G H I J K L M N O P Q R T U V	A B C D E F G H I J K L M N O P Q T U	F H L P Q T U	P Q T
IR3 7.5 - 10	R V W	W		
IR4 10 - 14.5	V W	W		
RADAR 1000 - ∞	ALL OF ABOVE	ALL OF ABOVE	ALL OF ABOVE	ALL OF ABOVE

FIGURE 34. Selection Matrix

performance of those materials, per se, and, in any event, such information is of critical interest to development of optimum properties of all the ceramics addressed in the program.

The next section discusses the potential for increasing the fracture toughness of the candidate materials.

SECTION 4

ENHANCED FRACTURE TOUGHNESS

SECTION 4

ENHANCED FRACTURE TOUGHNESS

4.1 Introduction

Improvements in the thermal shock and erosion resistance, and strength will be desirable, perhaps even necessary, for the various candidate materials. The 5μm cut-off requirement for the near IR eliminates most of the refractory materials with high inherent strengths or fracture toughnesses. The need is even more acute for the 8-14μm range where the covalent compounds or oxides with high strength, and/or low thermal expansion coefficient, α, are not transparent. The high molecular weight oxides, and the chalcogenide semiconductors generally have high expansions and low strength and fracture toughness.

The optically suitable materials are generally brittle at room temperature and perhaps through the entire service temperature range. The fracture strength:

$$\sigma_f = y \frac{K_{IC}}{\sqrt{a}} \qquad (1)$$

where y is of order unity, can be improved either from a reduction in flaw size, a, by careful processing, or by an increase in fracture toughness, K_{IC}, or fracture surface energy, γ_f, ($K_{IC} = \sqrt{2E\gamma_f}$, where E is Young's modulus). Improvements in K_{IC} reduce the sensitivity to processing induced flaws and the strength degradation from thermal shock or erosion.

Recently, improvements in K_{IC} have been obtained in a few ceramic materials using second phases, elongated grains, microcracks or combinations of these. Currently, the theoretical basis for understanding and optimizing these toughening mechanisms is incomplete.

4.2 Requirements

Following Hasselman[1], the critical temperature change which will cause propagation of cracks from thermal shock is:

$$\Delta T_{crit} = \left[\frac{\pi \gamma_f (1-2\nu)^2}{2E\alpha^2(1-\nu^2)}\right]^{1/2} \left[1 + \frac{16(1-\nu^2)Na_o^3}{9(1-2\nu)}\right] a_o^{-1/2} \qquad (2)$$

where N is the number of cracks per unit volume of initial size, a_o , and ν Poisson's ratio. The frequently used criterion for high strength materials is equivalent to the case where $(\gamma_f/E\alpha^2 a_o)^{1/2}$ is sufficiently high that $\Delta T < \Delta T_{crit}$ and no damage results. The thermal conductivity, K, is unimportant for rapid heating cases where $K/thc^{\nu} < 1$ (t is the thickness, h the heat transfer coefficient, and c^{ν} the volumetric heat capacity). If the thermal shock is too severe, propagation will occur with the final crack size given by:[1]

$$a_f = \left[\frac{3(1-2\nu)}{8(1-\nu^2)\, a_o N}\right]^{1/2} \qquad (3)$$

Thus, higher strength materials will be degraded more than weaker ones, and may fail catastrophically.

4.3 Toughening Approaches

Improved thermal shock resistance can be obtained by a high density of microcracks. The strength degradation is reduced, Eq. (3), as the crack density is increased. If the crack density is high enough, i.e., $a^3_o N > 1$, ΔT_{crit} is increased directly by reducing the total strain energy to cause crack propagation; in this case, cracks will be close enough together to interact which lowers the strength. At lower microcrack densities, indirect benefits may result from an increase in γ_f. This results because the microcracks can cause crack blunting, and branching and deflection and can reduce the stress intensity ahead of a larger crack.

The erosion resistance is also greatly improved by higher values of K_{IC} although it is also sensitive to flaw size and surface condition. Evans[2] has developed semi-empirical correlations showing that the threshold velocity for

damage increases with K_{IC}. Perhaps more importantly, the retained strength is proportional to $K_{IC}^{1.4}$ and the mass loss is proportional to $K_{IC}^{-1.5}$. Caution must be exercised in generalizing these correlations to two phase or microcrack toughened materials. To be beneficial, the size of the important microstructural elements must be finer than the size of the contact circle of the impacting particles or droplets. Possibly microcracks which decrease K_{IC} will lower the incubation time but still provide a reduction in the steady state rate of mass loss.

Optical requirements place restrictions on the size and distribution of second phases, cracks and pores in addition to those necessary to optimize mechanical properties. For any useful volume fraction, V_p, of second phase compound, it must also be transparent at the wavelength of interest and scattering must be sufficiently small. A guide to the size requirements can be obtained from the Raleigh scattering theory. For spherical particles of radius d, the transmitted intensity is[3]:

$$I = I_o e^{-St} \tag{4}$$

and for d

$$S = \frac{4\pi^4 V_p n_m^4}{d} \left(\frac{d}{\lambda_o}\right)^4 \left| \frac{(n_p/n_m)^2 - 1}{(n_p/n_m)^2 + 2} \right|^2 \tag{5}$$

when the fractional difference in the refractive index of the particles, n_p, and n_n is small, i.e., $\eta = (n_p - n_m)/n_m < 0.3$

$$S = \frac{16\pi^4 V_p n_m^4}{9d} \left(\frac{d}{\lambda_o}\right)^4 \eta^2 \left(1 - \frac{\eta}{3} - \frac{5}{12}\eta^2\right) \tag{5a}$$

Typically, λ_o/d must be 20-100 or larger. The effect of small whiskers or plates can be estimated using the volume equivalent sphere diameter.

Particle Toughening:

Recently, it has been shown that second phase particles which impede crack propagation can produce modest increases in K_{IC}. Strong particles apparently inhibit the propagation which increases crack front energy as it bows between particles.[4,5] Modulus mismatches or coherency strains from small precipitates may also increase K_{IC}. A relevant example is reported for single crystals of Al_2O_3 rich ($3Al_2O_3 \cdot MgO$) spinel; optimum aging produced an increase of K_{IC} from 1.5 to 2.6 $MN/m^{3/2}$. The highest toughness resulted from the presence of Al_2O_3 rich "pre-precipitates" or G. P. zones $\sim 40\text{Å}$ in size[6]. Several other more dramatic methods have also been demonstrated.

Fiber or Whisker Reinforcement:

For brittle matrices, fiber or whisker reinforcement will produce significant increases in K_{IC} only if the fiber is "stronger" than the matrix. Using 100 μm diameter SiC fibers in porous, reaction bonded Si_3N_4 values of K_{IC} = 8-12 $MN/m^{3/2}$ but with σ = 130-55 MPa were observed.[7] Obviously, this is only useful for $\lambda > 1$ mm, and the erosion resistance would be suspect.

For dense systems, toughening can be anticipated only if the K_{IC} (single crystal value) of the fiber is significantly greater than that of the matrix, or if there is a lower strength interface (e.g., a weaker glassy phase). There are few, if any, compounds with single crystal K_{IC} values proven to be high enough to reinforce the harder nitrides or oxides of current interest. However, a variant of this mechanism apparently explains the relatively high values of K_{IC}, 5-6.6 $MN/m^{3/2}$, obtained for dense Si_3N_4 in which the grains are elongated (K_{IC} = 3.1 $MN/m^{3/2}$ for equiaxed grains). This results from the anisotropy in K_{IC} in Si_3N_4 and/or from a glassy grain boundary phase.

Transformation Induced Toughening:

Significant toughening can be obtained by heat treating partially stabilized ZrO_2. Reported K_{IC} values are as high as 9.5 $MN/m^{3/2}$ for ZrO_2 + 3% CaO[9] and 6 $MN/m^{3/2}$ for ZrO_2 + 8% MgO[10] compared to 2.8 $MN/m^{3/2}$ for untreated ZrO_2. Strengths are 500 MPa. Optimum aging results in coherent precipitates of pure ZrO_2 which are 0.1 μm in diameter for the ZrO_2-CaO system[9] and are ellipsoids about 0.5 μm in diameter and 0.07 μm thick for the ZrO_2-MgO system[10].

The coherent precipitates are retained in the high temperature tetragonal (T) phase. In the stress field ahead of a crack, the precipitates transform to the low temperature monoclinic phase (M). The toughening apparently results from the lattice invariant plastic strain accompanying transformation, and the effect of the transformation induced strains around the particles on the stress field ahead of the crack tip[10].

Recently, similar toughening to $K_{IC} = 9\ MN/m^{3/2}$ has been reported[11] in Si_3N_4 with 20% ZrO_2 ($\sim 1\ \mu m$ diameter). The Si_3N_4 matrix is apparently strong enough to prevent the T→M transformation during cooling to room temperature. The requirement is for a second phase particles which undergo a phase transformation with a significant shape or volume change and which occurs martenstically so it is difficult, but not quite impossible to supress. The toughening will only be effective at temperatures below the T→M transformation temperature, about 1000-1100°C for ZrO_2.

Microcracked Systems:

Microcracks which are pre-existant or nucleate ahead of a larger crack or flaw, can produce toughening. Microcracking can be achieved using second phase particles with a lower expansion coefficient or from thermal expansion anisotropy of the matrix compound. An optimum particle size and volume loading are typically observed. This results because larger microcracks propagate more easily; if they are too large, they may provide less toughening and will lower the strength. Conversely, if the particles are less than a critical size, microcracks do not nucleate. The critical size can be reduced and the toughening further enhanced by increasing the volume misfit. This has been achieved in Al_2O_3 using unstabilized ZrO_2 in which the volume change accompanying the T→M transformation increases the misfit stresses with 15 v/o of 4 μm particles $K_{IC} = 10\ MN/m^{3/2}$ and $\sigma = 500$ MPa were obtained.[12]

Easy Cleavage Phases:

A variant of the microcrack toughening is to use a dispersion of a second phase with an easy cleavage plane. Such systems may not be precracked but provide similar benefits by crack nucleation with the particles. The machinable glass

ceramics have precipitated mica flakes, 50 μm in diameter, and 0.6 μm thick, which give K_{IC} = 2 MN/m$^{3/2}$, about a factor of 3 increase over glass. Mica flakes, 30 μm in diameter and 10 μm thick, added to Al_2O_3 produced K_{IC} = 8.5 MN/m$^{3/2}$ and σ = 400 MPa at 10 v/o.[14] The thermal shock resistance is significantly improved in these two materials,[13,14] and it has similarly been improved using hexagonal BN additions to Al_2O_3.[15] This technique is probably most effective with a material which has one easy cleavage plane and is strong in the other two directions.

4.4 Application to Window Materials

Toughness increases of a factor of 2-3 and improved thermal shock resistance have been achieved in several ceramics. These are summarized in Table 4-1 which includes calculated values of the parameter $(\gamma_f/E\alpha^2)^{1/2}$ which is a good measure of the crack stability under thermal shock.[1] Most of these have not been fully optimized for mechanical properties, and none of them have been made to optical quality. Typically, there are too many pores and absorbing impurities and the toughening particles are too coarse. Further, several of the materials are inappropriate for the wavelengths of interest, e.g., mica, BN, and Si_3N_4 cut-off at 3-4 μm or less. By applying these techniques to appropriate materials and developing adequate fabrication procedures, improved thermal shock and mechanical properties with satisfactory transparency can be anticipated.

Using typical values of n, λ, and V_p to calculate the scattering coefficient, Eq. (5), indicates the ranges of acceptable particle sizes. For transparency in the visible or near IR, the refractive index match between the two phases must be within a few percent, $\eta < 0.05$ to allow particles as large as 100-200 Å. For the mid- and far IR windows, particles can be 0.1-0.5 μm if $\eta < 0.05$. If the index match is poor, particles as fine as 200-300 Å may be required. When there are pre-existant microcracks, the additional scattering will require even finer particles.

ZrO_2/HfO_2

Partially stabilized ZrO_2 is attractive because toughening has already been demonstrated with second phase particles of an acceptable size for IR applications

TABLE 4-1. Fracture Toughness and Thermal Shock Resistance

Material	K_{IC}, $MN/m^{3/2}$	γ_f, J/m^2	E, GN/m^2	α, $°C^{-1}$	R@, $m^{1/2}$-°K
RB Si_3N_4 + 5% SiC Fiber†	12	900	73*	2.9×10^{-6}	38.
RB Si_3N_4 + 25% SiC Fiber†	8	200	146*	3.2	12.
Si_3N_4 + 20% ZrO_2	9	140	284*	4.2	5.3
Si_3N_4 (Elong. grns.)	6.6	70	310	2.8	5.4
Si_3N_4 (Equi. grns.)	3.1	16	310	2.8	2.5
ZrO_2 + 3% CaO	9.5	250	~180	~7	5.3
ZrO_2 + 8% MgO	6.0	100	~180	~8	2.9
Al_2O_3 + 15% ZrO_2	10	130	375*	8.3*	2.3
Al_2O_3 + 10% Mica	8.5	104	350	9	1.9
SiC	4.8	25	470	4.3	1.7
Al_2O_3	4.5	25	410	8.0	0.97
Al_2O_3 (Sing. Crys.)$(10\bar{1}1)$	2.2	6.0	410	8.0	0.47
Al_2O_3 (Sing. Crys.)(0001)	>5.8	>40	410	8.0	>1.3
$ZrSiO_4$	(2.3**)	(15**)	>170	5.6	(1.7)
$3Al_2O_3 \cdot 2SiO_2$	(2.6**)	(15**)	220	5.1	(1.6)
ZrO_2 (cubic)	2.8	16	250	10	0.79
$MgO \cdot 3Al_2O_3$ (Sing. Crys.)	1.5	4.7	~240	~9	0.49
$MgO \cdot 3Al_2O_3$ (S.C.-aged)	2.6	14	~240	~9	0.85
MgO	2.2	8	310	13.5	0.37
ThO_2	(2.3**)	(10**)	258	9	(0.69)
SiO_2 (glass)	0.82	4.7	72	0.5	16
Machinable Glass-Ceram.	21.	32	68	5.1	4.2
Pyroceram 9605	1.0	4	140	1.4	3.8
Pyroceram 9606	1.0	4	120	5.7	1.0
ZnSe	0.9	5.5	74	7.8	1.1
MgF_2	0.9	3.8	110	12	0.48

@ $R \equiv (\gamma_f/E\alpha^2)^{1/2} = K_{IC}/E\alpha\sqrt{2}$

* Estimated by Law of Mixtures

** Estimated

† Low density, low strength matrix; K_{IC} would probably overestimate erosion resistance.

References: K_{IC}, γ; 2, 6-14, 23-27

E, α; 7,9,13,14,27-29

eventhough its optical properties may be inferior to other mid IR candidates. The phase diagram for HfO_2-CaO is essentially the same as for ZrO_2-CaO[16], so similar toughening should be achievable. HfO_2 offers the additional advantages of lower α, presumably high IR cut-off, and a higher transformation temperature range for the T⟶M transformation, ~ 1600°C compared to ~ 1050°C for ZrO_2.

ZrO_2/HfO_2 - Toughening of Other Materials

Unstabilized ZrO_2 or HfO_2 can be used to toughen other mid IR candidate materials. At the fine particle sizes which are required, the T⟶M transformation may be suppressed giving the prospects of transformation induced toughening rather than pre-existant microcracking. This technique will be limited to materials which are unreactive with ZrO_2/HfO_2 and which do not stabilize the cubic phase of ZrO_2/HfO_2. The necessary phase diagrams are not available for most of the mid-IR candidate materials. Toughening of Y_2O_3 will not be possible based on existing phase diagrams.[16] Investigation of the stability with $BeSiN_2$, BP, the AlSiON compounds, and mixed oxides such as $B_4Al_{18}O_{13}$, cordierite ($Mg_2Al_4Si_5O_{18}$) and beryl ($Be_3Al_2Si_6O_{18}$) will likely indicate other possibilities.

Three obvious candidate systems can be identified. ZrO_2 or HfO_2 are stable with $ZrSiO_4$ or $HfSiO_4$.[16] The ternary phase diagram[16] indicates that ZrO_2 exists in equilibrium with mullite, $3Al_2O_3 \cdot 2SiO_2$. The effects of SiO_2 or Al_2O_3 on the M⟶T transformation have not been confirmed, however. The ThO_2 - ZrO_2 phase diagram[16] indicates that the T and M phases of ZrO_2 are equilibrium with ThO_2. Further, above 2000°C the ZrO_2 can be dissolved in ThO_2 and aging heat treatment to give fine, possibly coherent precipitates should be possible. ThO_2 plus ZrO_2 or HfO_2 offer particularly promising systems in which to developing high toughness in a material with a cut-off over 6 μ m.

Other transparent compounds with similar martensitic phase transformations could be used for toughening. No sulfides or other chalcogenides with appropriate transformations and transparencies in the far IR are presently known to the authors, although there are many such compounds with order-disorder or other second order transformations. Unfortunately, the volume and shape changes are usually small for these.

Easy Cleavage Phases

Another technique with the potential for toughening with dispersed particles of the order of 0.1 μm in size, is the use of dispersions of compounds with an easy cleavage plane. Many chalcogenides such as MoS_2 have hexagonal or distorted hexagonal crystal structures which cleave easily on the basal plane. Table 4-2 lists some of these layer compounds and relevant properties.[17, 18] The thermal properties of many of these compounds are not well established. Many are degenerate semiconductors or nearly metallic conductors and so the absorption coefficient will be too high; frequently, E_g is too small for transparency in the visible or even mid-IR.

The most promising of these compounds are HfS_2 or ZrS_2. The resistivities are high enough to suggest acceptable absorptivities[19]. Further, the sulfur vapor pressure over ZrS_2 is only 10^{-8} atm at 900°C[20] so vaporization rates may be low enough. For a dispersed phase, higher vaporization rates and lower melting points can be tolerated than for the matrix phase. Although much less refractory, GaS, GaSe and SnS_2, may also be useful. A dispersed phase of one of the layer compound sulfides or selinides in a compound such as $SrLa_2S_4$ or EuS offers a prospect for a higher toughness material for use in the far IR. Both the thermodynamic stability and the optical behavior of the "doped" compounds which have been equilibrated with each other must be determined before the most promising systems can be identified.

Microcracked Systems for the Radar Range

Systems with coarser particles or larger microcracks can be used in the radar range. Coarser (1-5 μm) ZrO_2 or HfO_2 particles can be used in any of the materials in which they are stable. The higher transformation temperature of HfO_2 may be a major advantage Dispersions of BN or mica can also be used in windows for the radar range BN is more refractory and probably stable with more compounds, but mica may provide better toughening. BN is probably stable with most of the compounds which would be of interest in the radar range such as $BeSiN_2$, AlSiON compounds and simple or mixed oxides. For these materials, the optimum particle sizes will be determined by thermal shock and erosion considerations, rather than scattering.

TABLE 4-2: Layer Compounds

Material	Structure	Tmp, °C	Comments
$CoSe_{1+x}$, $CoTe_{1+x}$,	$NiAs \rightarrow CdI_2$	~900	too conductive
GaS	hex	970	semiconductor
GaSe	hex	960	semiconductor
GaTe	monocl.	835	semiconductor
HfS_2	CdI_2-hex	high	Eg = 1.96, 2.1eV, $\rho \sim 10^8$ Ωcm
Hf_2S_3	$NiAs \rightarrow CdI_2$	high	
$HfSe_2$	CdI_2	high?	Eg + 1.13eV
MoS_2	MoS_2-hex	>1800	Eg = 1.1eV, metallic >200°C
$MoTe_2$	MoS_2	>1200	Eg = 1.9eV
NbS_2	hex	high	metallic
$NiSe_{1+x}$, $NiTe_{1+x}$	$NiAs \rightarrow CdI_2$	~900	too conductive
SnS_2	CdI_2	860	Eg = 2.2eV, $\rho \sim 10^8$ Ω-cm
TaX_2†	hex	high	metallic
Th_2X_3, U_2X_3	Sb_2S_3 -rhomb*	1500-2000+	prob. too conductive
ThX_2, UX_2	$PbCl_2$-rhomb@	1500-2000+	prob. too conductive
TiX_2	CdI_2		metallic
WS_2	MoS_2	>1800	Eg = 1.1eV, metallic?
WSe_2	MoS_2	high	Eg = 1.6 eV
ZrS_2	CdI_2	~1550	Eg = 1.68eV, $\rho \sim 10^8$ Ω-cm
$ZrSe_2$	CdI_2	high	Eg = 1.25 eV
$ZrTe_2$	CdI_2	high	prob. too conductive

References 17-19

† X = S, Se, Te

* Chain like bonding, therefore weak in two directions and strong in one.

@ Not strictly a layer structure, but an easy cleavage plane is probable.

Precipitate Strengthening

The restriction to particles with a good index match and sizes of 30-200 Å for the visible range, probably eliminates many of the techniques so far considered Precipitation from solid solution by aging can produce sufficiently small particles which may provide some toughness enhancement. The $BeSiN_2$-AlN is reported[21] to have complete solid solubility at high temperature. It is likely that phase separation or precipitation would occur on aging at lower temperature

Fiber/Whisker Strengthening

For the compounds suitable for the far IR, strengthening or toughening using strong fibers may be feasible in principle. To estimate scattering the equivalent spherical diameter would be 2.5 d for $\ell/d = 10$. If one of the simple covalent compounds, such as BP, had a sufficiently low absorption coefficient in the 8-14 μ m range, it could be used with a sulfide matrix which is compatible and has a suitable refractive index. If $\eta < 0.05$, whiskers with a diameter of 0.05 - 0.2 μ m would probably have sufficiently low scattering Production and handling of such small fibers and fabrication of a dense two-phase material would require advanced techniques.

For the mid-IR, the size requirements, fabrication difficulties, and stronger matrix materials available make whisker strengthening even less feasible. Particularly strong materials which only marginally meet the 6 μ m cut-off or which have oxidation or vaporization limitations, such as B_6P, could be used in more suitable, nonreactive matrices with better transparency.

Materials with noncubic structures which have significant anisotropy in the single crystal K_{IC} offer the potential for toughening with microstructure control, such as the development of elongated grains. Unfortunately, those same materials typically have poorer IR transmission, and if they are significantly bi-refringent, the grain size must be very fine.

4.5 Fabrication

To achieve the desired properties, the dispersed particles must be carefully controlled in size and spatial distribution. Powder processing is

probably more flexible than CVD for fabricating these two phase bodies. Sintering or hot pressing to high density will be necessary The porosity must either be as pores finer than approximately $\lambda/15n$ or the density must be greater than 99.99%. The easiest materials to control are those such as partially stabilized ZrO_2 or HfO_2 or $ThO_2 + ZrO_2$ in which the particles can be obtained by precipitation using a solutionizing and aging heat treatment.

For the materials which must be prepared by densification of powder mixtures, special techniques must be used to achieve the necessary size and distribution of second phase. Submicron ZrO_2 and HfO_2 with crystallite sizes of about 100 Å or about 300 Å are available from two different sources. These can be carefully milled and classified to remove or break up agglomerates. This can be done by vibromilling in a stable liquid suspension and centrifugally separating the powders by size for preparation of test samples. Fine powders of BN can probably be made by gaseous reactions and similarly classified. The matrix powders must be similarly fine to obtain an adequate dispersion of second phase. The classified powders can be mixed in suspension and then either deposited directly by slip casting or centrifugation or can be freeze- or spray-dried to prevent separation. Milling and centrifugal separation techniques have been used to produce dense ZrO_2 with a 0.16 μm grain size.[22]

Alternatively, for two component oxides, the powders can be made concurrently to achiev fine, well-mixed dispersions. If soluble salts of all the cations exist, coprecipitation, freeze drying or spray drying may be useful. If soluble salts are not available for all components similar techniques can be used to precipitate the soluble component into a fine suspension of the other powders. An alternative is to co-decompose volatile alkaloxides of the appropriate cations.

To establish phase stability and evaluate the toughness and other properties, samples should be made by the most expedient technique. The appropriate method of powder preparation will depend upon each particular

pair of materials. Evaluation samples can be hot pressed although scale-up to feasible techniques for production will likely warrant using sintering.

4.6 Toughness and Thermal Shock Evaluation

Fracture toughness, thermal shock resistance, and strength must be evaluated for the various materials. Preliminary toughness measurements can be made on small (~ mm) samples using the microhardness technique developed by Evans.[23] For the more promising materials, standard techniques such as double torsion or double cantilever measurements of fracture toughness should be done. For the best materials, toughness should also be measured at high temperature. This is particularly important for the ZrO_2 and HfO_2 toughened materials to determine the temperature above which the stress-induced T → M transformation no longer occurs. Comparison of the K_{IC} values from the microhardness technique and the larger samples may give an indication of the effectiveness of the particular techniques in inhibiting erosion.

Thermal shock resistance can be evaluated by relating the retained strength after quenching to the as-fabricated strength. Four point bend tests are satisfactory for the strength determinations. Samples should be quenched over a range of ΔT up to the maximum anticipated for service to determine ΔT_{crit} and the degree of degradation.

4.7 Scheduling and Screening

Although preparation of toughened window materials appears to be feasible, a considerable fabrication effort will be required to achieve optical quality and optimum mechanical properties. Consequently, evaluation and development should proceed in several steps. Thermodynamic stability, the melting range, and the mutual solubilities should be determined if they are unknown. Where there is uncertainty, the potential for suitable optical properties should be established by interdiffusing the two materials and then ascertaining the effect of the mutual doping. The optical absorption can be estimated by doing measurements on thin film samples or alternatively, on powders or samples with particles much larger than λ. The toughening

should be evaluated using materials and particle size restrictions with the potential for suitable optical performance. Those techniques and materials for which toughening and thermal shock resistance have been demonstrated and are otherwise suitable can then be considered for fabrication to optical quality and large sample preparation. For the small particle sizes required, there are uncertainties in the extent of toughening to be expected and the optimum volume loadings, sizes, spatial distributions, and aspect ratios. Where appropriate model studies using more readily available materials, such as MoS_2, may be desirable.

SECTION 5

PROGRAM PLAN

ADVANCED OPTICAL CERAMICS

PHASE I

SECTION 5

PROGRAM PLAN

ADVANCED OPTICAL CERAMICS - PHASE I

5.1 Introduction

The accompanying statement of work for the Advanced Optical Ceramics Phase I study (Section 5.4) defines the initial effort of a proposed three year DARPA sponsored investigation which will lead to identification and development of revolutionary advanced materials suitable for electro-optical/electro-magentic (EO/EM) windows, IR domes and radomes capable of meeting mission requirements anticipated for the 1990 decade and beyond. This statement of work is an output of the Advanced Optical Ceramics Phase "O" Study, ONR Contract N00014-77-C-0649. The data base used in assessing DoD 1990 time frame system needs and Advanced Optical Ceramics candidate selections is described in References 1 and 2, and in the body of this Final Report.

The initial candidate list has been selected based on known data and solid state physics considerations which permit narrowing of the list to manageable proportion and yields high confidence that the materials selected for development will be appropriate. This approach limits activity which predictably could not yield useful results and directs the activity to avenues expected to be fruitful. The candidate slates are partitioned on the basis of bandpass as follows:

UV	0.2 - 0.4 microns
VIS	0.4 - 0.7
IR 1	0.7 - 3.0
IR 2	3.0 - 5.5
IR 3	7.5 - 10.0
IR 4	10.0 - 14.5
RADAR	

Many candidates in these lists have dual mode capability. Since advanced missions are trending toward dual mode operation, the dual mode capability will be important.

In each case, the new candidates were judged relative to both the operational and the advanced materials currently under development by DoD for similar application. Criteria for selection were refractoriness, band pass (absorption coefficients), band gap, coefficient of thermal expansion, hardness, potential for fracture toughness enhancement, structure (cubic being preferred), chemical stability (including tendency to be sensitive to moisture).

A number of excellent candidates contain beryllium. The toxicity of Be is well recognized. However, it is judged that the beryllium industry has developed means to process beryllium compounds in conformance with OSHA requirements (BeO, Be metals) and, therefore, Be compounds are viable. Nevertheless, Be toxicity is an unfavorable factor when ranking candidates. Although the proposed three year program is designed to narrow the field of candidates and focus on a few materials leading in the third year to scale-up of the processes, a significant ongoing task will be to continuously monitor new material systems, data, and defense system requirements so that important trends or breakthroughs are factored into this program on a timely basis.

5.2 Review Board

During the course of this program, semi-annual reviews of progress and approaches will be conducted by a technical review panel selected with the concurrence of the contract monitor. The purpose of the semi-annual review will be to continuously incorporate into the program by an updating process the best technical knowledge available in the Nation in the fields of materials synthesis, characterization and applications technology related to the Advanced Optical Ceramics of interest.

Subject to further iteration, a tentative list of Advanced Optical Ceramics Review Board members has been drawn up. This Board will be a key to successful performance of the proposed Advanced Optical Ceramics program as well as the incorporation of the results of the program into new system developments.

5.3 General Approach for "Phase I Program Plan"

Specimens of each of the candidates will be located (as previously synthesized or naturally occurring crystals) and, if not available, will be synthesized. Many measurements can be performed on small samples on the order of 1 mm. In addition, some spectral data can be obtained on powders, while other measurements require large samples. Table 5-1 lists the screening characterizations to be made and the approximate sample size required for each measurement. The following list of properties will be obtained which will provide the basis for ranking of the candidate ceramics:

Density
Specific Heat (calculated)
Thermal Conductivity
Elastic Modulus
Modules of Rupture
Poisson's Ratio (estimated)
Coefficient of Thermal Expansion (CTE)
Dielectric Constant) for radome
Loss Tangent)
Absorption Coefficients for IR Domes and Visible Windows

Synthesis of specimens will be performed at various facilities, depending on the process chosen and the nature of the material.

The data derived from these characterizations will be used as a basis for estimates of properties as a function of temperature. Such data will be input to the Johns Hopkins University Applied Physics Laboratory Unified Radome Limitation (URLIM) Program[3] to assess probable useful performance envelopes. Along with the various figures of merit parameters for thermal shock Hasselman[4,5], the URLIM output will be considered when selecting candidates for further scale-up in the Year 2 program.

Additionally, the potential for optical success of the candidates will be assessed by use of analytical tools available at the Naval Weapons Center.

Candidates will be ranked and a selection of materials to carry on to the Year 2 program will be made by the contractor and contract monitor.

TABLE 5-1: Screening Characterizations

Measurement	Output	Minimum Sample Size	Facility
X-ray diffraction	crystal structure coefficient of thermal expansion	powder or small chips	GE-SSL, GE-CR&D
Weight and volume	density	1mm x 1mm x 1mm	GE-RESD
Hardness	Knoop Micro hardness	2-3mm dia. x 1-2 mm thick	GE-RESD, GE-CR&D
Near normal specular Transmittance	Absorption coefficient Deduce E_g	4-5mm dia. x .5 mm	GE-RESD, Oxford University (Elevated Temp.)
Near normal specular Reflectance	reflectance	4-5mm dia. x .5 mm	GE-RESD, Oxford University (Elevated Temp.)
Resonant cavity Dielectric constant	$\left.\begin{matrix}\epsilon_o \\ \text{loss tangent}\end{matrix}\right\}$ at X band	1 mm dia. x 25 mm long	GE-RESD, GE-CR&D, Cornell University
Thermal diffusivity	k, (based on calculated value of specific heat)	12 mm dia. x 1 mm thick	GE-RESD
Dilatometry	Bulk coefficient of thermal expansion		GE-RESD, Penn State Univ.
3 pt flexure test	E, Modulus of rupture	1mm x 1mm x 25 mm	GE-RESD
Ultrasound	E (Sonic modulus)	1mm x 1mm x 25 mm	GE-RESD
Fracture toughness	K_{IC} (micro) (macro)	1mm x 1mm x 25 mm 6mm x 1mm x 50mm	MIT NRL

5.4 Statement of Work - Advanced Optical Ceramics - Phase 1

Development of Advanced Optical Ceramics for Application to Advanced DoD Missions

TASK 1.0: Synthesis

Candidate materials will be synthesized (if not available naturally or from previous research work) which have been identified in the Phase "O" study. The specific candidates are summarized in Table 5-2.

For each candidate specimen, characterization measurements will be made, sufficient to determine the usefulness of the material in terms of band pass and thermostructural limitations. Measurements will be performed as indicated in Table 5-2, Screening Characterizations, although every specimen will not necessarily be subjected to every test.

The most promising formulation in each category of candidates will be further developed toward optimization of electro-magnetic and thermostructural properties. This optimization will include cation substitution in appropriate candidates to "fine tune" the band pass characteristics.

TASK 1.1: Non-silicate mixed oxides with IR cut off $> 5\mu m$, CTE $< 4.0 \times 10^{-6}/°C$

The following mixed oxides in this classification will be synthesized and characterized:

$2ZnO \cdot GeO_2$

$ThO_2 \cdot GeO_2$

$3CaO \cdot 5Al_2O_3$

These materials will be aimed primarily at the 3-5 um application.

TASK 1.2: Non-silicate mixed oxides with IR cut-off $> 5\mu m$, CTE near zero

The following mixed oxides in this classification will be synthesized and characterized:

TABLE 5.2. Summary of New Candidate Materials for Windows

Class	Materials	Max. Temp. °K	Band Pass*					
			UV	VIS	IR1	IR2	IR3	IR4
A	$2ZnO \cdot GeO_2$	1273		o	o	o		
B	$ThO_2 \cdot GeO_2$	1273		o	o	o		
C	$3CaO \cdot 5Al_2O_3$	1273	o	o	o	o		
D	$HfO_2 \cdot WO_3 \cdot Ta_2O_5$	1273		o	o	o		
E	$xTa_2O_5 \cdot yWO_3$	1273			o	o		
F	$xHfO_2 \cdot yTiO_2$	1773		o	o	o		
G	$Cs_2O \cdot Al_2O_3 \cdot 4SiO_2$	1273		o	o	o		
H	$ZrO_2 \cdot SiO_2$	1773	o	o	o	o		
I	$2ZnO \cdot SiO_2$	1273			o	o		
J	$3Al_2O_3 \cdot 2SiO_2$	1773	o	o	o	o		
K	$2MgO \cdot 2Al_2O_3 \cdot 5SiO_2$	1273	o	o	o	o		
L	$B_4Al_{18}O_{33}$	1773	o	o	o	o		
M	$Be_3Al_2(SiO_3)_6$	1273	o	o	o	o		
N	SnO_2	1273			o	o		
O	Nb_2O_5	1273			o	o		
P	ThO_2	2273	o	o	o	o		
Q	Y_2O_3	2273	o	o	o	o		
R	EuO	773			o	o	o	
S	$BeSiN_2$	2273	o	o	o			
T	$BeSiN_2$ - AlN (SS)	2273	o	o	o	o		

*All candidates good in RADAR range.

TABLE 5.2. Summary of New Candidate Materials For Windows
(continued)

Class	Materials	Max. Temp. ^{o}K	Band Pass*					
			UV	VIS	IR1	IR2	IR3	IR4
U	$Al_5Si_6O_{15}N_3$ $Al_2Si_9O_{12}N_6$ $Sc_2Si_9O_{12}N_6$	1773	o	o	o	o		
V	$CaLa_2S_4$ $SrLa_2S_4$ $BaLa_2S_4$	773		o	o	o	o	o
W	Diamond	1273	o	o	o		o	o

*All candidates good in RADAR range.

UV 0.2 - 0.4 microns
VIS 0.4 - 0.7
IR 1 0.7 - 3.0
IR 2 3.0 - 5.5
IR 3 7.5 - 10.0
IR 4 10.0 - 14.5

$HfO_2 \cdot WO_3 \cdot Ta_2O_5$

$XTa_2O_5 \cdot yWO_3$

$XHfO_2 \cdot yTiO_2$

These materials will be aimed primarily at the 3-5 μm application.

TASK 1.3: Silicate mixed oxides with IR cut-off $\sim$ 5 μm, CTE $<$ 5.6 x $10^{-6}/^{o}C$

The following mixed oxides in this classification will be synthesized and characterized:

$Cs_2O.Al_2O_3 \cdot 4SiO_2$

$ZrO_2 \cdot SiO_2$

$2ZnO \cdot SiO_2$

$3Al_2O_3 \cdot 2SiO_2$

$2MgO \cdot 2Al_2O_3 \cdot 5SiO_2$

$B_4Al_{18}O_{33}$

$Be_3Al_2(SiO_3)_6$

These materials will be aimed primarily at the 3-5 μm application.

TASK 1.4: Simple Oxides

The following simple oxides will be synthesized and characterized:

SnO_2

Nb_2O_5

These two materials have IR cut-off $\sim$ 7 μm and CTE $<$ 4.0 x $10^{-6}/^{o}C$

ThO_2

Y_2O_3

EuO

These three oxides have IR cut-off at 8, 9, 10 μm respectively, are cubic, and are considered good model systems for application of fracture toughening techniques.

TASK 1.5: Non-oxide candidates

The following non-oxide candidates will be synthesized and characterized:

$BeSiN_2$

$BeSiN_2$ - AlN solid solution

These materials will be useful from the UV up to the 5 μm band pass. In addition,

the $BeSiN_2$-AlN system will be a model system for the application of precipitation strengthening techniques.

TASK 1.6: Oxynitrides

At least one of the following predicted compounds will be synthesized (if possible) and characterized:

$Al_5Si_6O_{15}N_3$

$Al_2Si_9O_{12}N_6$

$Sc_2Si_9O_{12}N_6$

These are anticipated to have low CTE and improved oxidation resistance over the nitride candidates.

TASK 1.7: Ternary sulfides with the cubic Th_3P_4 structure

The following compounds will be synthesized and characterized:

$CaLa_2S_4$

$SrLa_2S_4$

$BaLa_2S_4$

These compounds are aimed at the 8-14 μm regime. These materials are also considered to be good model systems for the application of fracture toughness enhancement techniques.

TASK 2.0: Fracture Toughness Enhancement

Techniques will be developed to improve K_{IC} for the candidate materials. The approaches which will be investigated and evaluated for applicability will include the following:

a. Particle toughening
b. Fiber or whisker reinforcement
c. Microcracked systems
d. Inclusion of second phase particles with "easy cleavage planes"
e. Partially stabilized ZrO_2 inclusions
f. Precipitate strengthening

The emphasis in this task will be to identify those techniques which have the best chance for K_{IC} enhancement with acceptable degradation of optical properties for selected model systems in each band pass of interest.

Initial evaluation of toughness will be accomplished by microhardness measurements. For the more promising candidate systems, more standard techniques such as double cantilever fracture toughness measurements will be made.

Initial thermal shock performance will be evaluated by determining retained strength after quenching over a range of ΔT up to maximum service condition.

TASK 3.0: Thermostructural Analysis

Assessment of candidate material performance for various advanced mission trajectories will be accomplished after sufficient thermo-structural characterizations have been accomplished to provide the needed input data. It is anticipated that existing evaluation programs (such as the Johns Hopkins Applied Physics Laboratory URLIM program) will be made available to this study.

TASK 4.0: Modelling

Modelling of the effects of various flaws and added second phase particles on the optical performance of the candidates will be accomplished to provide guidance in performance of TASK 2.0.

TASK 5.0: Continuing Search for Improved Candidates

Throughout this study there will be a continuing effort to identify superior candidate materials. This will be accomplished by literature searches and personal contacts in the sensor window and materials sciences communities by all the co-investigators and consultants assigned to this program. If particularly promising candidates are identified, these will be characterized and assessed as part of this study.

TASK 6.0: Program Plan for Year 2

At the conclusion of this study, recommendations will be made for continuation of the work on a selected limited number of the more promising candidates.

A program plan will be prepared identifying in detail the specific materials to be optimized, the reasons for the selection, the synthesis procedures to be used, and the evaluation methods to be employed. Budget and schedule estimates will be provided.

TASK 7.0: Reporting

Progress of the study will be documented by three quarterly letter reports, and a comprehensive final report. Presentations to DARPA, the contract monitor, and the Steering Committee will be provided as appropriate.

Schedule

The schedule for the proposed 12-month Phase I study is shown in Figure 35.

FIGURE 34. Program Schedule

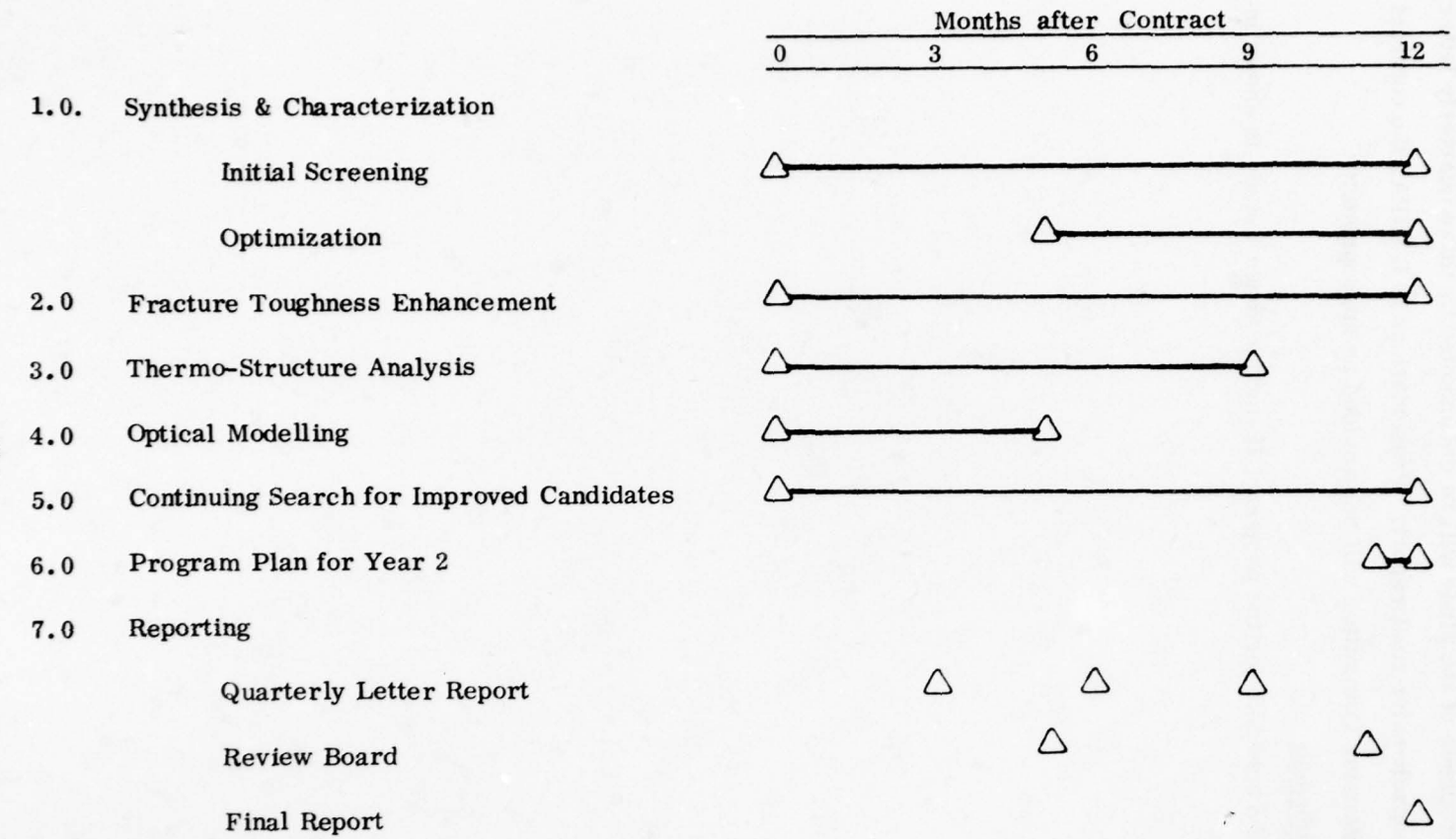

SECTION 6

REFERENCES

SECTION 6

REFERENCES

Section 2.0

1. Personal communication with Prof. W. A. Harrison, Stanford University, January, 1978.

2. A. N. Winchell and H. Winchell, Optical Properties of Artificial Minerals, Academic Press, p. 328 (1964).

3. A. G. Evans, et. al., "Impact Damage in Brittle Materials in the Plastic Response Regime", Technical Report SC 5023-9 TR, (ONR Contract No. N00014-75-C-0669).

Section 3.0

1. N. I. Minko, S. A. Fabrikant, and Yu. K. Platonov, Zh. Fiz. Khim., 46, p. 312 (1972) [Russ. J. Phys. Chem., 46, p. 184 (1972)].

2. D. Taylor, Mineral Mag., 38, p. 593 (1972).

3. W. Johnson and K. W. Andrews, Trans. Brit. Ceram. Soc., 55, p. 227 (1956).

4. H. Fizeau, Compt. Rend., 66, p. 1005 and 1072 (1868).

5. J. R. Benoit, J. Physique, 9, p. 253 (1889).

6. R. F. Geller and H. Insley, J. Res. U. S. Nat. Bur. Stand., 9, p. 35 (1932).

7. H. D. Erfling, Ann. Phys., 34, p. 136 (1939).

8. B. Morosin, Acta Crystallogr., B28, p. 1899 (1972).

9. M. Ushio and Y. Sumiyoshi, Nippon Kagako Kaishi (#10), 1730 (1975) [see Chem. Abstr., 83, p. 200475j (1975)].

10. E. A. Durbin and C. G. Harman, Battelle Memorial Institute Report #791, Columbus, Ohio, December 15, 1952.

11. R. F. Geller and H. Insley, J. Res. U. S. Nat. Bur. Stand., 9, p. 35 (1932).

12. G. R. Rigby and A. T. Green, Trans. Brit. Ceram. Soc., 41, p. 123 (1942).

13. F. A. Hummel and H. W. Reid, J. Am. Ceram. Soc., 34, p. 319 (1951).

14. M. D. Karkhanavala and F. A. Hummel, J. Am. Ceram. Soc., 36, p. 389 (1953).

15. C. Frondel and J. Ito, Amer. Min., 53, p. 943 (1968).

16. W. A. Deer, R. A. Howie, and J. Zussman, "Rock Forming Minerals", Wiley, New York, (1962).

17. H. P. Kirchner, Amer. Inst. Phys. Conf. Proc., 3, p. 269 (1971).

18. G. Bayer, Proc. Brit. Ceram. Soc., 22, p. 39 (1973).

19. S. Deganello, Z. Krist., 137, p. 127 (1973).

20. W. Ostertag, G. R. Fischer, and J. P. Williams, J. Amer. Ceram. Soc., 51, p. 651 (1968).

21. M. Czank and H. Schulz, Naturwiss, 58, p. 94 (1971).

22. R. A. Munson, J. Amer. Ceram. Soc., 50, p. 669 (1967).

23. W. Schreyer and J. F. Schairer, J. Petrol., 2, p. 324 (1961).

24. Y. S. Touloakian, R. W. Powell, C. Y. Ho, and P. G. Klemens, "Thermophysical Properties of Matter", Plenum, New York, 2, p. 802 (1970).

25. K. Horai and G. Simmons, Earth Planet. Sci. Letters, 6, p. 359 (1969).

26. G. A. Slack and S. B. Austerman, J. Appl. Phys., 42, p. 713 (1971).

27. G. A. Slack and S. F. Bartram, J. Appl. Phys., 46, p. 89 (1975).

28. T. Ormiston and R. A. Tanzilli, NASA Report CR-132331, October, 1973.

29. A. J. Perrotta and J. E. Young, Jr., J. Amer. Ceram. Soc., __, p. 441 (1973).

30. J. F. Lynch, C. G. Ruderer, and W. H. Duckworth, "Engineering Properties of Selected Ceramic Materials", pub. by Amer. Ceram. Soc., Columbus, (1966).

31. Y. S. Touloukian, et. al., "Thermophys, Props. High Temp. Solid Matter", 4, Macmillan, NY. (1967).

32. G. Oehlschlegel, A. Kochel, and A. Biedl, Glastech. Ber.,47, p. 441 (1974).

33. R. S. Krishnan, "Progress in Crystal Physics", 1, Viswanathan, Chetput (India), (1958).

34. J. L. Woolfrey,,J. Austrl, Ceram. Soc., 9, p. 33 (1973).

35. G. R. Rigby and A. T. Green, Trans. Brit. Ceram. Soc., 41, p. 123 (1942).

36. H. P. Singh, G. Simmons, and P. F. McFarlin, Acta Cryst., A31, p. 820 (1975), also C.M.B. Henderson and D. Taylor, Trans. J. Brit. Ceram. Soc., 74, p. 55 (1975).

37. T. G. Worlton, L. Cartz, A. Niravath, and H. Ozkan, High Temp. High Press., 4, p. 463 (1972).

38. G. Bayer, Thermochimica Acta, 3, p. 421 (1972).

39. J. B. Wachtman, Jr., T. G. Scuderi, and G. W. Cleek, J. Amer. Ceram. Soc., 45, p. 319 (1962).

40. S. M. Lang, Acta Cryst., 19, p. 210 (1965).

41. P. Wen, J. J. Brown and F. A. Hummel, "Dilatometer and X-ray Data for Zinc Compounds. I", Trans of the British Ceramic Society, 63, No. 9, pp. 501 508, September, 1964.

42. G. Bayer, "Thermal Expansion of ABO_4 - Compounds with Zircon and Scheelite Structures", J. of Less Common Metals, 26, pp. 255-262 (1972).

43. P. Tarte, "Etude Infra rouge des orthosilicates et des orthogermanates II Structures du type olivine et monticellite", Spectrochemica Acta, 19, pp. 25 47, (1963).

44. G. R. Rigby and A. T. Green, "The Thermal Expansion Charac teristics of Calcium Aluminates and Ferrites", Trans. of the British Ceram. Soc., 42, pp. 95-103, (1943).

45. R. W. Rice, "Possible New Irdome Materials for Transmission to 4.5 - 5.0 um", draft manuscript to be published by NRL.

46. C. E. Holcombe, et. al., "Survey of Low Expanding High Melting Mixed Oxides", UC-Y-12 Report Y-1913 (1974).

47. S. R. Skaggs, "Zero and Low Coefficient of Thermal Expansion Polycrystalline Oxides", Los Alamos Report LA-6918-MS, September, 1977.

48. C. E. Holcombe, Jr., "Properties of Thermally Contracting Tantalum Tungstates", UC-Y-12 Report Y-2071, February, 1977.

49. J. A. Kuszyk, R. C. Bradt, "Influence of Grain Size on Effects of Thermal Expansion Anisotropy in MgO . $2TiO_2$", J. Am. Ceram. Soc., 56, pp. 420-23 (1973).

50. P. J. Launer, "Regularities in the Infrared Absorption Spectra of Silicate Minerals", Am. Mineralogist, 37, pp. 764-784 (1952).

51. Mineral specimens and consultation was provided by the Curator of Minerals (R. Middleton) of the Philadelphia Academy of Natural Sciences during the Phase O program.

52. A translucent specimen of synthetic mullite was supplied on an earlier NRL program to GE RESD by K. S. Mazdiyasni of AFML (Personal Communication - Letter and Shipment dated 6 May 1976).

53. J. Quirk and C. G. Harmon, "Properties of a Tin Oxide Base Ceramic Body", J. Am. Ceram. Soc., 37, (1), pp. 24-26 (1954).

54. K. Nassau, "Cubic Zirconia - The Latest Diamond Imitation and Skull Melting", Lapidary Journal, Inc. (1977).

55. W. R. Manning, et. al., "Thermal Expansion of Nb_2O_5", J. Am. Ceram. Soc., 55, pp. 342-347 (1972).

56. A. Einstein, J. Appl. Phys., 17, p. 434 (1946).

57. E. M. Dudnik, G. V. Lashkarev, Yu. B. Paderno, and V. A. Obolonchik, Neorgan. Mater., 2, p. 980 (1966). [Inorgan. Mater., 2, (1966)]. (for EuS and EuSe).

58. Eu_2O_3 has $B = 10.3 \times 10^{-6}/^{o}K$ in Ref. 31.

59. P. H. Klein and W. J. Croft, J. Appl. Phys., 38, p. 1603 (1967).

60. C. E. Curtis, L. M. Doney and J. R. Johnson, J. Amer. Ceram. Soc., 37, p. 458 (1954).

61. J. D. Axe, J. Phys. Chem. Solids, 30, p. 1403 (1969).

62. K. P. Anath, P. J. Gielisse and T. J. Rockett, Mater. Res. Bull., 9, p. 1167 (1974).

63. G. Guentherodt, Phys. Condens. Matter, 18, p. 37 (1974).

64. T. B. Reed, R. E. Fahey and A. J. Strauss, J. Cryst. Growth, 15, p. 174 (1972).

65. P. L. Provenzano, S. I. Boldish and W. B. White, Mat. Res. Bull., 12, p. 939 (1977).

66. J. L. Browder and S. S. Ballard, Appl. Opt., 8, p. 793 (1969).

67. Eastman Kodak Co., "Kodak Irtran Infrared Optical Materials", publ. #U-72 (1971).

68. T. S. Moss, "Optical Properties of Semiconductors", Butterworths, London, (1961).

69. K. Kunc, Ann. Phys. (Paris), 8, p. 319 (1973-74).

70. D. A. Kleinman and W. G. Spitzer, Phys. Rev., 118, p. 110 (1960).

71. M. K. Farr, J. G. Traylor and S. K. Sinha, Phys. Rev., B11, p. 1587 (1975).

72. C. Muller, "Crystal Chemical Data for Ternary Chalcogenide and Pnictide Compounds", Scientific Report No. 1, AFCRL 72-0457, p. 155 (1972).

73. P. L. Provenzano and W. B. White, "Synthesis and Crystal Chemistry of Sulfides and Tellurides with the Th_3P_4 Structure", Scientific Report No. 5, AFCRL TR-74-0560, pp. 27 (1974).

74. P. L. Provenzano, S. I. Boldish and W. B. White, "Vibriational Spectra of Ternary Sulfides with the Th_3P_4 Structure", Mat. Res. Bull., 12, pp. 939-946 (1977).

75. C. M. B. Henderson and D. Taylor, Trans. J. Brit. Ceram. Soc., 74, p. 49 (1975).

76. Personal communication with R. Goehner, General Electric Research and Development Center.

77. T. B. Reed, "Free Energy of Formation of Binary Compounds", MIT Press, Cambridge (1971).

78. C. L. Hoenig and A. W. Searcy, J. Amer. Ceram. Soc., 50, p. 460 (1967).

79. G. A. Slack and T. F. McNelly, J. Cryst. Growth, 34, p. 263 (1976).

80. R. D. Pehlke and J. F. Elliott, Trans. A.I.M.E., 215, p. 781 (1959).

81. R. T. Coyle and A. W. Searcy, High Temp. Sci., 5, p. 335 (1973).

82. M. E. Washburn, Amer. Ceram. Soc. Bull., 46, p. 667 (1967).

83. K. H. Jack, J. Mater. Sci., 11, p. 1135 (1976).

Section 4.0

1. D. P. H. Hasselman, "Unified Theory of Thermal Shock Fracture Initiation and Crack Propagation in Brittle Materials", J. Am. Ceram. Soc., 52, p. 600 (1969).

2. A. G. Evans, et. al., "Impact Damage in Brittle Materials in the Plastic Response Regime", Tech. Report SC-5023-9-TR, Contract N00014 75 C 0669.

3. H. C. Vande Hulst, Light Scattering By Small Particles, Wiley N.Y. (1957).

4. F. F. Lange, "Interaction of Crack Front With Second Phase Dispersions", Phil. Mag., 22, p. 983 (1970).

5. F. F. Lange, "Effect of Microstructure on Strength of Si_3N_4-SiC Composite System", J. Am. Ceram. Soc., 56, p. 445 (1973).

6. G. K. Bansal and A. H. Heuer, "Precipitation Strengthening in Non-Stoichiometric Mg Al Spinel", in Fracture Mechanics of Ceramics, ed. R. C. Bradt, et. al., Plenum, N.Y., p. 677 (1974).

7. M. W. Lindley and D. J. Godfrey, "Silicon Nitride Ceramic Composites with High Toughness", Nature, 229, p. 192 (1971).

8. F. F. Lange, "Relation Between Microstructure, Fracture Energy, and Microstructure of Hot Pressed Si_3N_4", J. Am. Ceram. Soc., 56, p. 518 (1973).

9. R. C. Garvie and R. T. Pascoe, "Strengthening of Partially Stabilized Zirconia by Post Sintering Heat Treatment", presented at Processing of Crystalline Ceramics, North Carolina State Univ., November 7-9, 1977.

10 D. L. Porter and A. H. Heuer, "Mechanisms of Toughening Partially Stabilized Zirconia (PSZ)", J. Am. Ceram. Soc., 60, p. 183 (1977).

11. L. J. Gauckler, "Densification of β-Si_3N_4 Solid Solution During Chemical Reactions", in Ref. 9.

12. N. Claussen, J. Steeb and R. F. Pabst, "Effect of Induced Microcracking on the Fracture Toughness of Ceramics", Bull. Am. Ceram. Soc., 56, p. 559 (1977).

13. K. Chyung, "Fracture Energy and Thermal Shock Resistance of Mica Glass Ceramics", p. 495 in Ref. 6.

14. Personal communication with J. McAuley, AMMRC, Watertown, MA.

15. Personal communication with R. Rice, NRL, Washington, D.C.

16. E. M. Levin, C. R. Robbins and H. F. McMurdie, Phase Diagrams for Ceramists, 1969 Supplement, 1975 Supplement, Am. Ceram. Soc., (1964), (1969), (1975).

17. a) M. Hansen, Constitution of Binary Alloys, McGraw Hill, NY (1958).
    b) R. P. Elliot, Constitution of Binary Alloys First Supplement, McGraw Hill, NY (1965).
    c) F. A. Shunk, Constitution of Binary Alloys Second Supplement, McGraw Hill, NY (1969).

18. J. P. Suchet, Crystal Chemistry and Semiconduction in Transition Metal Binary Compounds, Academic Press, N.Y. (1971).

19. L. E. Conroy, Kyu Chang Park, "Electrical Properties of Group IV Disulfides", Inorg. Chem., 7, p. 459 (1968).

20. A. H. Larsen and A. W. Schlechten, "A Thermodynamic Study of the Zirconium-Sulfur System in the Region $ZrS_{1.49}$ to $ZrS_{2.00}$", Trans. AIMF, 230, p. 862 (1964).

21. Personal communication with L. J. Gauckler, Max Planck-Institute, Stuttgart, Germany.

22. T. Vasilos and W. H. Rhodes, "Fine Particulates to Ultrafine Grain Ceramics", in Ultrafine Grain Ceramics, ed. J. J. Burke, et. al., Syracuse Univ. Press., p. 137 (1970).

23. A. G. Evans and E. A. Charles, "Fracture Toughness Determinations by Indentation", J. Am. Ceram. Soc., 59, p. 371 (1976).

24. R. W. Davidge, "Effect of Microstructure on the Mechanical Properties of Ceramics", p. 447, in Ref. 6.

25. S. W. Freiman, K. R. McKinney, and H. L. Smith, "Slow Crack Growth in Polycrystalline Ceramics", p. 659, in Ref. 6.

26. R. W. Rice, "Fractographic Identification of Strength Controlling Flaws and Microstructure", p. 323, in Ref. 6.

27. C. R. Andrews and C. L. Strecker, Proceedings of the Fourth Annual Conference on Infrared Laser Window Materials", ARPA (1975).

28. J. F. Lynch, et. al., "Engineering Properties of Selected Ceramic Materials, Am. Ceram. Soc. (1966).

29. W. H. Kohl, Materials and Techniques for Vacuum Devices, Reinhold, N.Y. (1967).

Section 5.0

11. S. Musikant, et. al., "Advanced Optical Ceramics Midterm Report", ONR Contract N00014-77-C-0649, November 30, 1977.

2. J. Greshock, "Task 1 Report Advanced Mission Survey and Ceramic Window Performance Requirements", ONR Contract N00014-77-C-0649, November 30, 1977. GE No. 78SDR2196

3. R. K., Frazer, "A General Application Heat Transfer Computer Program", Johns Hopkins University, Applied Physics Laboratory, Silver Spring, MD.

4. D. P. H. Hasselman, "Thermal Shock by Radiation Heating", J. Am. Ceram. Soc., 46, (5), pp. 229-34 (1963).

5. D. P. H. Hasselman, "Unified Theory of Thermal Shock Fracture Initiation and Crack Propagation in Brittle Ceramics", J. Am. Ceram. Soc., 52 (11), pp. 600-604 (1969).

APPENDIX I

ABSORPTION COEFFICIENTS FOR

SOME SINGLE CRYSTAL MATERIALS

APPENDIX I

ABSORPTION COEFFICIENTS FOR SOME SINGLE CRYSTAL MATERIALS

REF. Advanced Materials for Optical Windows
General Electric Company
TIS No. 78-SDR-2199, May 15, 1978
Dr. G. A. Slack

The following charts present absorption coefficient data for a number of refractory single crystal materials as a function of photon wavenumber.

Figure No.	Material	Figure No.	Material
A-1	β-Boron, B_6P	A-10	MgF_2
A-2	Diamond	A-11	BP
A-3	Cubic BN	A-12	Si_3N_4
A-4	BeO	A-13	Si
A-5	α-SiO_2	A-14	$Y_3Al_5O_{12}$
A-6	Cubic SiC	A-15	Y_2O_3
A-7	MgO	A-16	ZnSe
A-8	α-Al_2O_3	A-17	ThO_2
A-9	AlN		

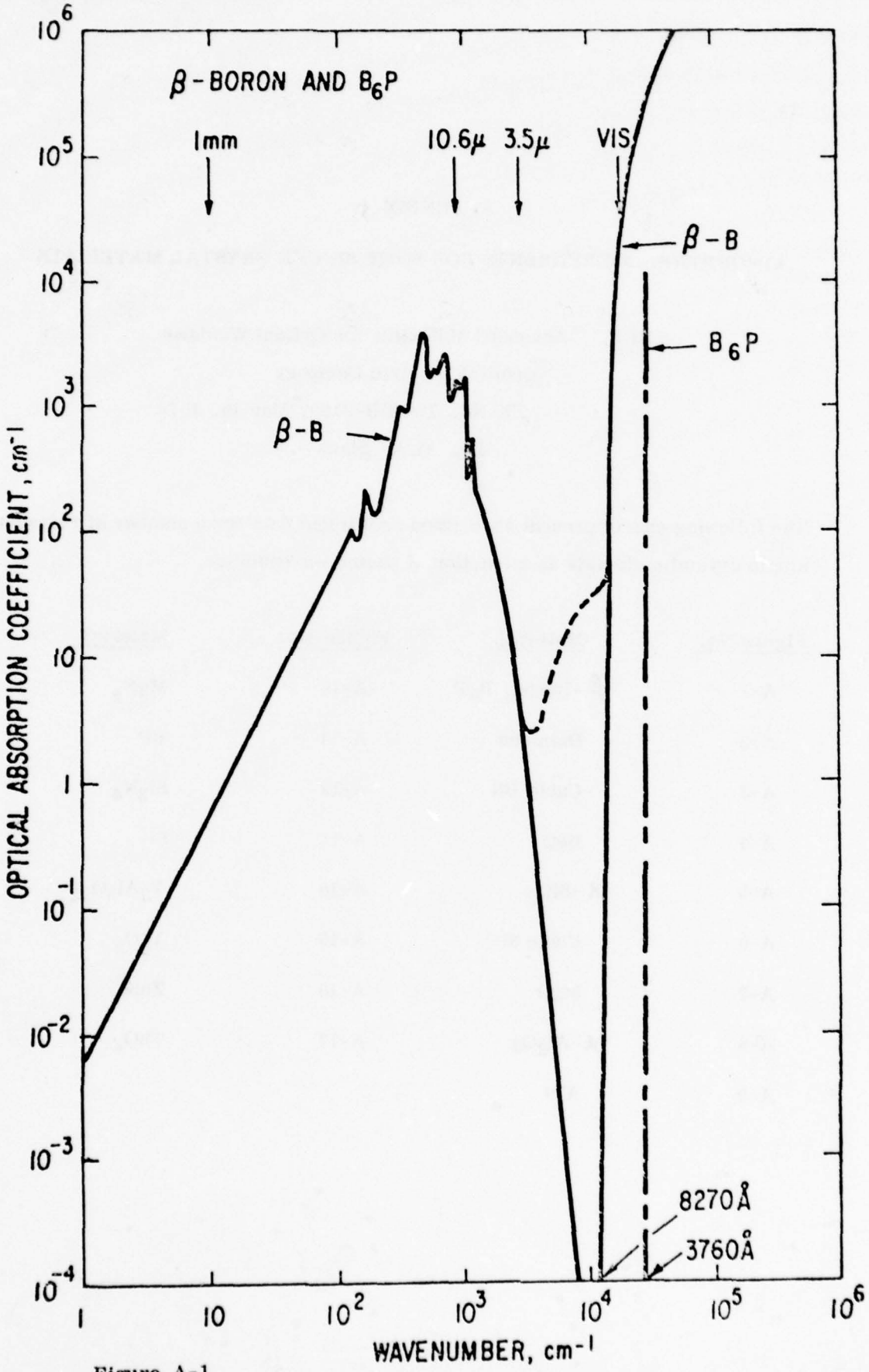
β-BORON AND B_6P
1mm
10.6μ
3.5μ
VIS
β-B
B_6P
β-B
8270Å
3760Å
OPTICAL ABSORPTION COEFFICIENT, cm^{-1}
WAVENUMBER, cm^{-1}
10^6
10^5
10^4
10^3
10^2
10
1
10^{-1}
10^{-2}
10^{-3}
10^{-4}
1
10
10^2
10^3
10^4
10^5
10^6

Figure A-1

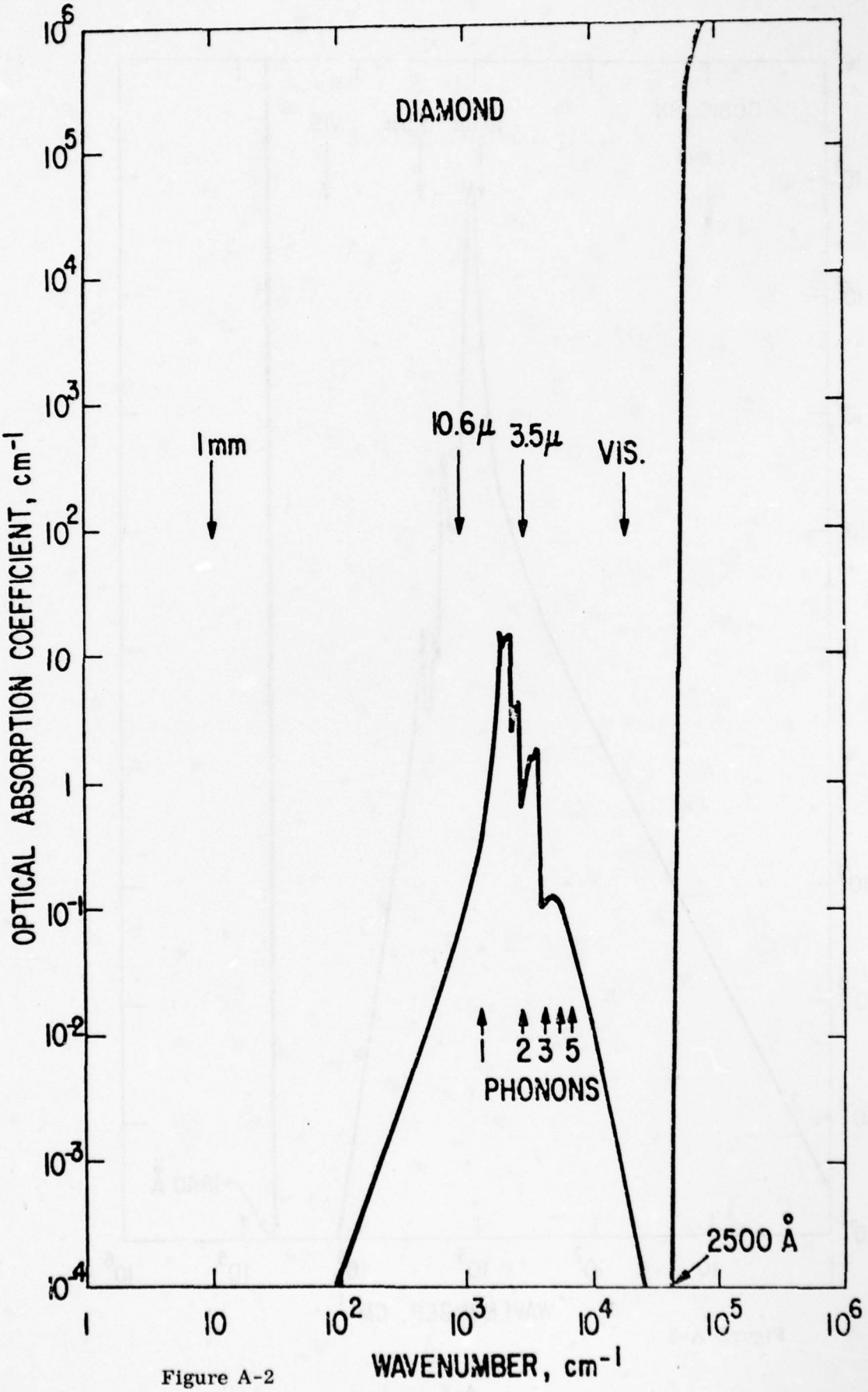
DIAMOND
1mm
10.6μ
3.5μ
VIS.
2500 Å
1 2 3 5
PHONONS
OPTICAL ABSORPTION COEFFICIENT, cm⁻¹
WAVENUMBER, cm⁻¹
10⁶
10⁵
10⁴
10³
10²
10
1
10⁻¹
10⁻²
10⁻³
10⁻⁴
1
10
10²
10³
10⁴
10⁵
10⁶

Figure A-2

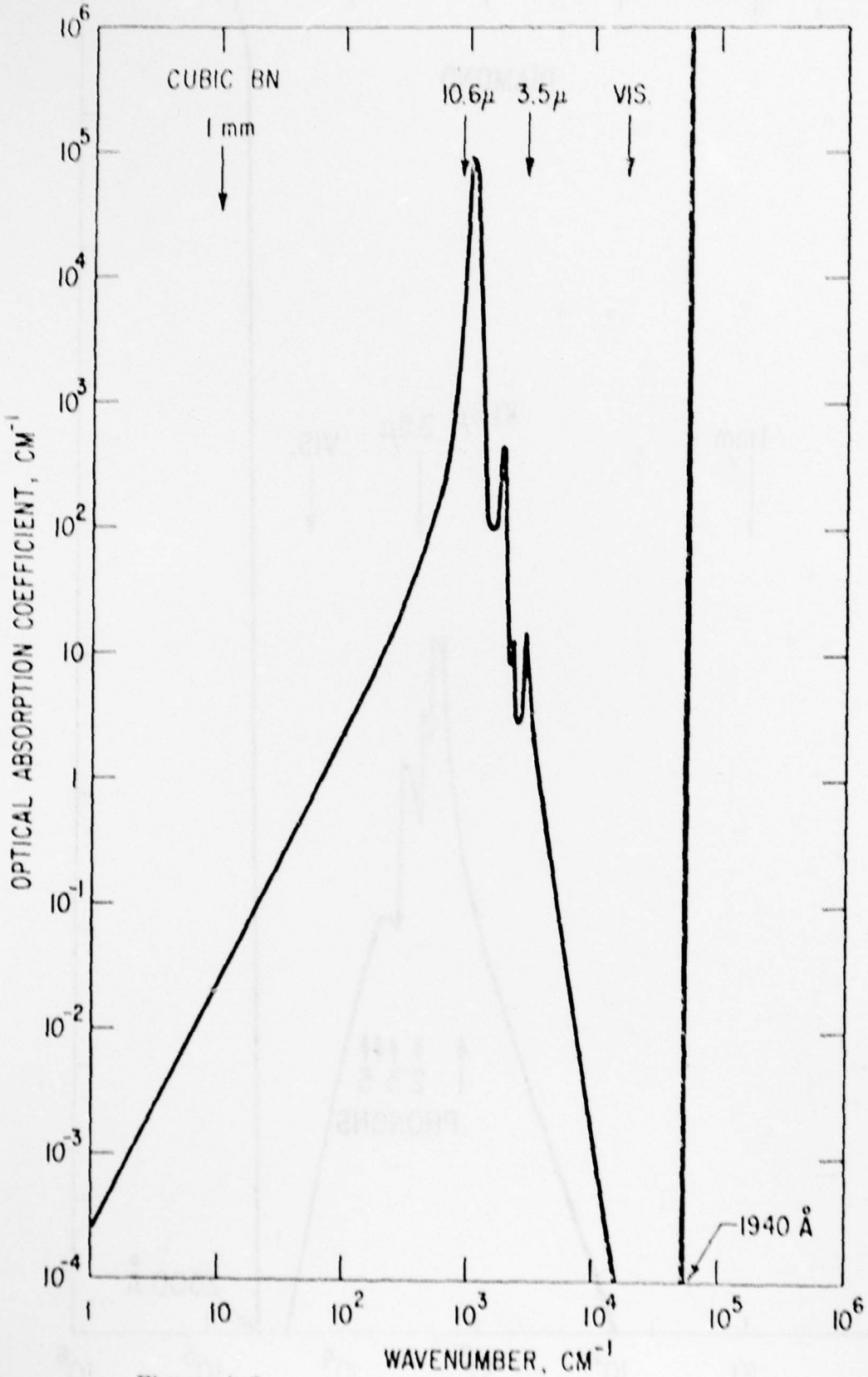
CUBIC BN
1 mm
10.6μ
3.5μ
VIS
1940 Å
OPTICAL ABSORPTION COEFFICIENT, CM⁻¹
WAVENUMBER, CM⁻¹
10⁶
10⁵
10⁴
10³
10²
10
1
10⁻¹
10⁻²
10⁻³
10⁻⁴
1
10
10²
10³
10⁴
10⁵
10⁶

Figure A-3

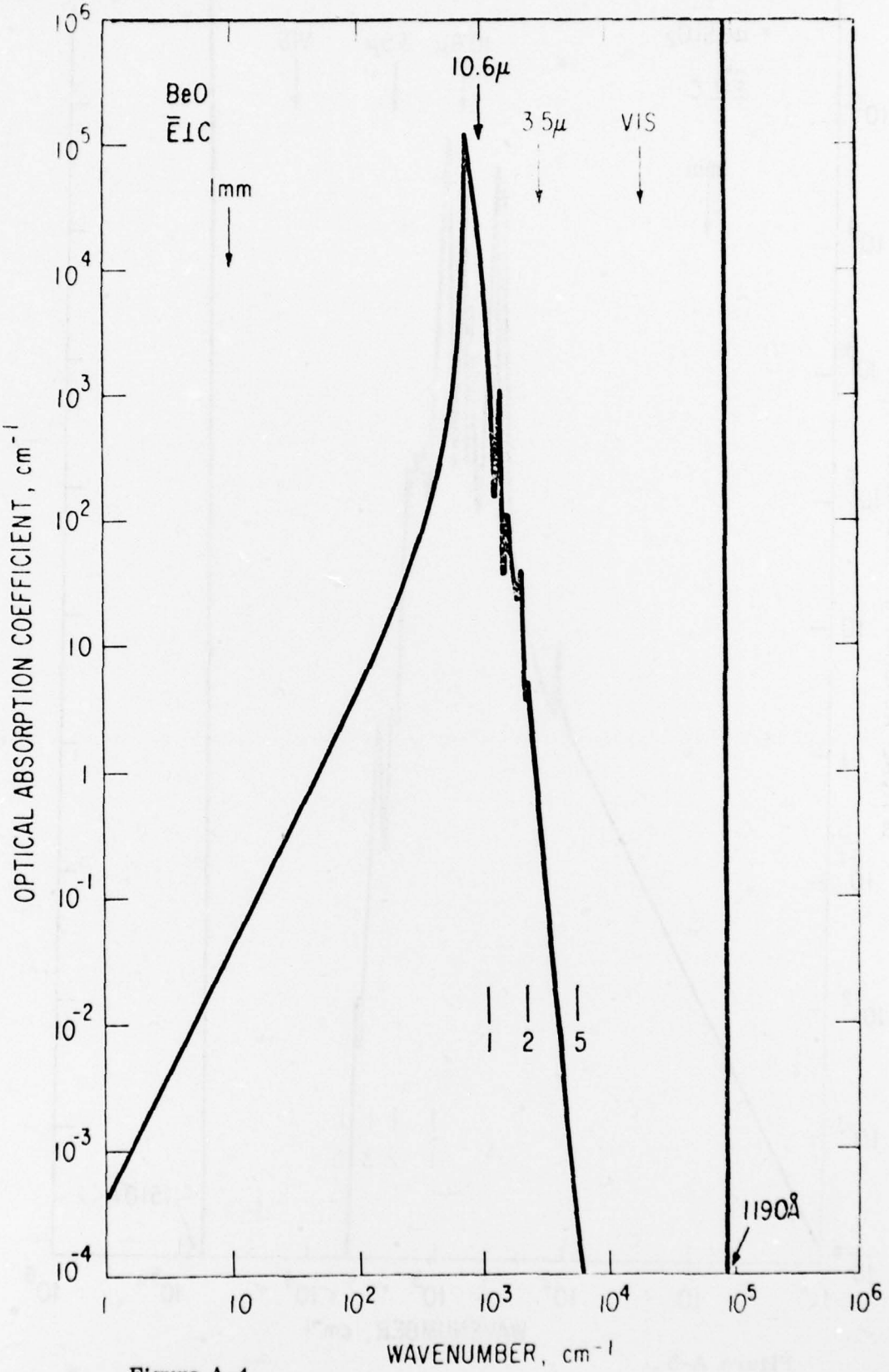
BeO
E⊥C
10.6μ
3.5μ
VIS
1mm
1190Å
1
2
5
OPTICAL ABSORPTION COEFFICIENT, cm⁻¹
WAVENUMBER, cm⁻¹
10⁶
10⁵
10⁴
10³
10²
10
1
10⁻¹
10⁻²
10⁻³
10⁻⁴
1
10
10²
10³
10⁴
10⁵
10⁶

Figure A-4

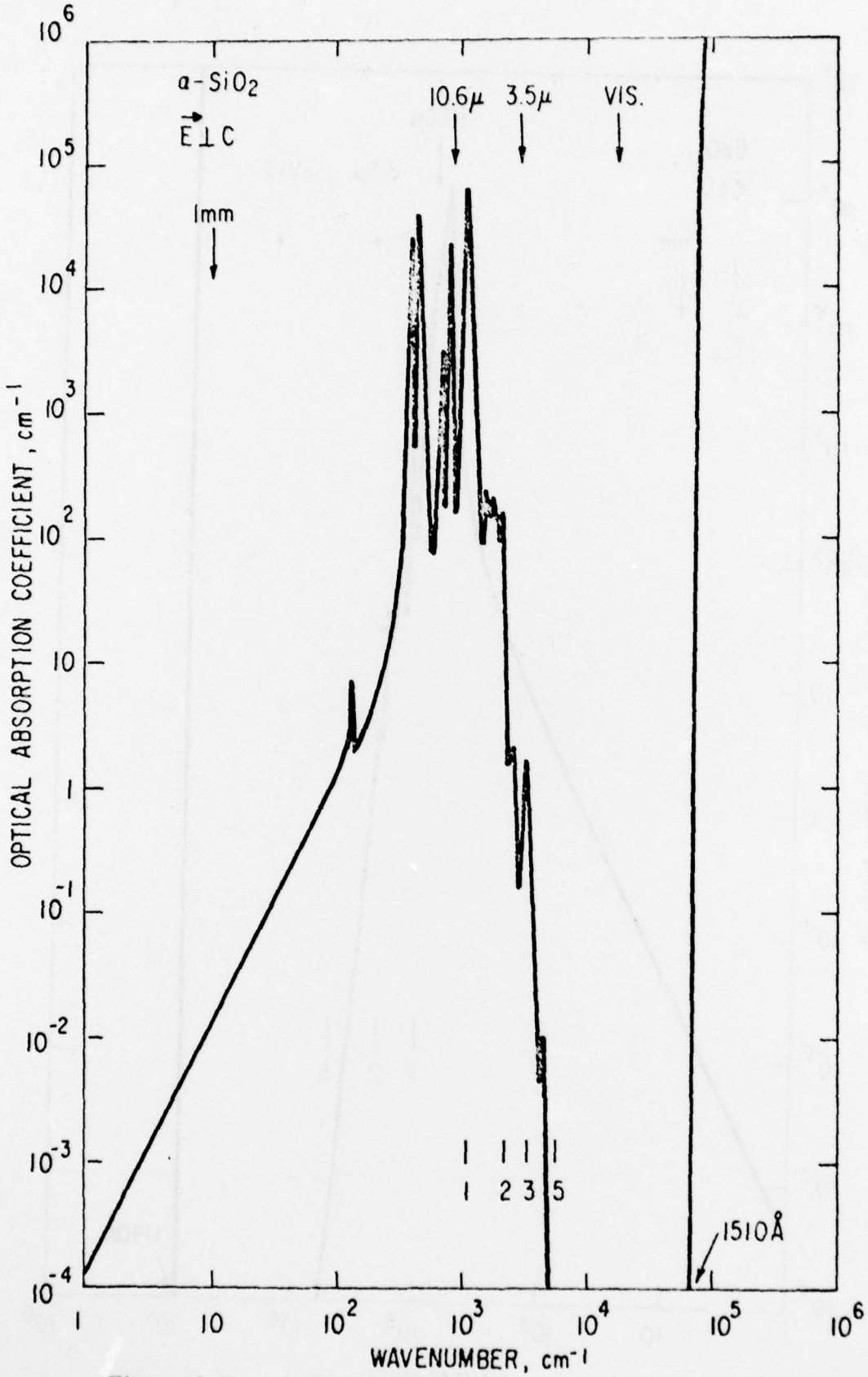
a-SiO2
E⊥C
1mm
10.6μ
3.5μ
VIS.
1510Å
1 1 1 1
1 2 3 5
OPTICAL ABSORPTION COEFFICIENT, cm⁻¹
WAVENUMBER, cm⁻¹
10⁶
10⁵
10⁴
10³
10²
10
1
10⁻¹
10⁻²
10⁻³
10⁻⁴
1
10
10²
10³
10⁴
10⁵
10⁶

Figure A-5

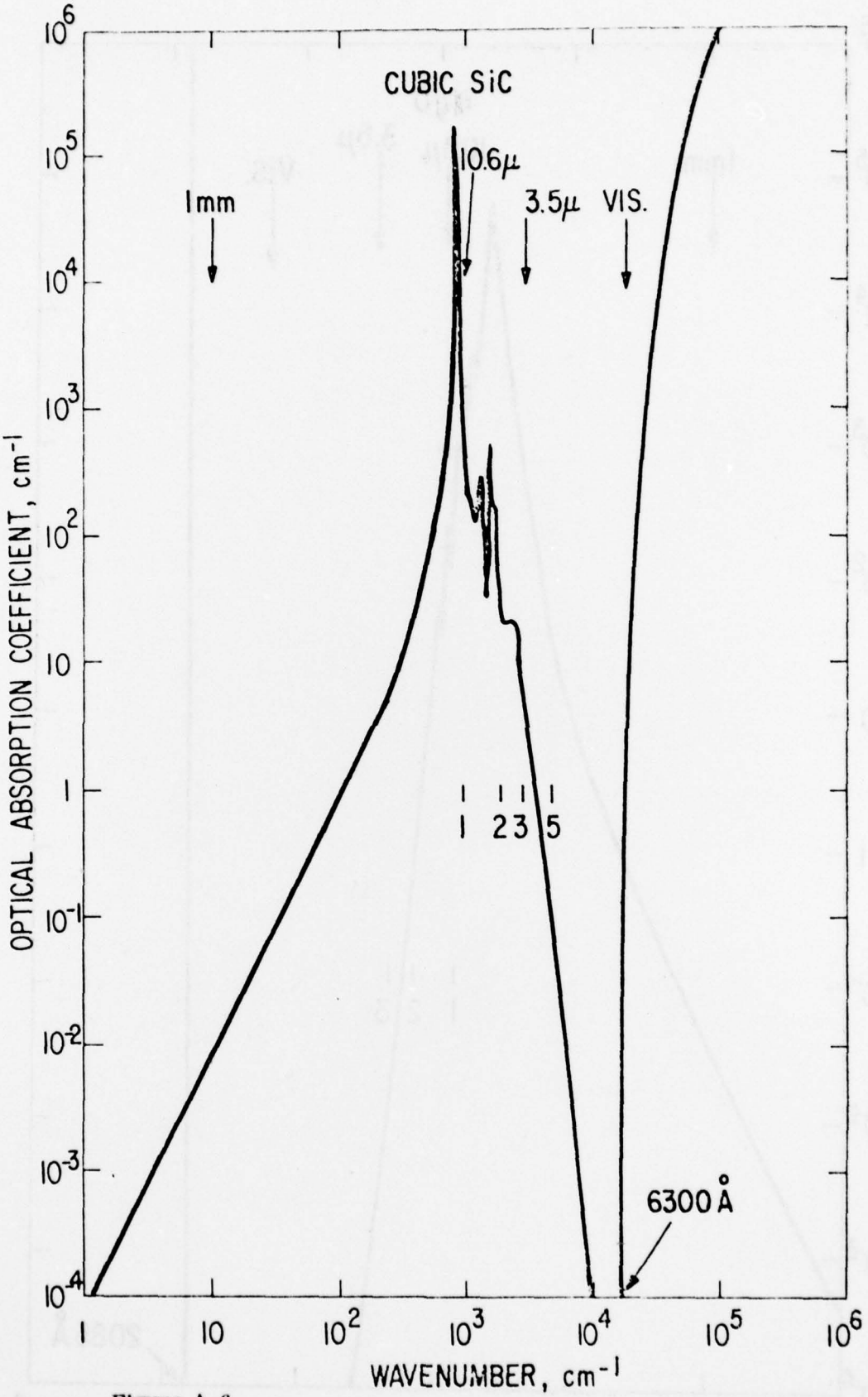
CUBIC SiC
10.6μ
1mm
3.5μ
VIS.
6300 Å
1
2
3
5
OPTICAL ABSORPTION COEFFICIENT, cm⁻¹
WAVENUMBER, cm⁻¹
10⁶
10⁵
10⁴
10³
10²
10
1
10⁻¹
10⁻²
10⁻³
10⁻⁴
1
10
10²
10³
10⁴
10⁵
10⁶

Figure A-6

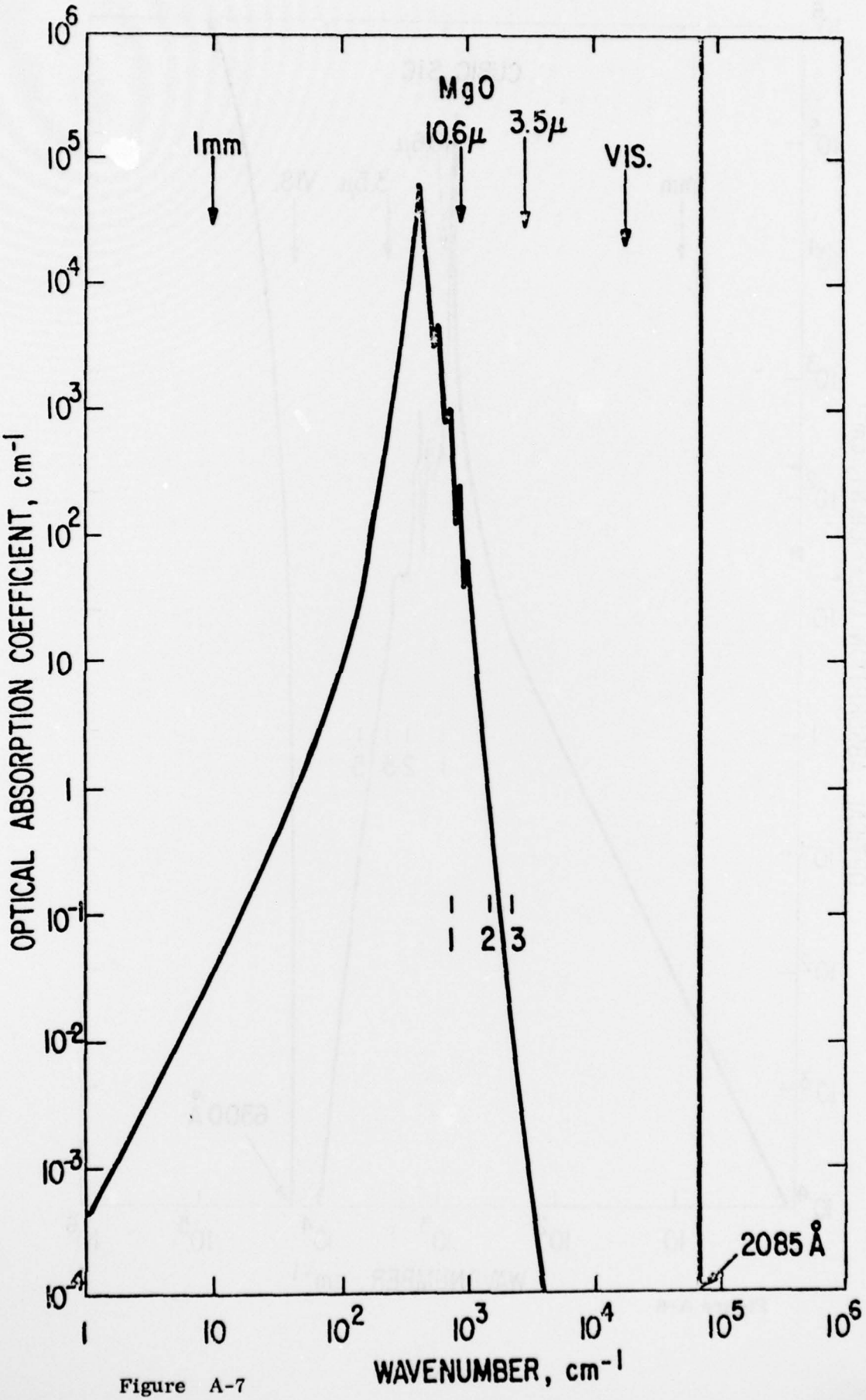
MgO
10.6μ
3.5μ
1mm
VIS.
2085 Å
1 1 1
1 2 3
OPTICAL ABSORPTION COEFFICIENT, cm⁻¹
WAVENUMBER, cm⁻¹
10⁶
10⁵
10⁴
10³
10²
10
1
10⁻¹
10⁻²
10⁻³
10⁻⁴
1
10
10²
10³
10⁴
10⁵
10⁶

Figure A-7

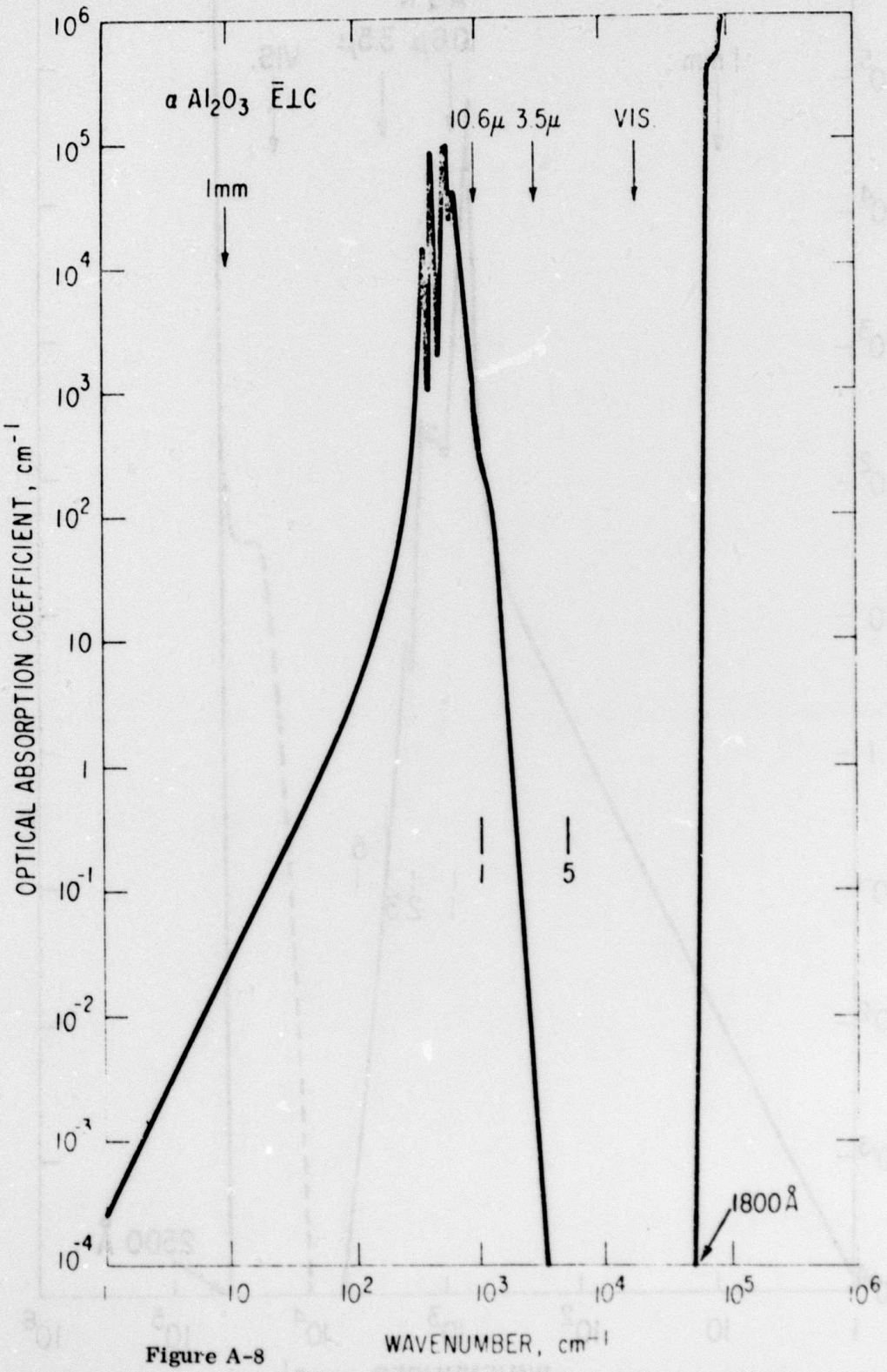
α Al2O3 E⊥C
10.6μ 3.5μ VIS
1mm
1
5
1800 Å
OPTICAL ABSORPTION COEFFICIENT, cm⁻¹
WAVENUMBER, cm⁻¹
10⁶
10⁵
10⁴
10³
10²
10
1
10⁻¹
10⁻²
10⁻³
10⁻⁴
1
10
10²
10³
10⁴
10⁵
10⁶

Figure A-8

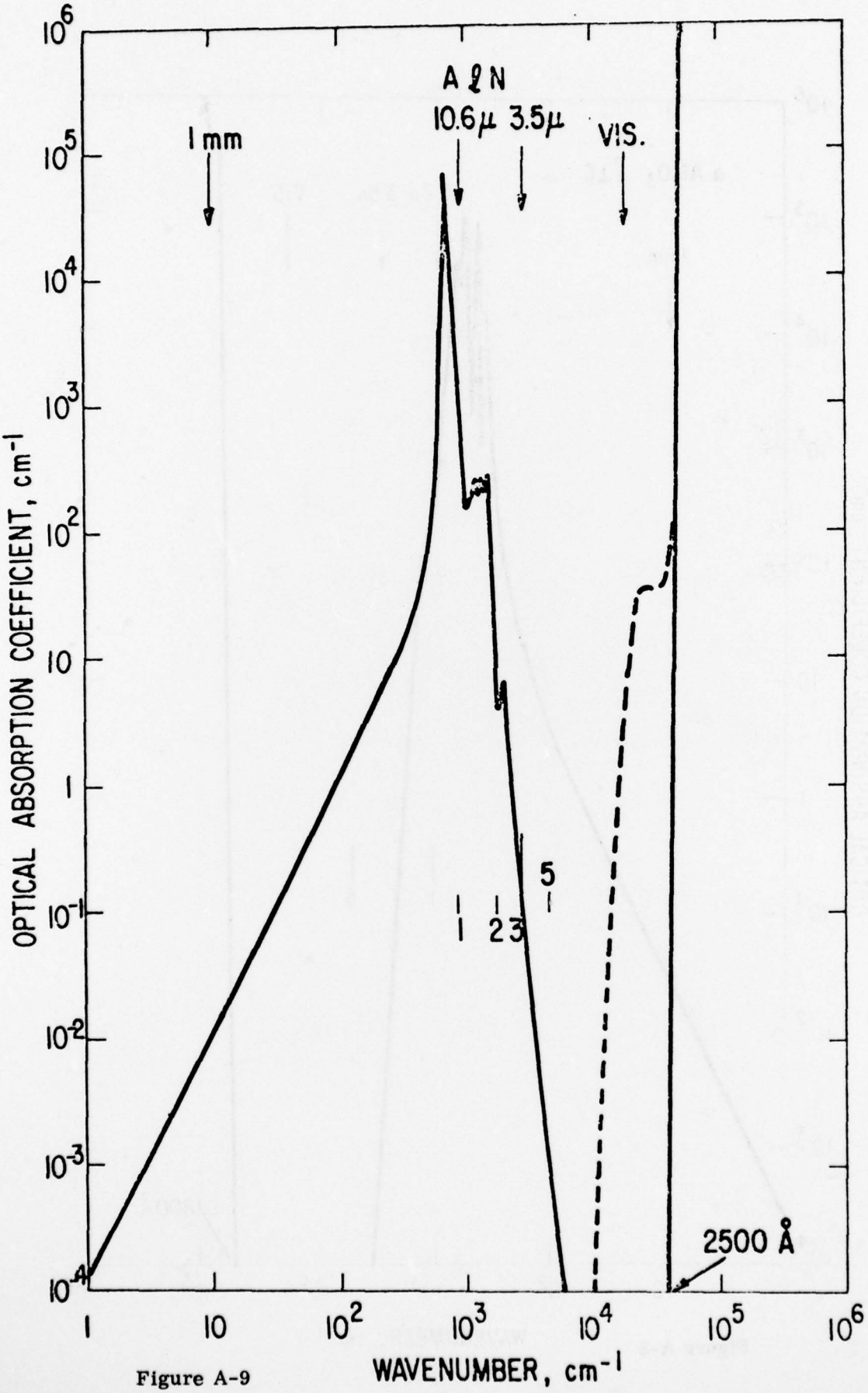
OPTICAL ABSORPTION COEFFICIENT, cm⁻¹
WAVENUMBER, cm⁻¹
1 mm
A ℓ N
10.6μ 3.5μ
VIS.
2500 Å
5
1
1
2
3
10⁶
10⁵
10⁴
10³
10²
10
1
10⁻¹
10⁻²
10⁻³
10⁻⁴
1
10
10²
10³
10⁴
10⁵
10⁶

Figure A-9

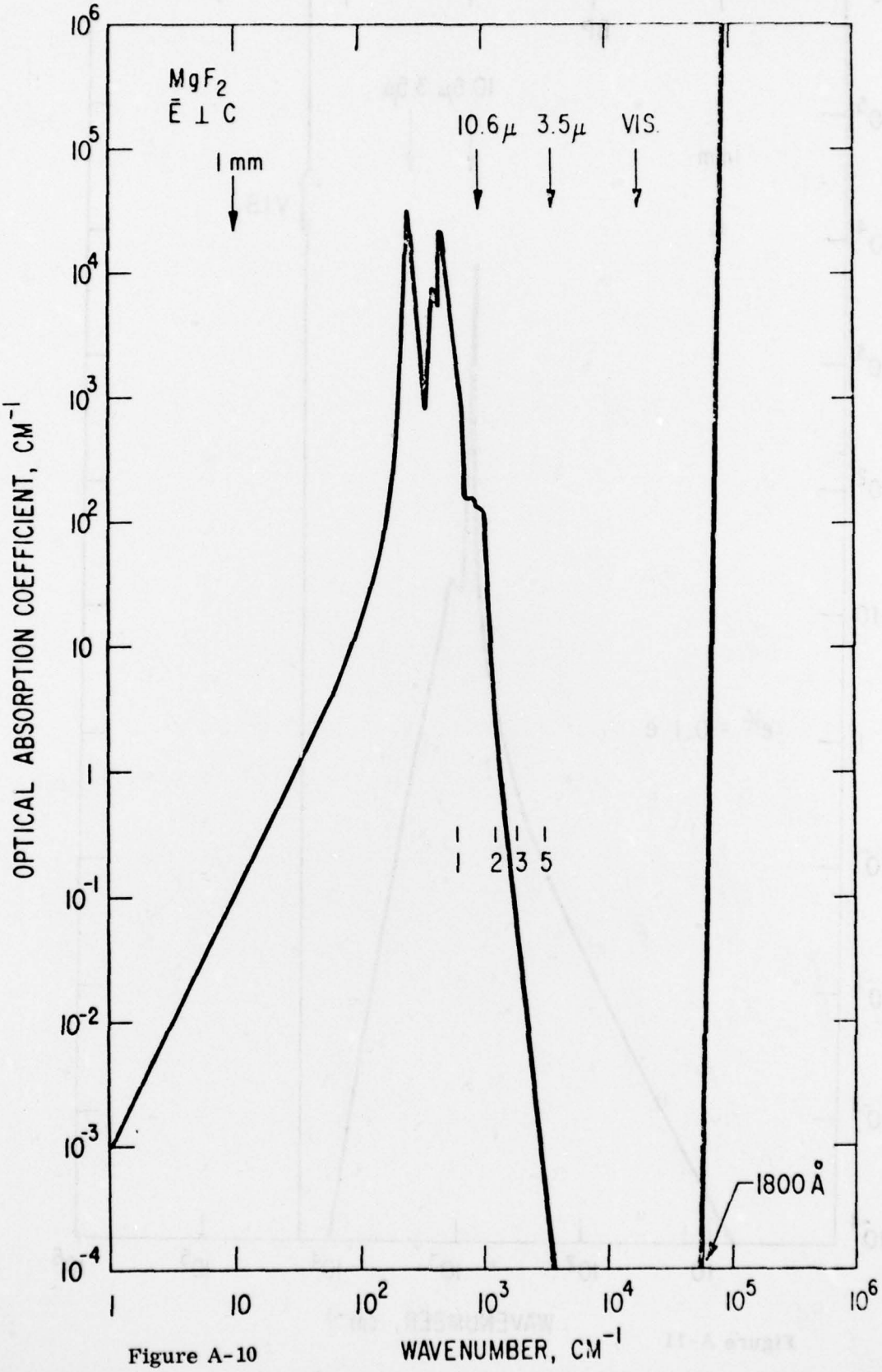
MgF2
E ⊥ C
1 mm
10.6μ
3.5μ
VIS.
1800 Å
1 1 2 3 5
OPTICAL ABSORPTION COEFFICIENT, CM-1
WAVENUMBER, CM-1
10^6
10^5
10^4
10^3
10^2
10
1
10^-1
10^-2
10^-3
10^-4
1
10
10^2
10^3
10^4
10^5
10^6

Figure A-10

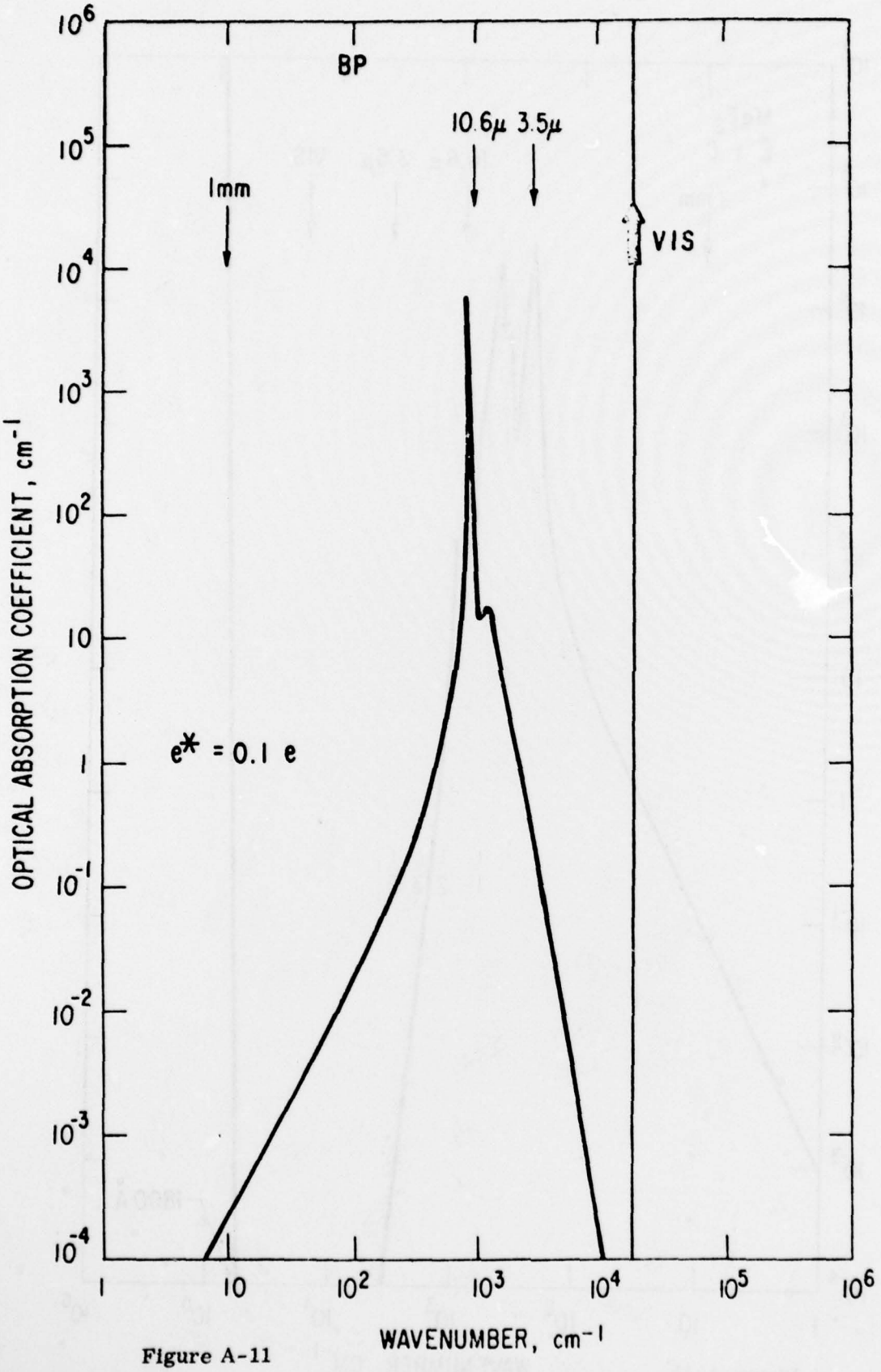
BP
10.6μ 3.5μ
1mm
VIS
e* = 0.1 e
OPTICAL ABSORPTION COEFFICIENT, cm⁻¹
WAVENUMBER, cm⁻¹
10⁶
10⁵
10⁴
10³
10²
10
1
10⁻¹
10⁻²
10⁻³
10⁻⁴
1
10
10²
10³
10⁴
10⁵
10⁶

Figure A-11

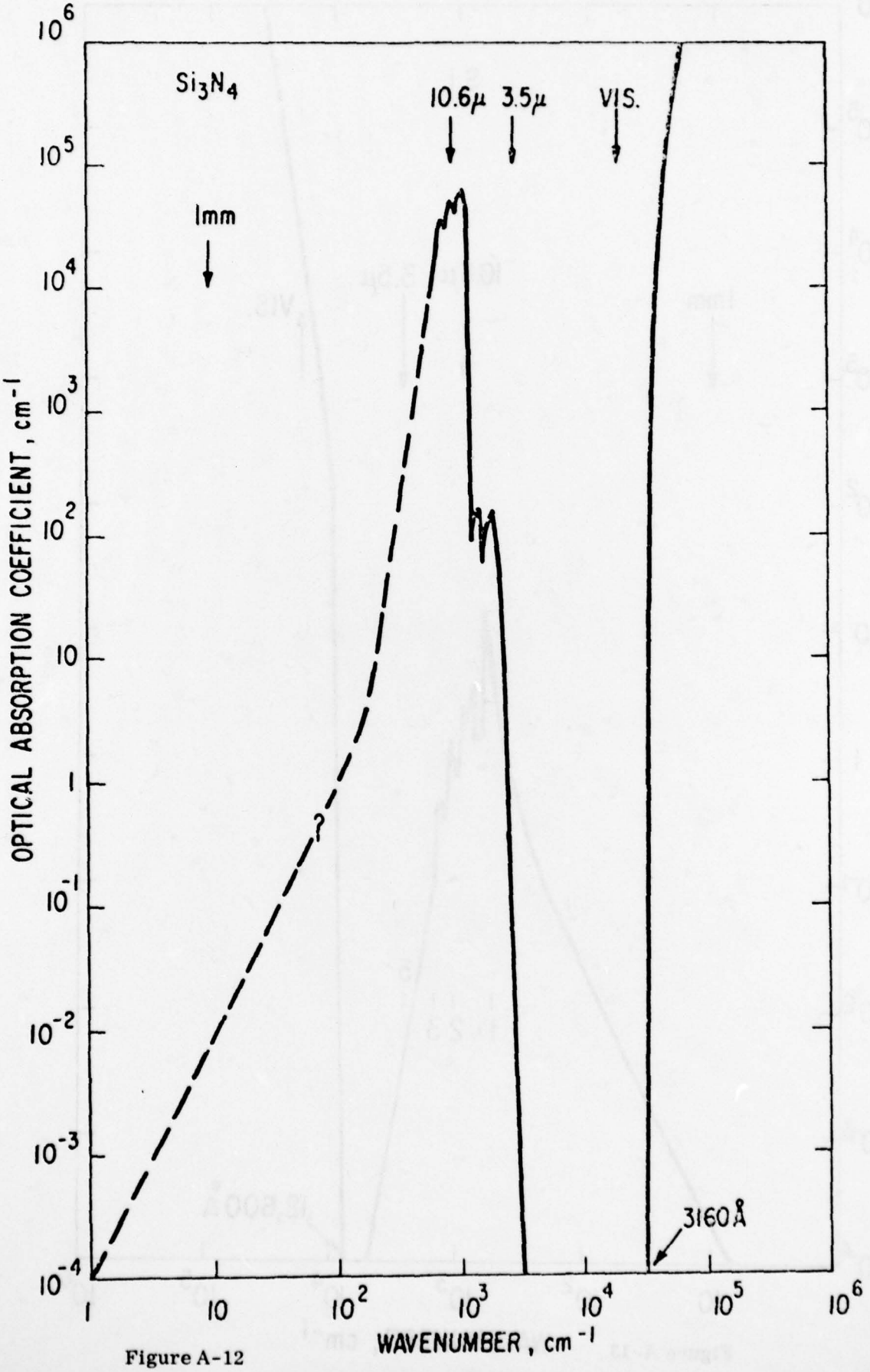
Si_3N_4
10.6μ
3.5μ
VIS.
1mm
3160 Å
?
OPTICAL ABSORPTION COEFFICIENT, cm^{-1}
WAVENUMBER, cm^{-1}
10^6
10^5
10^4
10^3
10^2
10
1
10^{-1}
10^{-2}
10^{-3}
10^{-4}
1
10
10^2
10^3
10^4
10^5
10^6

Figure A-12

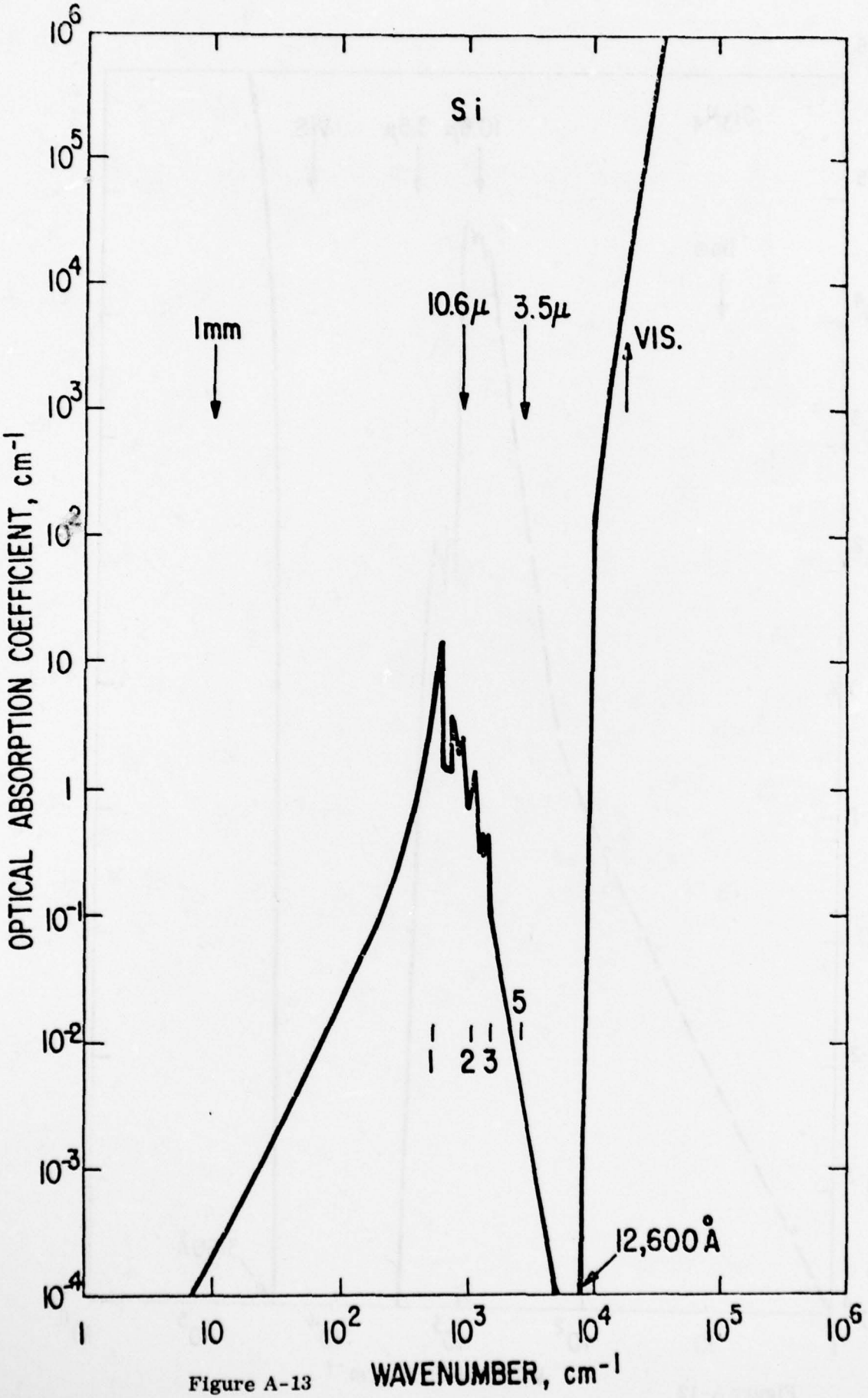
Si
1mm
10.6μ
3.5μ
VIS.
12,600 Å
1
2
3
5
OPTICAL ABSORPTION COEFFICIENT, cm⁻¹
WAVENUMBER, cm⁻¹
10⁶
10⁵
10⁴
10³
10²
10
1
10⁻¹
10⁻²
10⁻³
10⁻⁴
1
10
10²
10³
10⁴
10⁵
10⁶

Figure A-13

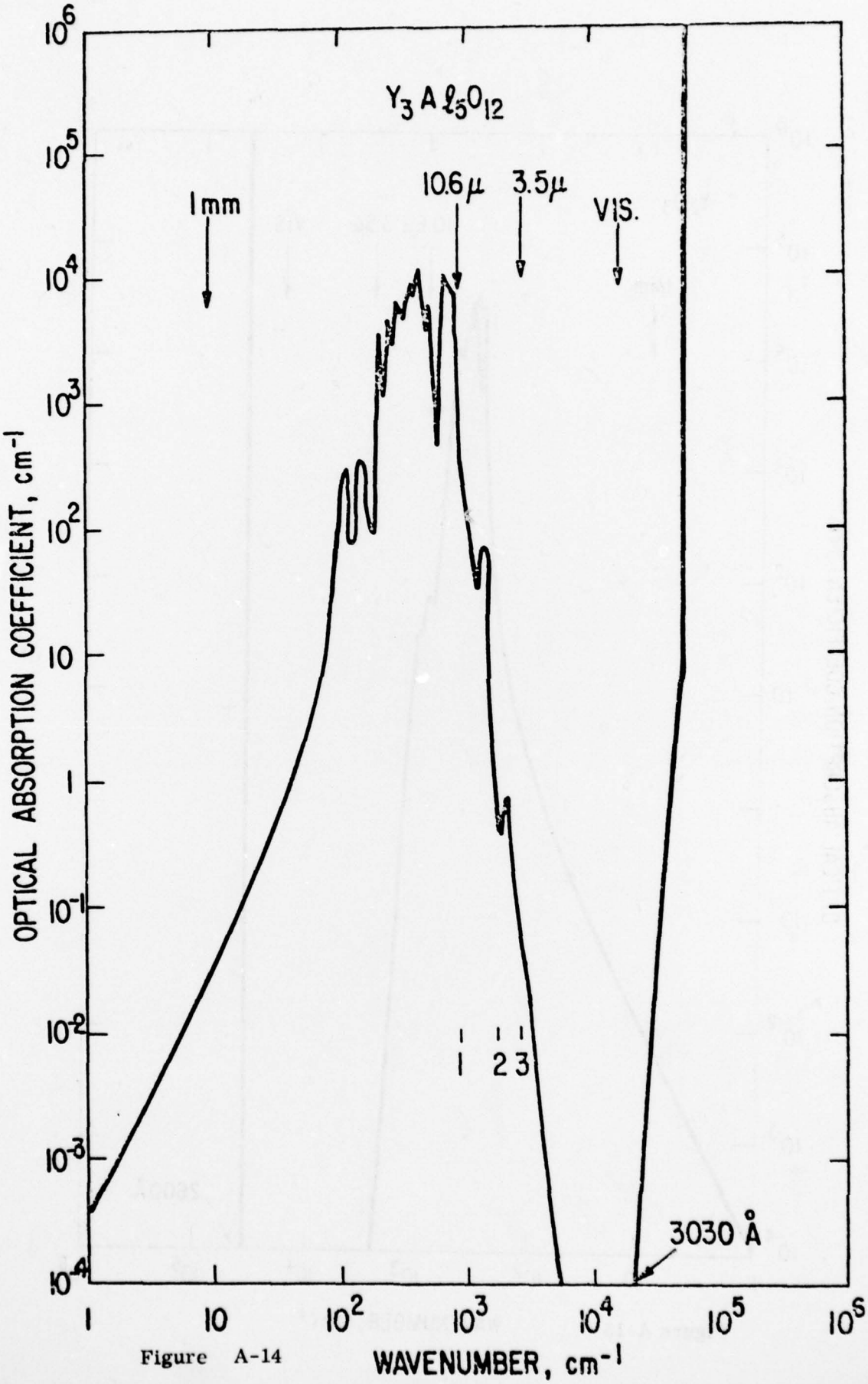
$Y_3 A\ell_5O_{12}$
1mm
10.6μ
3.5μ
VIS.
1
2
3
3030 Å
OPTICAL ABSORPTION COEFFICIENT, cm⁻¹
WAVENUMBER, cm⁻¹
10⁶
10⁵
10⁴
10³
10²
10
1
10⁻¹
10⁻²
10⁻³
10⁻⁴
1
10
10²
10³
10⁴
10⁵
10⁶

Figure A-14

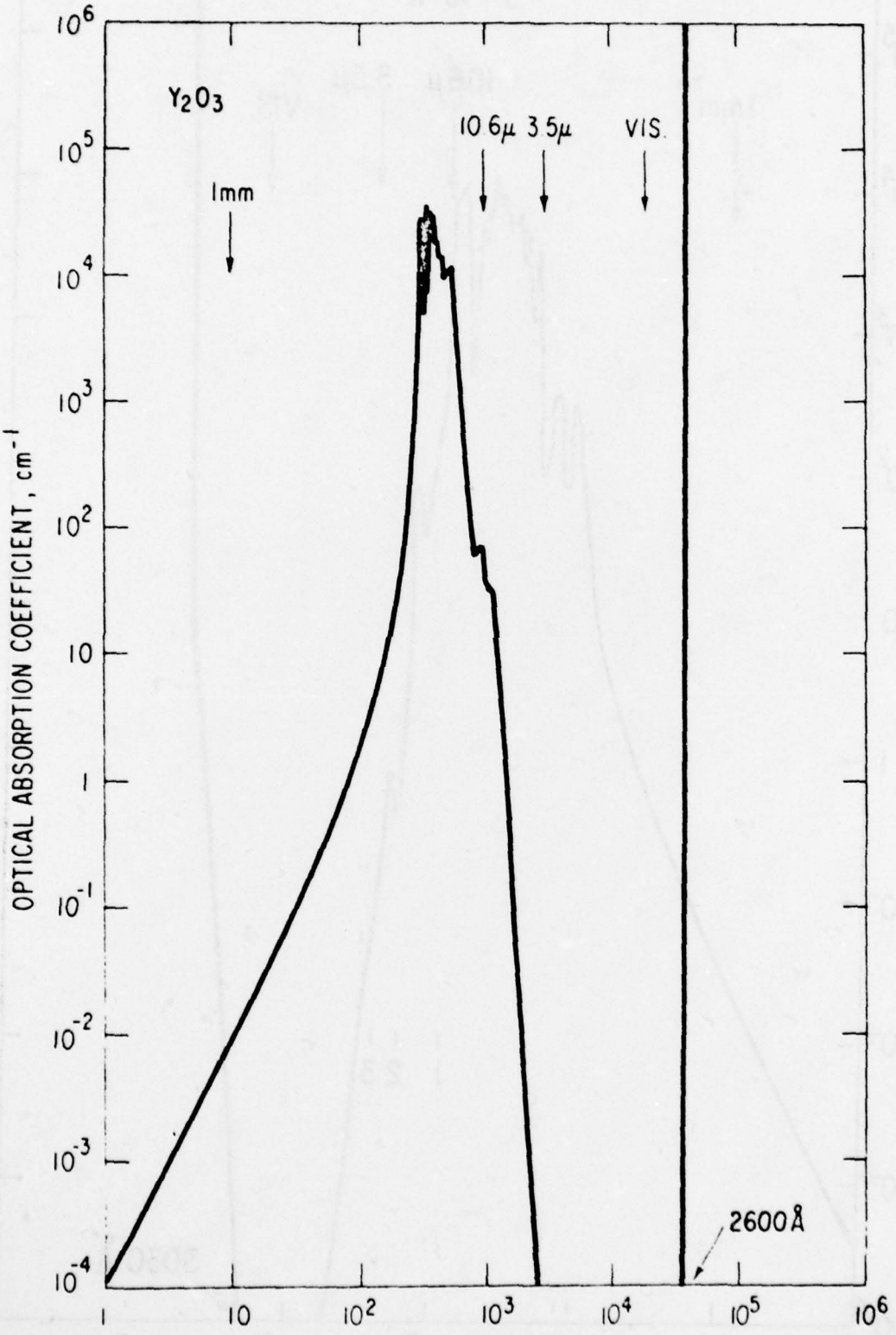
Y_2O_3
1mm
10 6μ
3 5μ
VIS.
2600Å
OPTICAL ABSORPTION COEFFICIENT, cm^{-1}
WAVENUMBER, cm^{-1}
10^6
10^5
10^4
10^3
10^2
10
1
10^{-1}
10^{-2}
10^{-3}
10^{-4}
1
10
10^2
10^3
10^4
10^5
10^6

Figure A-15

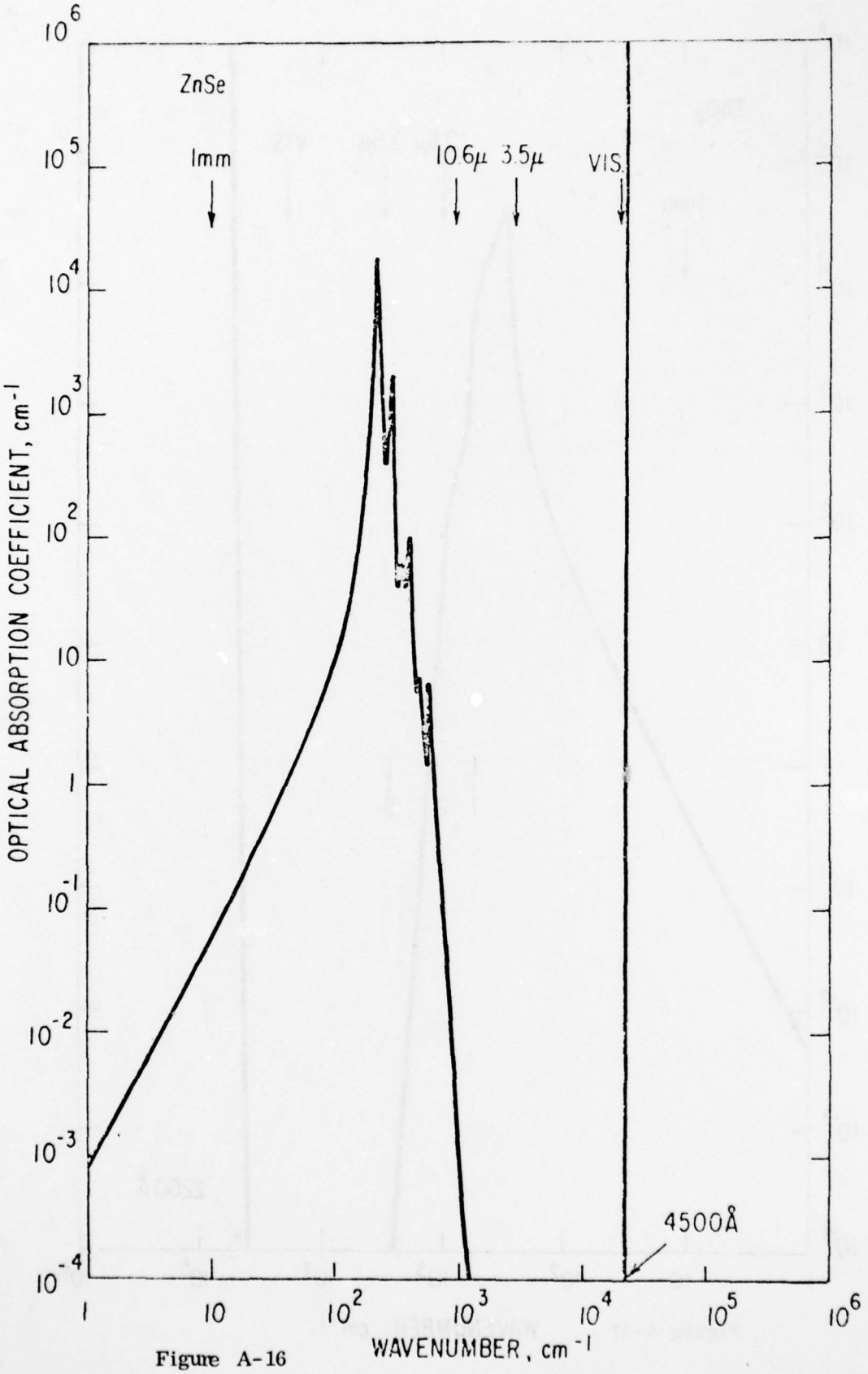
ZnSe
1mm
10.6μ
3.5μ
VIS.
4500Å
OPTICAL ABSORPTION COEFFICIENT, cm⁻¹
WAVENUMBER, cm⁻¹
10⁶
10⁵
10⁴
10³
10²
10
1
10⁻¹
10⁻²
10⁻³
10⁻⁴
1
10
10²
10³
10⁴
10⁵
10⁶

Figure A-16

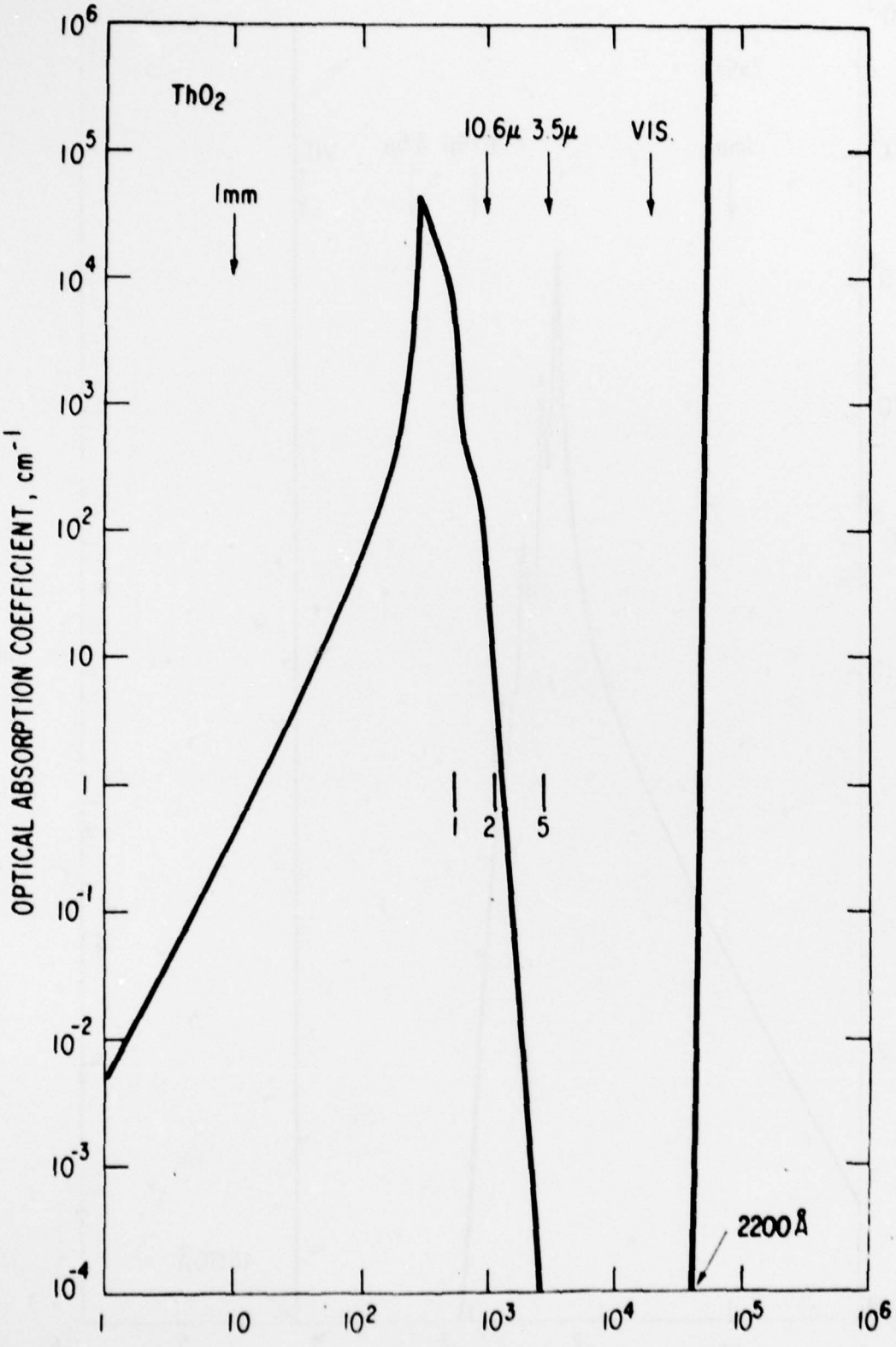
ThO2
1mm
10.6μ
3.5μ
VIS.
1
2
5
2200Å
OPTICAL ABSORPTION COEFFICIENT, cm⁻¹
WAVENUMBER, cm⁻¹
10⁶
10⁵
10⁴
10³
10²
10
1
10⁻¹
10⁻²
10⁻³
10⁻⁴
1
10
10²
10³
10⁴
10⁵
10⁶

Figure A-17